Propriétés électroniques des semiconducteurs magnétiques dilués: Ga1-xMnxN, Ga1-xMnxAs, Ge1-xMnx

Andrey Titov

▶ **To cite this version:**

Andrey Titov. Propriétés électroniques des semiconducteurs magnétiques dilués: Ga1-xMnxN, Ga1-xMnxAs, Ge1-xMnx. Condensed Matter [cond-mat]. Université Joseph-Fourier - Grenoble I, 2006. English. NNT : . tel-00113864

HAL Id: tel-00113864
https://theses.hal.science/tel-00113864

Submitted on 12 Dec 2006

Université Joseph Fourier – Grenoble I

A. M. Prokhorov General Physics Institute of the Russian Academy of Sciences

A dissertation for the degree of

Doctor of the Joseph Fourier University – Grenoble I

Specialty: Physics

Presented and defended by

TITOV Andrey

December 7, 2006

Electronic properties of the diluted magnetic semiconductors:

$$\text{Ga}_{1-x}\text{Mn}_x\text{N}, \text{Ga}_{1-x}\text{Mn}_x\text{As}, \text{Ge}_{1-x}\text{Mn}_x$$

Advisory committee:

President:	Michel ZIGONE
Reporter:	Patrick BRUNO
Reporter:	Frédéric PETROFF
Thesis co-adviser:	Henri MARIETTE
Thesis adviser:	Erkin KULATOV
Thesis adviser:	Joël CIBERT

Grenoble – 2006

Acknowledgements

Contents

Introduction

Electrical and magnetic properties of materials are used in the modern information technology. The information processing is performed in solid state circuits where the logical states "1" and "0" are associated to the electric potential. The electron spin is not used during the processing. However to store a large volume of information we use the magnetic record, i.e. electron spin in ferromagnetic metals. The aim of the spin electronics (spintronics) is to create new electronic components which would use both the electrical and spin dependent phenomena for the information processing.

Giant magneto-resistance sensor is an example of such spintronic components. It consists of two ferromagnetic metal layers separated by a nonmagnetic metal layer [1]. It was shown that the electric resistance of the multilayer structure depends on the directions of the magnetization in the ferromagnetic layers: if the magnetizations of the layers are parallel, the resistance is small. The resistance increases when the magnetizations of the ferromagnetic layers become anti-parallel. Today the magneto-resistance sensor is used in the read head in hard disks and it allows information recording with the density as high as 19 Gbit/cm^2 [2].

The magneto-resistance sensor has a simple structure, small size and a high speed. Therefore the component can be used as a storage cell in the random access memory. The memory based on the magneto-resistance sensors is called the magnetic random access memory (MRAM). It is interesting that the sensor can also perform the basic logical operations a+b, a×b and the inversion. Therefore a full functional microprocessor can be created where the magneto-resistance cells keep and process information [3]. Many other possible spintronic components were proposed during the last years [1,4], however the lack of suitable materials prevents practical realization of the components.

The usual semiconductors which are used in the microelectronics (Si,GaAs) are not ferromagnetic. On the other hand it is quit difficult to use ferromagnetic metals (Fe,Ni) together with conventional semiconductors, because of complicate properties of metal-semiconductor interfaces. The concentrated magnetic semiconductors ($CuCr_2S_4$, Sr_2FeMoO_6,

Sr$_2$CrReO$_6$) are ferromagnetic at high temperature. However the crystal structure of these materials does not allow incorporating them in modern microelectronic devices [4].

In order to use semiconductors in microelectronics we change their electric properties: donor or acceptor impurities should be incorporated to obtain *n*-type and *p*-type semiconductors. Just as in the case of electric properties, the magnetic properties of semiconductors can be changed by doping with magnetic impurities. For a long time much attention has being paid to II-VI semiconductors, where the valence of the cation coincide to the valence of well studied magnetic ions (Mn, Cr). However antiferromagnetic interactions are very important in the semiconductors and obtained values of the Curie temperature are very low (a few K in ZnMnTe [5]).

Another way is to make conventional nonmagnetic semiconductors ferromagnetic. Silicon based semiconductors would be very important for practical applications however the Si layers doped with Mn are not homogeneous and they contain clusters like Si$_3$Mn$_5$ [4]. This work is dedicated to three conventional semiconductors doped with Mn: (Ga,Mn)N, (Ga,Mn)As and (Ge,Mn).

The diluted magnetic semiconductor (Ga,Mn)N was studied experimentally and theoretically. According to a theoretical prediction [6], *p* type Ga$_{1-x}$Mn$_x$N crystals would be ferromagnetic above room temperature. This implies however the incorporation of *x*=0.05 of Mn into GaN, substituting Ga in the form of Mn^{2+} ions. Experimental works following this prediction did not give any clearcut conclusion about the magnetic properties of (Ga,Mn)N: ferromagnetic properties at room temperature [7,8], as well as paramagnetic properties at very low temperature [9,10,11] were reported. In addition contradictory conclusions were drown about the valence state of Mn in (Ga,Mn)N. In bulk (Ga,Mn)N, with a very low content of Mn, the 2+ valence state was detected by the electron paramagnetic resonance in agreement with the strong *n* type character of the samples [12]. In similar samples the 3+ valence state was deduced from magneto-optical measurements upon co-doping with Mg [11], which is a usual acceptor in GaN. The Mn content in these samples is very low, a few 10^{18} cm^{-3} therefore the valence state of Mn can be influenced by a small content of a donor impurity. Various types of valence states from 2+ to 4+ were invoked to explain optical spectra of epilayers with a larger Mn content [13,14]. Also *p* type (Ga,Mn)N layers were reported that implies the 2+ valence state of Mn in (Ga,Mn)N. Therefore additional investigation is necessary to clarify

electronic and magnetic properties of (Ga,Mn)N. The most part of the work is devoted to this semiconductor.

The diluted magnetic semiconductor (Ga,Mn)As is another promising material for spintronic applications. A recent progress in semiconductor technology allowed incorporation a high concentration of Mn in GaAs epilayers [15]. The Curie temperature of the $Ga_{1-x}Mn_xAs$ (x=0.053) was found to be 110 K. It was also shown that annealing of the samples increases the Curie temperature [16] and the highest Curie temperature obtained in (Ga,Mn)As is 173 K [17]. In this work (Ga,Mn)As semiconductor is used as a reference system: on the one hand this semiconductor is close to the III-V semiconductor (Ga,Mn)N, therefore numerous experimental and theoretical results obtained on (Ga,Mn)As samples will be useful in investigation of (Ga,Mn)N semiconductor; on the other hand the electronic structures of (Ga,Mn)As and (Ge,Mn) semiconductors are similar, therefore the same results obtained on (Ga,Mn)As samples will be also used to predict electronic properties of (Ge,Mn). In the third chapter the x-ray absorption spectrum of a (Ga,Mn)As sample is shown. This sample was grown by molecular beam epitaxy at the University of Nottingham [18].

The third diluted magnetic semiconductor studied in the work is (Ge,Mn). First experimental results indicated that (Ge,Mn) was a high temperature ferromagnetic semiconductor (T_C=116K [19], 285K [20]). However later investigations did not confirm the ferromagnetic properties of (Ge,Mn) [21,22]. The electronic structure of (Ge,Mn) was calculated in this work. According to this calculation the valence state of Mn in (Ge,Mn) is 2+. This assumption can be checked using the K-edge x-ray absorption spectra of Mn in (Ge,Mn).

In the first chapter the structure of (Ga,Mn)N samples is described. The electronic structure of the samples was further investigated using x-ray absorption measurements. Therefore the experimental equipment used for the measurements is also described in this chapter. Finally the obtained K-edge x-ray absorption spectra of Mn in the (Ga,Mn)N samples are presented.

In the second chapter I describe the *ab-initio* methods that were used to calculate the electronic structure of the semiconductors. Such *ab-initio* calculations are used very often in interpretation of complicated experimental data. As we will see later the calculations allow us to link together the real band structure and observable properties of crystals.

In the third chapter the electronic properties of (Ga,Mn)N, (Ga,Mn)As and (Ge,Mn) are investigated using the *ab-initio* methods described in the chapter II. The results of the calculations were further compared to experimental x-ray absorption spectra of (Ga,Mn)N, (Ga,Mn)As and (Zn,Mn)Te. An interpretation of the x-ray absorption near edge structure of Mn is proposed. This interpretation allows determining the valence state and the distribution of the Mn in diluted magnetic semiconductors with a tetrahedral arrangement of ligands.

The magnetic properties of the three semiconductors are outlined in the fourth chapter. Different possible exchange mechanisms are considered. The observed magnetic properties of the three diluted magnetic semiconductors are analyzed; the analysis is based on the study of electronic properties of the semiconductors.

Chapitre I. Etude expérimentale de DMS

Une étude expérimentale des couches de (Ga,Mn)N est présentée dans cette chapitre. Les couches de Ga$_{1-x}$Mn$_x$N (x=0,003-0,057) ont été préparées par épitaxie par jets moléculaires [1,2,3]. La structure wurtzite de ces échantillons a été confirmée par des mesures de diffraction des rayons X. La forte dynamique de ces mesures a montré également que les couches de (Ga,Mn)N ne contiennent pas de phases secondaires comme GaMn$_3$N [2].

Les propriétés structurales et électroniques de (Ga,Mn)N ont été étudiées par spectroscopie d'absorption des rayons X au seuil K du Mn. Les spectres d'absorption ont été enregistrés au Synchrotron Européen (ESRF, ligne BM30B) à Grenoble [10]. Cette méthode a plusieurs avantages. Premièrement, elle permet d'étudier séparément les différents éléments chimiques dans un alliage complexe. Deuxièmement, l'intensité de ces spectres peut souvent être directement associée à la densité d'états p au dessus du niveau de Fermi. En outre, les spectres d'absorption au seuil K sont moins influencés par la surface des échantillons que les spectres au seuil L. Les spectres au seuil K permettent donc d'étudier les propriétés intrinsèques du cristal. Enfin, cette méthode est couramment utilisée à Grenoble et des résultats préliminaires étaient disponibles dans notre équipe. Une simulation de la partie EXAFS des spectres d'absorption au seuil K du Mn a confirmé que les atomes de Mn substituent les atomes de Ga dans GaN [10]. Nous présentons une étude de l'état électronique et de la distribution du Mn dans (Ga,Mn)N à partir de la partie XANES des spectres d'absorption des rayons X au seuil K du Mn. La forme des spectres XANES enregistrés ne dépend pas de la concentration du Mn dans Ga$_{1-x}$Mn$_x$N (x=0,003-0,057). L'état électronique du Mn et la structure cristalline locale autour du Mn sont donc les mêmes dans tous nos échantillons. Cependant, il est assez compliqué de trouver un lien entre le XANES et la structure électronique du cristal. Nous utiliserons des calculs *ab-initio* pour obtenir une information quantitative à partir de ces spectres.

Chapter I. Experimental investigation of DMS

1.1 (Ga,Mn)N samples

Electronic and magnetic properties of (Ga,Mn)N semiconductor were studied on (Ga,Mn)N layers grown by nitrogen-plasma-assisted molecular beam epitaxy (MBE). This method of growth is widely used in the modern microelectronic technology and it allows us to prepare very pure crystals of good quality. The technology of (Ga,Mn)N samples was described in detail in [1,2,3]. The aim of this chapter is to outline main parameters of obtained (Ga,Mn)N samples.

GaMnN MBE
GaN MBE
GaN MOCVD
Al_2O_3 (0001)

Fig. 1.1. Structure of (Ga,Mn)N samples. The (Ga,Mn)N films were grown by nitrogen-plasma assisted molecular beam epitaxy (MBE) on a GaN buffer layer. The buffer layer was previously grown by the metal-organic chemical vapor deposition (MOCVD) on a sapphire substrate.

Sapphire crystals were used as a substrate in the samples. The sapphire crystals have hexagonal structure and the surface (0001) was chosen as a growth surface. Thermal stability

and transparency of the sapphire substrate allow creating thermally stable elements and investigation of (Ga,Mn)N layers using optical spectroscopy methods. There is a considerable mismatch between the sapphire and GaN crystal structures [4], therefore a GaN buffer layer was grown by metal-organic chemical vapor deposition (MOCVD) on the sapphire substrate to relax this mismatch. The thickness of the buffer layer is approximately 3 micron. A thin MBE buffer layer (20 nm) was further grown on the MOCVD layer to create first high quality mono-layers. Finally, the "active" (Ga,Mn)N layer was grown by molecular beam epitaxy. The thickness of the (Ga,Mn)N layer is approximately 200 nm. The structure of (Ga,Mn)N samples is shown in fig. 1.1.

The manganese content in the (Ga,Mn)N layers was measured by secondary emission mass spectroscopy (SIMS). The presence of any secondary phase was checked *in situ* by reflection high-energy diffraction (RHEED) and *ex situ* by x-ray diffraction (XRD) measurements. The XRD measurements were performed using the Seifert 3003 PTS-HR system. A beam concentrator in front of the two-bounce Ge (220) monochromator and a soller slit of 0.15 degrees aperture inserted in front of the detector were used in the measurements (E. Bellet-Amalric in [3,5]). The wavelength of x-ray light was 0.154 nm. During the measurements the (Ga,Mn)N samples were fixed on a 2 degrees vicinal Si monocrystal in order to reduce the background. Achieved large dynamic range (10^6) allows detecting possible inclusions in a very small amount. For example, the secondary phase $GaMn_3N$ was detected in a $Ga_{1-x}Mn_xN$ sample with $x=0.00007$). Therefore the XRD measurements allow detecting inclusions of such a small concentration.

Special attention was paid to different growth regimes. It was shown that the highest concentration of Mn in GaN can be incorporated using the nitrogen-rich regime (growth regime in excess of nitrogen) [2]. Under optimal conditions, pure wurtzite $Ga_{1-x}Mn_xN$ layers with Mn content x up to 5.7% were obtained; additional inclusions like $GaMn_3N$ or Mn_4N clusters were not detected.

1.2 X-ray absorption spectroscopy

X-ray absorption spectroscopy is a very powerful investigation method of solid state physics which is used to study the structural, electronic and magnetic properties of materials. An x-ray photon can be absorbed by a core electron of an atom. The excited photoelectron moves to an empty state above the Fermi level. The probability of the transition depends on the energy of the absorbed photon. The absorption probability as a function of the photon energy (x-ray absorption spectrum) can be related to empty electronic states in the solid. Intense electronic transitions fulfill the dipole selection rules: the orbital and total moments of initial and final states change according to the relations $\Delta l = \pm 1$, $\Delta j = 0, \pm 1$. Quadrupole transitions are less intensive and in this case the orbital and total moments of initial and final states are related by the quadrupole selection rules: $\Delta l = 0, \pm 2$ and $\Delta j = 0, \pm 1, \pm 2$. If the excited core level has the principal number $n=1$ the corresponding x-ray absorption spectrum is called K-spectrum; if $n=2$ then absorption spectrum is called L-spectrum [6].

X-ray absorption spectroscopy methods have a number of important advantages as compared to other methods. First of all, there is only one initial state of the excited electron, i.e. a localized core state (in optical spectra we have several initial states). That is why the x-ray absorption spectrum of a solid can be directly related to electronic states above the Fermi level. In addition, the dipole selection rules allow a separate investigation of electronic states of different symmetries. Another important advantage of x-ray absorption spectroscopy it is the element selectivity. Energy positions of absorption edges of different atoms are very different. Therefore electronic states of each element in a complex alloy can be studied separately. These two advantages allow a very detailed study of structural and electronic properties of solids.

However there is a serious drawback that limits the possibilities of the x-ray absorption spectroscopy: it is limited resolution of the x-ray absorption spectra. The resolution is determined by natural widths (lifetimes) of initial and final states, and by resolution of the monochromator. While the resolution of the monochromator in principle can be chosen sufficiently small, the natural width of the core level can not be changed. For example the natural width of 1s level in Mn is 1.16 eV. Therefore the band structure of Mn compounds can not be studied with a higher precision than 1.16 eV using the K-edge absorption spectra of

Mn. Usually the natural width of shallow core levels is smaller. Therefore the soft x-ray radiation allows a more precise study of the electronic states.

X-ray absorption measurements can be performed using three main devices: x-ray radiation source, optical system and detector. Synchrotron can be used as a source of x-ray radiation. It allows obtaining a very intense x-ray light that is necessary to investigate diluted compounds like the diluted magnetic semiconductors. There are two main functions of the optical system. The first function is to concentrate as much as possible of x-ray radiation in a narrow beam. It is quite difficult to manipulate x-ray light because of lack of materials with necessary properties in the x-ray energy region [7]. The second function of the optical system is to pick out radiation with a fixed energy and the intensity of the obtained monochromatic light should not be too weak. The experimental equipment which is intended to perform these two functions is called the beamline. A scheme of a typical beamline at the European Synchrotron Radiation Facility (ESRF, Grenoble) is shown in fig. 1.2.
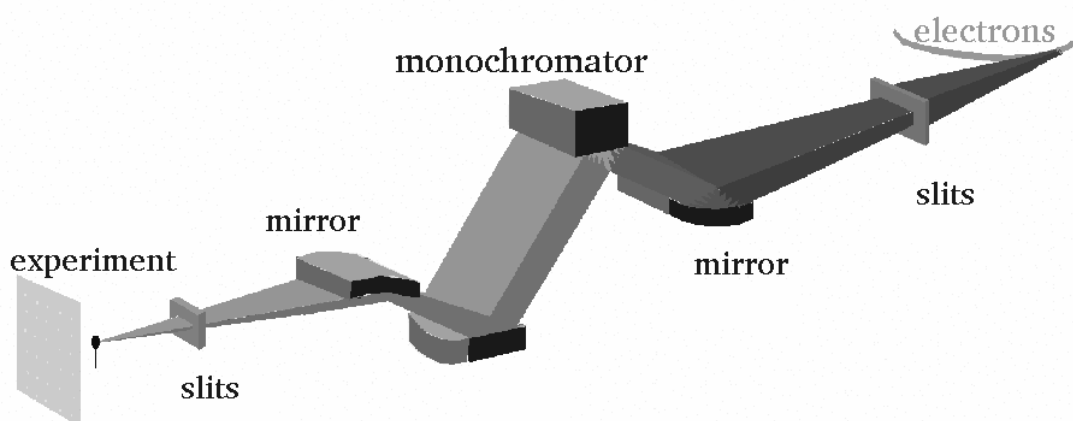
Fig. 1.2. Main elements of a typical beamline at the European Synchrotron (ESRF) in Grenoble [8].

The synchrotron beam is formed by the horizontal and vertical slits which are placed just on the entry of the beamline. The slits pick out a parallel beam which will be further transformed by the optical system. The acceptance angle should be sufficiently small because it is quite difficult to transform a very diverging beam into a parallel one. At the same time a too small acceptance angle will lead to a weak intensity of the beam. Therefore a compromise between the energy resolution (which is related to the beam divergence) and the intensity of the beam should be found. In the beamline BM30B the acceptance angle is about 2 mrad [9].

The x-ray beam is further transformed by the first mirror. This mirror transforms the diverging beam into a parallel beam before it enters in the monochromator. This transformation is necessary to obtain the highest possible energy resolution of the beam after all transformations. The second important role of the mirror is to suppress higher harmonics in the initial beam. It is clear that this mirror dissipates a high amount of heat. Therefore the material of the mirror should be stable at high temperature. In order to decrease the heating, a small incidence angle is used and the mirror is coated by a heavy metal to increase the reflectivity coefficient. In addition the first mirror supplied by a cooling system. Polished Si monocrystals coated with rhodium are used as mirrors at the beamline BM30B [9].

Two Si monocrystals with the active surface (220) are used in the monochromator at the beamline BM30B. The monocrystals of Si are stable at high temperature and at high radiation level. The plane (220) allows obtaining a good resolution (~0.45 eV) at energy 6539 eV (K-egde of Mn). The first Si monocrystal dissipates a high amount of energy. Therefore it is provided by a cooling system.

The obtained monochromatic beam is further focused by two mirrors on a small point (250×250 µm² in BM30B beamline) to obtain the highest possible intensity of photons with the chosen energy. Such a high intensity is necessary to study diluted materials where the "useful" signal may be very weak.

1.3 X-ray absorption spectra of (Ga,Mn)N

The K-edge x-ray absorption spectra of Mn in $Ga_{1-x}Mn_xN$ (x=0.003–0.057) were recorded at the European Synchrotron Radiation Facility (ESRF, Grenoble) at the beamline BM30B. The measurements were organized by X. Biquard [10] and I had an opportunity to participate in these measurements. The x-ray absorption measurements were performed at the K-edge of Mn (6539 eV) in fluorescence mode: the $1s$ hole of Mn created by an x-ray photon is filled by a $2p$ electron of Mn. This transition $2p{\rightarrow}1s$ causes an emission of another photon (fluorescence, K_α lines); number of the emitted photons equals to number of excited $1s$ electrons. The energy dependence of the fluorescence from the two K_α lines of Mn was

measured during the x-ray absorption experiments. This method is very efficient when the "useful" signal of Mn is only a small part of the total absorption. Such a situation is usual in diluted systems.

The achieved energy resolution of the x-ray beam was ~0.45 eV, such a good resolution is necessary to study the band structure of semiconductors. As it was mentioned above, the final resolution of x-ray absorption spectra is limited by the natural width of the excited core level. In our case of Mn the natural width of the $1s$ level is 1.16 eV, therefore this is the fundamental limit for the energy resolution of x-ray absorption spectra. However this resolution is sufficient to distinguish main features in the band structure of (Ga,Mn)N. The incidence angle of the beam was kept 30°±10° with respect to the sample surface. Bragg diffraction peaks from the sample saturate detectors; therefore only signals from the unsaturated fluorescence detectors were included in final x-ray absorption spectra.

There are two different parts in the K-edge absorption spectrum. The first part is the Extended X-ray Absorption Fine Structure (EXAFS). This part is situated above E_{edge}+30 eV (E_{edge} is the absorption edge energy, energy position where the absorption coefficient achieves 50% of its maximum value). In this energy region the excited photoelectron has a high kinetic energy. So the electron wave function is strongly dispersed by nearest neighbor atoms of Mn. The dispersion of the wave function caused by the crystal potential is not so strong. That is why this part of the x-ray absorption spectrum is very useful to identify the local atomic structure around the atom-absorber. The local atomic structure of the atom-absorber depends on the position of the atom in crystal; therefore the position of the atom-absorber in the crystals can be determined from a simulation of the EXAFS spectrum. The EXAFS spectrum can be simulated using the multiple-scattering approach: only crystal structure around the atom-absorber is used to simulate the EXAFS part, the particular form of the crystal potential is not taken into account. This simulation can be done using the FEFF code [11]; efficiency of the code was confirmed by numerous simulations of experimental spectra. A simulation of the measured EXAFS spectra of Mn in $Ga_{1-x}Mn_xN$ (x=0.003–0.057) demonstrated that the Mn atoms substitute the Ga atoms in the (Ga,Mn)N samples [10].

Another part of the x-ray absorption spectrum (under E_{edge}+30 eV) is called the X-ray Absorption Near-Edge Structure (XANES) and it contains information about the electronic structure of the crystal: the shape of the XANES is essentially determined by the density of states above the Fermi level. Because the density of states depends on the local atomic

structure around the atom-absorber, the shape of the XANES is sensible to the local crystal structure. In addition the XANES spectra allow studying the electronic state of the atom-absorber. As we will see late a more distant crystal structure can be also studied using the XANES spectra. However interpretation of the XANES is not as straightforward as it was in the case of the EXAFS: a calculation of the band structure of the crystal is necessary to extract quantitative information from the XANES spectra.

The XANES part of K-edge absorption spectra of Mn in $Ga_{1-x}Mn_xN$ (x=0.003–0.057) is shown in fig. 1.3. The shape of the spectra does not depend on the Mn content in (Ga,Mn)N. Therefore the Mn atoms have the same valence and local crystal structure in all the samples. It is quite difficult to obtain more information from the spectra using such a simple reasoning. *Ab-initio* calculation methods described in the chapter II will be used to determine the valence state of Mn in (Ga,Mn)N from the XANES spectra. In addition the shape of the XANES spectra points to a homogeneous distribution of Mn in (Ga,Mn)N. These questions will be discussed in the chapter III in detail.
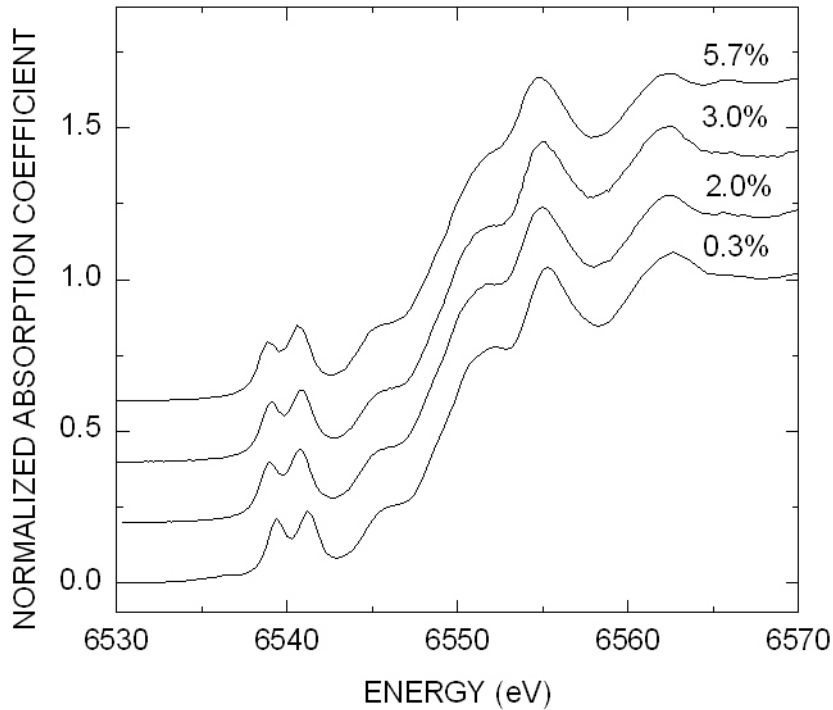
Fig. 1.3. Normalized K-edge x-ray absorption spectra of Mn in $Ga_{1-x}Mn_xN$ (x=0.003–0.057), near-edge structure is shown. The Mn content is indicated in the figure. The x-ray absorption spectra were recorded by X. Biquard et al. [10].

Summary for chapter I

The $Ga_{1-x}Mn_xN$ epilayers were grown by molecular beam epitaxy on a sapphire substrate [2]. The wurtzite structure of the layers was confirmed by x-ray diffraction measurements. Special growth conditions are necessary to avoid formation of Mn-rich clusters. At optimal growth conditions (N-rich mode, Mn/Ga flux ration less than 15%) samples having a Mn content up to $x=0.057$ were obtained. The x-ray diffraction measurements show that the samples do not contain precipitations like $GaMn_3N$ and Mn_4N.

Structural and electronic properties of the samples were studied using the x-ray absorption spectroscopy. This method allows a separate investigation of local atomic structure around different atoms in complex compounds. In addition the electronic states of different symmetries can be studied separately by appropriate choice of the absorption edge (K-edge for empty p states and L-edge for empty d states). However the natural width of excited core level limits the accuracy of the investigation: only well separated electronic states can be distinguished in x-ray absorption spectrum.

The K-edge x-ray absorption spectra of Mn in (Ga,Mn)N epilayers were recorded at the European Synchrotron Radiation Facility in Grenoble [10]. The achieved resolution of the monochromator was ~0.45 eV. A simulation of the part EXAFS of the spectra confirmed the substitutional position of Mn in the (Ga,Mn)N epilayers [10]. The shape of the XANES spectra (edge region of the absorption spectra) does not depend on the concentration of Mn. This implies the same valence state and local atomic structure around the Mn atoms. However additional calculations are necessary to identify the valence state of Mn in the samples. The calculations will be presented in the chapter III. As we will see late the distribution of Mn in (Ga,Mn)N can be studied using the XANES spectra.

Chapitre II. Calcul de la structure de bandes

Des méthodes de calcul *ab-initio* sont décrites dans ce chapitre. Des calculs de ce type permettent de prédire des propriétés électroniques différentes des matériaux, et en principe aucune information expérimentale n'est nécessaire pour effectuer ces calculs. La théorie de la fonctionnelle de densité permet de simplifier fortement le problème: l'équation multiélectronique de Schrödinger peut être transformée à une autre équation pour un électron dans un champ effectif. Et cette dernière équation peut être résolue à l'aide des ordinateurs modernes. C'est pourquoi les calculs *ab-initio* sont devenus aujourd'hui très populaire dans le monde scientifique.

Deux méthodes *ab-initio* ont été utilisées pour calculer la structure de bandes des semiconducteurs: LAPW et LMTO. Ces méthodes sont très efficaces (elles sont linaires) et assez précises. Des cristaux avec plusieurs centaines d'atomes par une maille élémentaire peuvent être calculer assez facilement par ces deux méthodes. Les méthodes LAPW et LMTO sont donc décrites en détail dans ce chapitre.

Chapter II. Band structure calculations

The aim of this chapter is to describe the basic principles of *ab-initio* band structure calculations. Such calculations allow us to investigate and to predict different electronic properties of solids. Progress in computer technology made it possible to investigate atomic systems which contain several hundred atoms. That is why the *ab-initio* calculations became so popular in the scientific community and they are widely used as a complimentary component of experimental investigations.

Ab-initio methods allow us to calculate different properties of a crystal and to do that one does not need any experimental parameter of the crystal, therefore the band structure and other properties of a crystal can be investigated without synthesizing the crystal. This particularity of *ab-initio* methods allows us to predict the properties of a material and to estimate the benefit of the material for future applications.

The electronic structure of a crystal (eigenfunctions and eigenvalues of energy) can be calculated using a multi-particle Hamiltonian in the Schrödinger equation [1]:

$$\mathbf{H} = -\frac{\hbar^2}{2}\sum_i \frac{\nabla_i^2}{m_e} - \frac{\hbar^2}{2}\sum_i \frac{\nabla_i^2}{M_i} - \frac{1}{4\pi\varepsilon_0}\sum_{i,j}\frac{e^2 Z_i}{\left|\mathbf{R}_i - \mathbf{r}_j\right|} + \frac{1}{8\pi\varepsilon_0}\sum_{i\neq j}\frac{e^2}{\left|\mathbf{r}_i - \mathbf{r}_j\right|} + \frac{1}{8\pi\varepsilon_0}\sum_{i\neq j}\frac{e^2}{\left|\mathbf{R}_i - \mathbf{R}_j\right|}, \quad (2.1)$$

here M_i is the mass of the nucleus at point $\mathbf{R}_i$, m_e is the mass of a free electron at point $\mathbf{r}_i$. The first two terms are kinetic energy operators for electrons and nuclei, respectively. The last three terms describe electrons-nuclei, electrons-electrons and nuclei-nuclei Coulomb interactions. Today it is not possible to solve the Schrödinger equation containing this Hamilton operator for several hundred particles. Therefore no exact solution of the problem can be found. However we do not need an exact solution of quantum mechanical problems to perform a comparison between theoretical predictions and available experimental data because the experimental data always contain an error and an acceptable error of our

calculation can be of the same order as the experimental error. Therefore some approximations can be accepted to simplify the problem of band structure calculation.

First of all, the positions of the nuclei will be fixed (Born-Oppenheimer approximation). This allows us to reduce the problem to a simpler one: motion of electrons in an external field of the nuclei. This problem is still complicated because the Schrödinger equation should be solved for several hundred electrons. Therefore further simplifications are necessary.

The next approximation was proposed by Hohenberg, Kohn and Sham in [2,3]. According to this approach the ground state of an electronic system can be described by an electron density functional of $E[\rho]$. The exact form of the functional is still unknown, but there are good approximations for the functional for different electronic systems [4]. This approach allows us to replace the multi-particle Schrödinger equation by a single-particle equation where an external effective field describes the interaction between electrons.

2.1 Electron density functional

According to the electron density functional theory all properties of the ground state of an electron system can be described by the electron density functional. The electron density functional can be written in this form [4]:

$$E[\rho] = \int d\mathbf{r}\rho(\mathbf{r})V_{ext}(\mathbf{r}) + \frac{1}{8\pi\varepsilon_0}\iint d\mathbf{r}d\mathbf{r}'\frac{\rho(\mathbf{r})\rho(\mathbf{r}')}{|\mathbf{r}-\mathbf{r}'|} + G[\rho], \qquad (2.2)$$

here V_{ext} is an external field which includes the electric field of nuclei, functional $G[\rho]$ includes the kinetic and exchange-correlation energy of electrons. The ground state of an electron system can be found by minimization the electron density functional and the total energy of the ground state is the minimum of the electron density functional. It was proposed that the $G[\rho]$ functional can be rewritten in the form:

$$G[\rho] = T[\rho] + V_{xc}[\rho].$$

(2.3)

The functional $T[\rho]$ is the kinetic energy of non-interacting electrons and the functional $V_{xc}[\rho]$ takes into account exchange interaction between electrons and correlation effects. The electron density can be presented as a sum of squared wave functions of electrons:

$$\rho(\mathbf{r}) = e\sum_{i=1}^{N}|\varphi_i(\mathbf{r})|^2,$$

(2.4)

N is the number of electrons. Minimization of the functional (2.2) using the new variables φ_i leads to one-particle Kohn-Sham equations [1,4]:

$$\left[-\frac{\hbar^2}{2m_e}\nabla^2 + \frac{1}{4\pi\varepsilon_0}\int\frac{\rho(\mathbf{r'})}{|\mathbf{r}-\mathbf{r'}|}d\mathbf{r'} + V_{ext}(\mathbf{r}) + V_{xc}(\mathbf{r})\right]\varphi_i = \varepsilon_i\varphi_i,$$

(2.5)

where ε_i are Lagrange coefficients used for the minimization of the functional (2.2), the exchange-correlation is given by the functional derivative [1]:

$$V_{xc} = \frac{\delta V_{xc}[\rho]}{\delta\rho}.$$

(2.6)

Thus to calculate the band structure of a crystal we have to solve a set of Schrödinger equations for one-particle wave functions φ_i. This problem is much simpler than the initial one (2.1). However the problem is still difficult. First of all the Hamiltonian in equation (2.5) contains the electron wave functions φ_i (they are present as the electron density) that we want to find. Therefore several iterations are necessary to find a self-consistent solution of the Schrödinger equations. Secondly, we can find a solution of the equations (2.5) if the form of the exchange-correlation potential V_{xc} is known. Therefore, constructing the exchange-correlation potential is the main problem of the electron density functional theory. Actually the exact form of the potential is not known. However several good approximations for the exchange-correlation potential were found during the last decades.

The most popular approximation of the exchange-correlation potential is the Local Density Approximation (LDA). According to this approximation, the exchange-correlation energy can be calculated using the formula [1]:

$$E_{xc}^{LDA} = \int \rho(\mathbf{r})\varepsilon(\rho(\mathbf{r}))d\mathbf{r}, \tag{2.7}$$

where $\varepsilon(\rho)$ is the exchange-correlation function for a homogeneous electron gas (this function is numerically known). The exchange-correlation energy due to a particular density $\rho(\mathbf{r})$ could be found by dividing the material in infinitesimally small volumes with a constant density. Each such volume contributes to the total exchange correlation energy by an amount equal to the exchange correlation energy of an identical volume filled with a homogeneous electron gas [1]. It is expected that this approximation should be sufficiently good in electron systems where the electron density $\rho(\mathbf{r})$ changes slowly. Numerous practical calculations show that the local density approximation allows us to obtain good calculation results for different materials. The properties of magnetic materials can be calculated using a modification of the LDA approximation, which is called Local Spin-Density Approximation (LSDA) [4]:

$$E_{xc}^{LSDA} = \int \rho(\mathbf{r})\varepsilon(\rho^{\uparrow}(\mathbf{r}), \rho^{\downarrow}(\mathbf{r}))d\mathbf{r}. \tag{2.8}$$

The local density approximation can be improved if we take into account not only the electron density in the infinitesimal volume where we calculate the exchange energy, but also the electron density in neighbor volumes. This approach allows a better estimation of the exchange-correlation energy in systems where the electron density $\rho(\mathbf{r})$ changes rapidly. The calculation scheme mentioned above is realized in the Generalized Gradient Approximation (GGA).

Very often the crystal potential (last three terms in Hamiltonian in (2.5)) is represented by a superposition of the potentials of the atoms:

$$V^{cryst}(\mathbf{r}) = \sum_i V_i^{atom}(\mathbf{r} - \mathbf{R}_i), \tag{2.9}$$

$\mathbf{R}_i$ is the position of *i*-th atom, the atomic potential V_i^{atom} is obtained as a result of the self-consistent calculation. Usually the symmetry of the potential is quite complicated and further simplifications are necessary for practical calculations. There are two main approximations for the crystal potential: the Muffin-Tin (MT) and Atomic Sphere (AS) approximations. According to the MT-approximation, all atoms in a crystal are placed in non-overlapping MT-spheres. Therefore the crystal space is divided into two different parts: crystal space in the MT-spheres and interstitial space out of the spheres. The crystal potential in MT-spheres is atomic-like and it changes rapidly with distance from the atomic nucleus. In contrast, in the interstitial part the crystal potential practically does not change. According to this, the crystal potential can be chosen as a constant V_c in the interstitial part and as a spherically symmetric function in the MT-spheres [4]:

$$V(\mathbf{r}) = \begin{cases} V(|\mathbf{r}|), r < R_{MT} \\ V_c, \quad r > R_{MT} \end{cases} \tag{2.10}$$

The MT-approximation considerably simplifies calculation of band structure and it is widely used in practice. Within the AS approximation, overlapping atomic spheres are used and the total volume of the spheres should be equal to the volume of the crystal. Therefore there is no interstitial space in this case and the problem of band structure calculation become again simpler. There are however calculation methods (full potential methods) where no particular shape of the potential is imposed. In this case the crystal potential is represented by the following form [5]:

$$V(\mathbf{r}) = \begin{cases} \sum_{L,M} V_{LM}(r) Y_{LM}(\mathbf{r}), r < R_{MT} \\ \sum_{\mathbf{K}} V_{\mathbf{K}} e^{i\mathbf{K}\mathbf{r}}, \quad r > R_{MT} \end{cases} . \tag{2.11}$$

Now after all the simplifications the equation (2.5) can be solved for a large number of electrons. The procedure can be divided into two steps: solution of the Schrödinger equation (2.5) for a given crystal potential, and construction of the potential.

As we know, the initial multi-particle Schrödinger equation (2.1) can be reduced to a set of simplified one-particle equations with the following form [4]:

$$\left[-\frac{\hbar^2}{2m_e}\nabla^2 + V(\mathbf{r})\right]\Psi(\mathbf{r}) = E\Psi(\mathbf{r}),\qquad(2.12)$$

where $V(\mathbf{r})$ is a periodic crystal potential. There is a general approach which is used in most computational methods to solve equation (2.12). According to this approach, the one particle wave function $\Psi(\mathbf{r})$ is represented as a linear combination of basis functions $\varphi_j(\mathbf{r})$:

$$\Psi(\mathbf{r}) = \sum_j C_j\varphi_j(\mathbf{r}).\qquad(2.13)$$

Then, the wave function (2.13) is substituted into (2.12), the obtained equation is multiplied by $\varphi_i{}^*(\mathbf{r})$, and integration in the real space is performed [4]:

$$\sum_{j=1}^{N} C_j(H_{ij} - EO_{ij}) = 0,\quad j=1..N,\qquad(2.14)$$

where N is the number of basis wave functions, H_{ij} and O_{ij} are matrix elements:

$$\begin{aligned} H_{ij} &= \int \varphi_i^*(\mathbf{r})H\varphi_j(\mathbf{r})d\mathbf{r} \\ O_{ij} &= \int \varphi_i^*(\mathbf{r})\varphi_j(\mathbf{r})d\mathbf{r} \end{aligned},\qquad(2.15)$$

here H is the Hamiltonian in equation (2.12). The eigenvalues of energy $E(\mathbf{k})$ are roots of the secular equation

$$\det\left\|H_{ij} - EO_{ij}\right\| = 0.\qquad(2.16)$$

Actually, different computation methods differ by the choice of the basis wave functions. And a computation method will be more efficient if the basis functions are closer to the real electron wave functions in the investigated material. There are two extreme cases: electrons are free in a crystal, or they are strongly localized near atoms. In the first case (which is

realized in metals) the wave functions of quasi-free electrons is represented as a linear combination of plane waves. This method permits to obtain good computation results for valence electrons in metals. However a too large set of plane waves is necessary to describe localized valence orbitals in insulators and semiconductors. In the second case (electron wave functions are localized) the wave functions are expanded in atomic-like orbitals near each atom in the crystal. This method is very efficient for insulators and it was realized for example in the Tight-Binding Local Muffin-Tin Orbital method (TB-LMTO [6]).

There are however some "universal" methods that allows us to calculate the band structure of both metals and insulators. These methods have advantages of the two extreme approaches: localized electron wave functions near atomic nuclei are expanded in atomic-like orbitals, but free-like parts of the same wave functions in the interstitial space are represented as sums of plane waves. In this case we do not need a large number of plane waves to construct the electronic wave function near the nuclei. The method is realized in the Augmented Plane Wave + Local Orbitals (APW+lo) program [7]. In the next three sections, I will describe briefly the peculiarities of the basis functions in the APW, in its linear modification LAPW, and in the TB-LMTO methods.

2.2 Augmented Plane Wave Method (APW)

According to the muffin-tin approximation the crystal space is divided into two parts: inside MT-spheres (S_α for the αth atom) and out of the spheres (I – interstitial part). The electron wave function is expanded in different basis functions in these two parts. The electron wave function changes rapidly near atomic nuclei, therefore it is quite natural to use a solution of the Schrödinger equation for a free atom to represent the wave function in the MT-spheres. In the interstitial part of crystal electrons are quasi-free, and the electronic wave function can be well represented by a set of plane waves. Thus the basis functions have the following form [1]:

$$\varphi_{\mathbf{K}}^{\mathbf{k}}(\mathbf{r}, E) = \begin{cases} \dfrac{1}{\sqrt{V}} \exp[i(\mathbf{k} + \mathbf{K})\mathbf{r}], & \mathbf{r} \in I \\ \displaystyle\sum_{l,m} A_{l,m}^{\alpha,\mathbf{k}+\mathbf{K}} u_l^{\alpha}(r', E) Y_{l,m}(\mathbf{r}'), & \mathbf{r} \in S_{\alpha} \end{cases}, \tag{2.17}$$

where V is crystal volume, $\mathbf{K}$ is a translation vector in the reciprocal space, $Y_{l,m}$ are spherical functions, u_l^{α} is radial solution of the Schrödinger equation for a free atom,

$$\mathbf{r}' = \mathbf{r} - \mathbf{r}_{\alpha}. \tag{2.18}$$

The A coefficients in (2.17) can be determined if we impose the condition of continuity of the basis functions on the MT-spheres.

2.3 Linear Augmented Plane Wave Method (LAPW)

Now we can use the basis functions defined in (2.17) to obtain the matrix elements in (2.15). In this case the matrix elements will depend on the eigenvalues of the Hamiltonian which we try to find in (2.16). Therefore, equation (2.16) should be solved iteratively, and this forces us calculate the determinant (2.16) 100-200 times at the same $\mathbf{k}$-point. However this energy dependence of the determinant can be eliminated if we expand the radial part of the basis functions in Taylor series near a fixed energy E_0 [1]:

$$u_l^{\alpha}(r', \varepsilon_{\mathbf{k}}^n) = u_l^{\alpha}(r', E_0) + (E_0 - \varepsilon_{\mathbf{k}}^n)\dot{u}_l^{\alpha}(r', E_0) + O(E_0 - \varepsilon_{\mathbf{k}}^n)^2, \tag{2.19}$$

where $\varepsilon_{\mathbf{k}}^n$ is the eigenvalues that we want to find, and the derivative of u_l^{α} function is calculated at the fixed energy E_0. The difference $E_0 - \varepsilon_{\mathbf{k}}^n$ is not known; therefore we can replace it by a coefficient B:

$$\varphi_{\mathbf{K}}^{\mathbf{k}}(\mathbf{r},E) = \begin{cases} \dfrac{1}{\sqrt{V}}\exp[i(\mathbf{k}+\mathbf{K})\mathbf{r}], & \mathbf{r}\in I \\[2mm] \sum\limits_{l,m}\Big[A_{l,m}^{\alpha,\mathbf{k}+\mathbf{K}}u_l^\alpha(r',E_0)+B_{l,m}^{\alpha,\mathbf{k}+\mathbf{K}}\dot{u}_l^\alpha(r',E_0)\Big]Y_{l,m}(\mathbf{r}'), & \mathbf{r}\in S_\alpha \end{cases}. \tag{2.20}$$

Now there are two undetermined coefficients and they can be found if we impose the condition of continuity for the u function and its derivative on MT-spheres.

The smaller difference $E_0-\varepsilon_{\mathbf{k}}^{n}$, the better the precision of the linearization. Therefore the energy E_0 should be as close as possible to the eigenvalue $\varepsilon_{\mathbf{k}}^{n}$. Different atomic orbitals have different energy positions. It would reasonable to take different linearization energies for different orbital. Therefore the basis functions of the LAPW method can be represented in the following form [1]:

$$\varphi_{\mathbf{K}}^{\mathbf{k}}(\mathbf{r},E) = \begin{cases} \dfrac{1}{\sqrt{V}}\exp[i(\mathbf{k}+\mathbf{K})\mathbf{r}], & \mathbf{r}\in I \\[2mm] \sum\limits_{l,m}\Big[A_{l,m}^{\alpha,\mathbf{k}+\mathbf{K}}u_l^\alpha(r',E_l^\alpha)+B_{l,m}^{\alpha,\mathbf{k}+\mathbf{K}}\dot{u}_l^\alpha(r',E_l^\alpha)\Big]Y_{l,m}(\mathbf{r}'), & \mathbf{r}\in S_\alpha \end{cases}. \tag{2.21}$$

The LAPW method was realized in the WIEN2k code [7]. In addition the crystal potential in MT-spheres was represented according to formula (2.11), therefore there is no imposed restriction to the shape of the potential and this method refers to the full-potential approach.

2.4 Linear Muffin-Tin Orbital Method (LMTO)

The LMTO method can be realized using the MT- as well as the AS-approximations. However numerous calculations shows that the AS-approximation in general leads to a better agreement between experimental data and calculated electronic properties.

Let us consider a crystal which contains one atom per primitive cell. Now we put the atom in an atomic sphere which an atomic sphere which volume equals the volume of the primitive cell. The crystal potential in the atomic sphere is supposed to be spherically symmetric. At the same time the potential is constant out of the sphere (V_0) and we suppose

that the difference $E - V_0$ is 0 out of the atomic sphere [8]. In this case we have the Schrödinger equation which contains a symmetric potential inside the sphere; electron function should be solution of Laplace equation out of the sphere [4]:

$$\nabla^2 \Psi = 0. \tag{2.22}$$

The radial solution of the equation (2.22) is $\Psi = a_l r^l + b_l r^{-l-1}$. Therefore the radial part of basis functions in the LMTO method can be represented as [4]:

$$\Phi_l(r,E) = \begin{cases} u_l(r,E), & r \leq S \\ \left[\dfrac{D_l + l + 1}{2l+1}\left(\dfrac{r}{S}\right)^l + \dfrac{l - D_l}{2l+1}\left(\dfrac{r}{S}\right)^{-l-1} \right] u_l(S,E), & r > S \end{cases}, \tag{2.23}$$

where u_l is the radial solution of the Schrödinger equation in the atomic sphere (S is the radius of the atomic sphere), D_l is the radial derivative

$$D_l = \frac{S u_l'(S)}{u_l(S)}. \tag{2.24}$$

The basis functions (2.23) contain a divergent part which is proportional to $(r/S)^l$. Therefore the divergent part should be subtracted from the functions to construct local basis orbitals Ψ_l. The Bloch sum of the obtained local orbitals should be constructed to take into account contribution of neighbor atoms in the chosen atomic sphere. This sum can be used as basis functions of the LMTO method [4]:

$$\varphi_{l,m}^{\mathbf{k}}(\mathbf{r},D) = \sum_{\mathbf{R}_s} e^{i\mathbf{k}\mathbf{R}_s} i^l Y_{l,m} \Psi_l(r,D). \tag{2.25}$$

The obtained muffin-tin orbitals are energy dependent and the matrix elements in (2.15) will also energy dependent. Therefore a large number of iterations are necessary to solve the equation (2.16). Linearization of the MT-orbitals permits to increase the efficiency of the method. The LMTO approach was realized in the TB-LMTO (ASA) code [6].

The Wien2k code (LAPW method) [7] will be used in the next chapter to calculate the band structure of (Ga,Mn)N, (Ga,Mn)As and (Ge,Mn). The same code will be also used to calculate the x-ray absorption spectra of Mn in (Ga,Mn)N. An additional calculation of the band structure of $Ge_{1-x}Mn_x$ (x=0.0156) will be performed using the TB-LMTO (ASA) code [6]: this code is very efficient and it allows calculating very large supercells with a great number of atoms. Such large supercells are necessary to calculate properties of crystals with low concentrations of impurities.

Chapitre III. Propriétés électroniques de (Ga,Mn)N, (Ga,Mn)As et (Ge,Mn)

La structure de bandes de (Ga,Mn)N a été calculée dans cette chapitre. En effet les propriétés magnétiques des semiconducteurs magnétiques dilués sont liées à leurs propriétés électroniques. Les résultats de ce chapitre seront donc utiliser dans la chapitre IV pour expliquer un ferromagnétisme à basse température que nous observons dans (Ga,Mn)N. La distribution du Mn dans (Ga,Mn)N est un autre facteur important qui influence fortement sur les propriétés magnétiques. C'est pourquoi ce problème a été également étudié en détail. En outre, la structure électroniques de (Ga,Mn)As et (Ge,Mn) ont été calculée. En effet, les propriétés de (Ga,Mn)As sont déjà bien connues et de nombreux résultats expérimentaux et théoriques sont disponibles. Dans ce travail nous utilisons (Ga,Mn)As comme une référence pour profiter de ces nombreux résultats. Le semiconducteur (Ge,Mn) est un autre matériau qui peut trouver de nombreux applications en électronique de spin: d'une part, la technologie de croissance du germanium est bien développée et d'autre part, des propriétés ferromagnétiques de (Ge,Mn) à température élevée ($T_C \sim 285K$) ont été observées. Dans ce travail la structure de bande de (Ge,Mn) a été calculée pour déterminer l'état électronique du Mn dans (Ge,Mn).

Une information expérimentale sur les propriétés électroniques de ces semiconducteurs a été obtenue a partir des spectres d'absorption des rayons X et des mesures de transport électrique. Une interprétation de la partie XANES de ces spectres a été proposée. Elle permet d'étudier l'état électronique et la distribution du Mn dans (Ga,Mn)N. Pourtant, la précision de cette méthode est limitée par la largeur naturelle du niveau $1s$ du Mn. La spectroscopie optique permet une étude beaucoup plus précise de la structure de bande parce que la résolution du monochromateur peut être moins que 0,5 eV. Une étude de l'état électronique et de la distribution du Mn dans (Ga,Mn)N par spectroscopie optique est décrite brièvement dans ce chapitre ce qui permet de mettre en évidence des avantages de ces deux spectroscopies.

Chapter III.   Electronic   properties   of (Ga,Mn)N, (Ga,Mn)As and (Ge,Mn)

Electronic properties of (Ga,Mn)N, (Ga,Mn)As and (Ge,Mn) semiconductors are studied in this chapter. The results of this study will be further used to explain their magnetic properties. Actually the magnetic properties are closely related to the electronic structure; therefore a detailed investigation of the electronic properties is necessary in order to clarify observable magnetic phenomena in the diluted magnetic semiconductors. The specific distribution of magnetic impurity in diluted magnetic semiconductor is another important factor that significantly changes magnetic interaction between the atoms of the magnetic impurity. That is why a considerable attention was paid to the problem of Mn distribution in this chapter.

The present work is essentially devoted to investigation of (Ga,Mn)N semiconductor. In addition, (Ga,Mn)As and (Ge,Mn) diluted magnetic semiconductors were also considered. Properties of (Ga,Mn)As are well studied today and the obtained results can be very useful in investigation of the other III-V semiconductor – (Ga,Mn)N. In addition the band structures of (Ga,Mn)As and (Ge,Mn) are similar, and properties of (Ge,Mn) can be predicted if the same properties of (Ga,Mn)As are known. The (Ge,Mn) semiconductor is less studied, but interesting magnetic properties of (Ge,Mn) were reported by several groups (see the chapter IV). Therefore a detailed study of the electronic properties of (Ge,Mn) is necessary.

The electronic properties and the distribution of Mn in the semiconductors were studied by x-ray absorption spectroscopy. As we will see later, the method allows a detailed study of the electronic and structural properties of semiconductors. However the precision of the study is limited by the natural width of the core level ($1s$ level in the K-edge spectroscopy). At the same time the optical spectroscopy allows a much more detailed investigation of the electronic structure (the resolution of optical spectra can be lower than 0.5 meV). Therefore it is very interesting to compare advantages and drawbacks of the two different methods in order to find the best ways to investigate different aspects the electronic

structure problem. With that end in view, a paragraph devoted to optical spectra modeling was included.

Two different crystal structures of (Ga,Mn)N are considered in this chapter: zinc-blende and wurtzite structures. Although the studied in this work (Ga,Mn)N samples have the wurtzite structure, a lot of calculation results for the zinc-blende (Ga,Mn)N are available today and these results are widely used in the analysis of our experimental data. The validity of application of the theoretical results obtained for the zinc-blende (Ga,Mn)N to experimental data obtained on wurtzite (Ga,Mn)N samples is discussed.

Finally some limitations of *ab-initio* calculations are considered. Actually some band structure parameters of semiconductors obtained from the *ab-initio* calculations are not confirmed by our experimental results: for example, according to our *ab-initio* calculations a high density of Mn *p* states should be present near the Fermi level in (Ga,Mn)As, however these states are not observed experimentally. Therefore the *ab-initio* calculations should not be considered as a method which replaces the experimental investigation. However the *ab-initio* description facilitates interpretation of experimental data and it provides us with additional information which can not be obtained directly from experiment.

3.1 Crystal structures of GaN
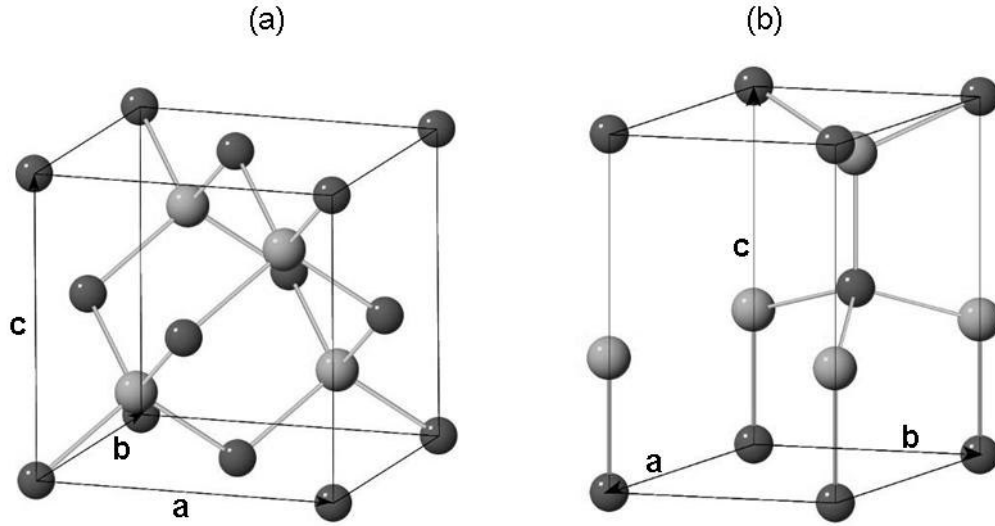
Fig. 3.1. Unit cells of (a) zinc-blende and (b) wurtzite GaN crystals. Ga and N atoms are denoted by dark and light circles respectively.

Crystals of zinc-blende GaN can be represented as a Ga and a N cubic face-centered sublattices; one of the sublattices is shifted relatively to the other one by a vector $(1/4,1/4,1/4)a_0$, where a_0 is the lattice parameter of GaN [1]. The unit cell of the zinc-blende GaN crystal is a cube (fig. 3.1a). Coordinates (x,y,z) of Ga atoms in the cube are

$$(0,0,0) \quad (0,1/2,1/2) \quad (1/2,0,1/2) \quad (1/2,1/2,0),$$

here the coordinates are represented in the basis vectors **a**, **b**, and **c** (fig. 3.1a). Coordinates of N atoms are

$$(1/4,1/4,1/4) \quad (3/4,1/4,3/4) \quad (3/4,3/4,1/4) \quad (1/4,3/4,3/4).$$

The primitive cell of zinc-blende GaN crystal is based on three vectors $\mathbf{p}_1$, $\mathbf{p}_2$ and $\mathbf{p}_3$:

$$\mathbf{p}_1=(\mathbf{a}+\mathbf{b})/2 \quad \mathbf{p}_2=(\mathbf{b}+\mathbf{c})/2 \quad \mathbf{p}_3=(\mathbf{a}+\mathbf{c})/2,$$

and the primitive cell contain only one Ga atom in the position (0,0,0) and one N atom in the position (1/4,1/4,1/4). Several band and crystal parameters of zinc-blende GaN are listed in tab. 3.1.

Tab. 3.1. Parameters of zinc-blende GaN crystals.

parameter	value	reference
band gap (eV)	3.299	[2]
lattice parameter at T=300K (Å)	4.50	[2]
crystal volume per atom (Å^3)	11.39	calculation
number of nearest neighbors for a Ga atom distance to the atoms (Å)	4 N atoms 1.95	calculation
number of second neighbors for a Ga atom distance to the atoms (Å)	12 Ga atoms 3.18	calculation

Tab. 3.2. Parameters of wurtzite GaN crystals.

parameter	value	reference
band gap (eV)	3.507	[2]
lattice parameters at T=300K (Å) a_0 (Å) c_0 (Å) u	3.189 5.185 0.375	[2]
crystal volume per atom (Å^3)	11.42	calculation
number of nearest neighbors for a Ga atom distance to the atoms (Å)	1 N 3 N 1.944 1.952	calculation
number of second neighbors for a Ga atom distance to the atoms (Å)	6 Ga 6 Ga 3.180 3.189	calculation

The primitive cell of wurtzite GaN crystals are shown in fig. 3.1b. This cell contains four atoms: two Ga atoms are placed in the positions (a,b,c)

$$(0,0,0) \qquad (1/3,2/3,1/2),$$

while two N atoms are placed in the positions

$$(0,0,u) \qquad (1/3,2/3,1/2+u),$$

here the coordinates are calculated in the basis of **a**, **b** and **c** vectors (fig. 3.1b). Parameters a_0 and c_0 of wurtzite GaN crystals are listed in the tab. 3.2. The u parameter is not the same in different wurtzite crystals, however it is always close to 0.375. The distances between a Ga atom and its nearest neighbor N atoms are not the same in wurtzite GaN. However the difference is very small (0.4%) and such a distortion does not significantly alter the tetrahedral symmetry around Ga atoms in wurtzite GaN.

3.2 (Ga,Mn)N crystals: experiment *vs* theory

Usually GaN crystallizes in the wurtzite structure (also called hexagonal GaN or α-GaN) [3]. The crystal quality of the samples is usually superior to that of the zinc-blende GaN samples. That is why all experimental results described in this work were obtained on wurtzite GaN crystals.

On the other hand zinc-blende GaN crystals (also called cubic GaN or β-GaN) are of great interest to theoretical investigation. First of all this is connected with a higher symmetry of the zinc-blende structure as compared with the wurtzite one. The number of symmetry operations which transform the unit cell of a crystal into itself is larger for cubic GaN. This implies also a higher symmetry of the Brillouin zone for zinc-blende GaN, as compared to the symmetry of the Brillouin zone for wurtzite GaN. To describe the electronic structure of a crystal we have to calculate the eigenvalues of the Hamiltonian and the eigenfunctions for a set of **k**-points in the first Brillouin zone. To do this we have to diagonalize the Hamiltonian for every **k**-point in the Brillouin zone. Actually this part of the calculation is the most time consuming one. But we can avoid a long calculation using the symmetry of a crystal: we can calculate eigenvalues only in a part of the first Brillouin zone (irreducible part of the Brillouin zone) and after it we can obtain eigenvalues of Hamiltonian in other part of the first Brillouin zone using available symmetry operations. This procedure allows us to reduce the time necessary to calculate the band structure of a crystal. The efficiency of the procedure depends on the number of symmetry operations which can be applied to the crystal. The zinc-blende

GaN crystals have higher symmetry as compared to wurtzite crystals, i.e. the zinc-blende structure is simpler from the point of view of calculation.

There is another factor which makes the zinc-blende structure more attractive for calculation. Each crystal structure has several parameters which can change from one material to other. The zinc-blende structure has only one structural parameter to be determined – the lattice parameter. In the case of the wurtzite structure we have at least three such parameters (a_0, c_0, u, see tab. 3.2). To find the real ground electronic state of our crystal we have to optimize these parameters in our model. This optimization could take much time (especially then we consider a large supercell) and the "cost" of the optimization increases very rapidly with the number of crystal structural parameters to be optimized. The two factors described here explain why the greatest part of theoretical investigations was devoted to the zinc-blende structure.

Thus there is a contradiction between experiment and theory: experimental works are mostly concentrated of the wurtzite structure, while theoretical works are often focused on the zinc-blende structure. But it seems that this contradiction is not very important when we want to describe some properties of the Mn impurity in (Ga,Mn)N which are determined by the local crystal structure. Indeed, the local atomic structures around Mn atoms in both zinc-blende and wurtzite (Ga,Mn)N are very similar: in both cases the Mn atoms have four nearest-neighbor N atoms. If we put a Mn atom in the center of a regular tetrahedron these four N atoms would be in the corners of the tetrahedron. In other words Mn atoms have tetrahedral arrangement of ligands (four atoms of N) in both zinc-blende and wurtzite (Ga,Mn)N. The Mn-N distance has the same value (1.95 Å, see tab. 3.1) for all nearest-neighbor N atoms in zinc-blende (Ga,Mn)N. At the same time this distance is slightly different for one nearest-neighbor N atom and three other nearest-neighbor N atoms (1.944 Å and 1.952 Å respectively, see tab. 3.1) in wurtzite (Ga,Mn)N. Such a distortion however does not significantly alter the tetrahedral symmetry of the Mn atoms in wurtzite (Ga,Mn)N. The second neighbors of Mn in both zinc-blende and wurtzite (Ga,Mn)N are 12 Ga atoms. Just as in the case of N atoms, we have identical Mn-Ga distances (3.18 Å, see tab. 3.1) for all 12 Ga atoms in zinc-blende (Ga,Mn)N and the distances are slightly different for 6 Ga atoms as compared with the other 6 second neighbor Ga atoms (3.180 Å and 3.189 Å respectively, see tab. 3.2).

Thus we can conclude that the local atomic structures around Mn atoms are very similar in the zinc-blende and wurtzite (Ga,Mn)N. This allows us to assume that the electronic properties of (Ga,Mn)N determined by the local atomic structure are also similar in the zinc-blende and wurtzite (Ga,Mn)N. As we will see late, x-ray absorption spectra at the K-edge of Mn and optical absorption spectra in infrared can be attributed to this type of electronic properties. For this reason I describe the electronic structures of the both zinc-blende and wurtzite (Ga,Mn)N in this chapter. The band structure of zinc-blende (Ga,Mn)N is well known today from different theoretical reports and we can use these numerous results to understand the general trends and common features for the both crystal structures. Complementary calculations for wurtzite (Ga,Mn)N were performed to compare our experimental results obtained on wurtzite samples to the most direct predictions derived from the band structure calculations. These calculations allow us to obtain new information about electronic state and distribution of Mn in (Ga,Mn)N.

3.3 Band structure of (Ga,Mn)N

Before describing some results of band structure calculations, it is worth to give some details about the method which was used to calculate electronic properties of crystals with defects. Initially the band calculation methods described in chapter II were intended for ideal crystals, where a unit cell can be found. In a real crystal with defects (for example Mn in GaN) the distribution of the defects in the lattice is random and in this case no unit cell can be found. However the real crystal with a disordered distribution of defects can be replaced by another crystal with an ordered distribution and the same average concentration of defects. In this case a unit cell can be found for the crystal and the band structure problem for the crystal can be resolved by LMTO or LAPW methods.

When we replace one problem by another one, we suppose that the electronic properties of crystals with ordered and disordered defects are essentially the same. This is true if the assumed ordered distribution of defects well corresponds to the disordered distribution in a real crystal. For example a disordered homogenous distribution should be modeled by an

ordered homogeneous distribution. If the defects form clusters in a real crystal, these clusters should be included in the unit cell of ordered crystal. As we will see later a specific type of defect distribution in a real crystal can be deduced from experimental investigations.

A supercell approach was used in this work to calculate the band structure and electronic properties of crystals with impurities. According to this approach a supercell has to be found for the crystal with impurities. The supercell is an elementary cell of the crystal, but usually it is larger than the primitive cell of the crystal without impurities. The size of the supercell should be sufficiently large to obtain the desirable concentration of impurities in the supercell. By translating this supercell in the space we obtain a crystal with the same concentration of impurity. For example if we want to calculate the band structure of a $Ga_{1-x}Mn_xN$ (x=0.0625) crystal, we can put a Mn atom in a supercell which contains also 15 Ga and 16 N atoms:

$$x = \frac{N_{Mn}}{N_{Mn} + N_{Ga}}, \qquad\qquad (3.1)$$

where N is the number of atoms (Mn or Ga) in the supercell. If we want to calculate the properties of a $Ga_{1-x}Mn_xN$ (x=0.03125) crystal the size of the supercell should be 2 times as large. Thus, the smaller the concentration of impurities, the larger the supercell which is necessary to construct the crystal. The computing time increases very quickly with the size of supercell, and this time increases more quickly than N^2, where N – is the total number of atoms in the supercell. Therefore it is easier to calculate the properties of crystals with a high concentration of impurities while usually real crystals have a very low concentration of impurities. This fact induces us to look for a compromise between our experimental and theoretical possibilities.

For this reason the smallest possible supercell of a crystal, with one impurity atom, is usually chosen to calculate the properties of the crystal. However there are problems where two, three or more atoms of impurity should be considered. This is necessary when we study the magnetic properties of materials or if we consider problems of impurity precipitation. For example, it is possible to estimate the exchange integral between magnetically active atoms in a material. To do this we may put two atoms in a supercell. Then two calculations should be performed where the spins of the two atoms have the same, and opposite, directions. The

difference in the total energy between these two states is the exchange energy, which can be related to the exchange integral. Obviously the supercell with two impurity atoms is two times bigger than the supercell containing only one impurity atom for the same concentration of impurity.
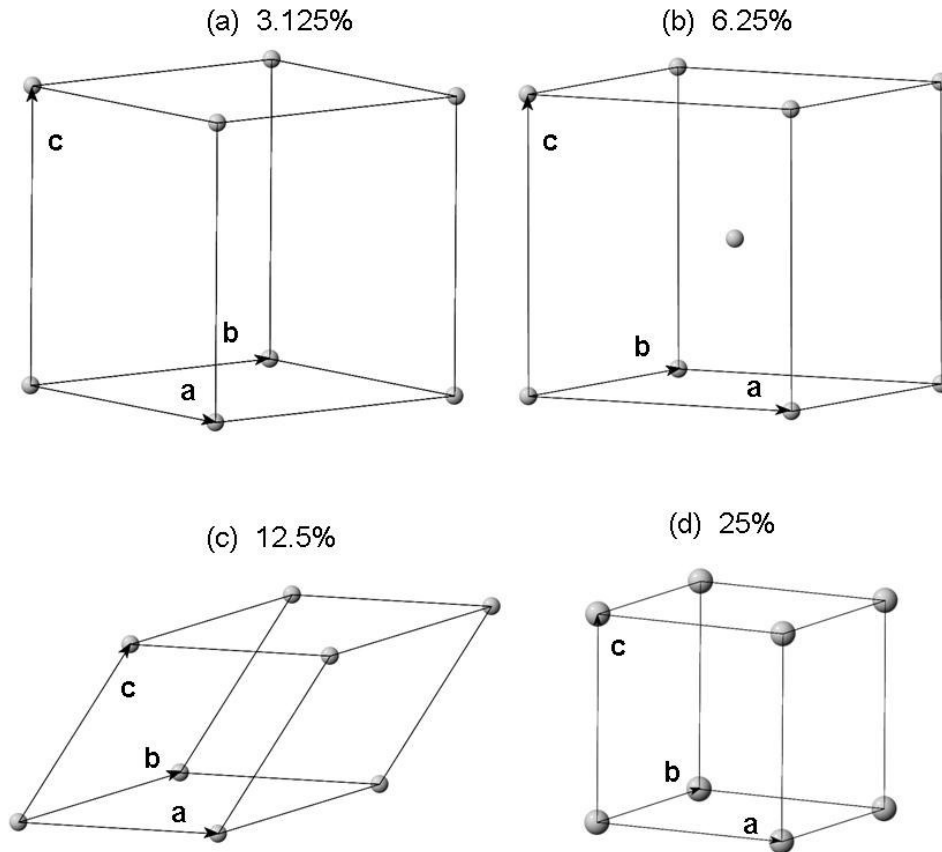
Fig. 3.2. Supercells of zinc-blende $Ga_{1-x}Mn_xN$ (x=0.03125, 0.0625, 0.125, 0.25) used in the band structure calculations. For clarity Mn atoms only are shown in these supercells.

Tab. 3.3. Values of primitive translation vectors for zinc-blende $Ga_{1-x}Mn_xN$ (x=0.03125, 0.0625, 0.125, 0.25) supercell shown in fig. 3.2. The values are given in units of a_0.

concentration of Mn atoms, x	a (a_0)	b (a_0)	c (a_0)
0.03125	2	2	2
0.0625	2	2	2
0.125	$\sqrt{2}$	$\sqrt{2}$	$\sqrt{2}$
0.25	1	1	1

The band structure of zinc-blende $Ga_{1-x}Mn_xN$ (x=0.03125, 0.0625, 0.125, 0.25) was calculated in [4] using four different supercells shown in fig. 3.2. The primitive translation vectors **a**, **b**, and **c** for the lattices are listed in tab. 3.3. The lattice parameter a_0 was chosen to be 4.5 Å (the experimental value of the lattice parameter for zinc-blende GaN, see tab. 3.1).
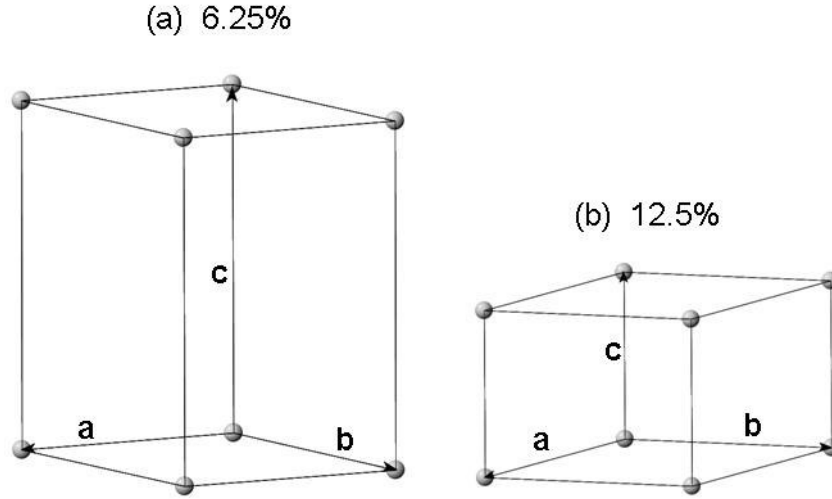
Fig. 3.3. Supercells of wurtzite $Ga_{1-x}Mn_xN$ (x=0.0625, 0.125) used in the band structure calculations. For clarity Mn atoms only are shown in these supercells.

Tab. 3.4. Primitive translation vectors for wurtzite $Ga_{1-x}Mn_xN$ (x=0, 0.0625, 0.125) supercells shown in fig. 3.1 and fig. 3.3.

concentration of Mn atoms, x	a, b	c	u
0	a_0=3.23Å	c_0=5.28Å	u_0=0.375
0.0625	$2a_0$	$2c_0$	u_0
0.125	$2a_0$	c_0	u_0

Two different supercells were used in band structure calculations for wurtzite $Ga_{1-x}Mn_xN$ (x=0.0625,0.125). The supercells are shown in fig. 3.3; the values of primitive vectors for the supercells are given in tab. 3.4. These supercells were chosen so as to make the nearest-neighbor Mn-Mn distances as isotropic as possible: in the first case (6.25%) the distance between two nearest Mn atoms along the c axis of the wurtzite structure is longer

than along the *a* axis (the ratio is ~1.6) while it is shorter in the second case (12.5%, the ratio is ~0.8). As it was mentioned above the wurtzite crystal structure has three lattice parameters – a_0, c_0 and u. These three parameters were optimized on the primitive cell of wurtzite GaN (fig. 3.1b). The optimization allows us to find a true fundamental state of the crystal. To perform this optimization the ratio c_0/a_0 has been changed. The total energy of the GaN supercell was calculated for different values of the ratio c_0/a_0. The dependence of the calculated total energy E on the ratio c_0/a_0 is shown in fig. 3.4. And the minimum of the function $E(c_0/a_0)$ corresponds to the optimal value of c_0/a_0. Two energy functions $E(u)$ and $E(V)$ were also calculated to find optimized values for the three structure parameters (a_0, c_0 and u, see fig. 3.4). The optimized values are listed in tab. 3.4.
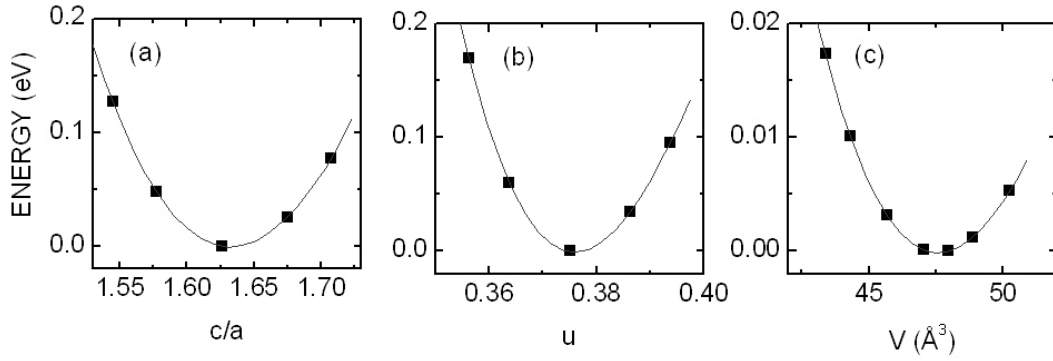
Fig. 3.4. Calculated total energy of the GaN primitive cell as a function of (a) ratio c_0/a_0, (b) parameter u, (c) volume of the cell. The calculated values (symbols) were interpolated by a cubic polynomial (solid line).

Actually there is no agreement about the necessity of the optimization today. On the one hand, the optimization allows calculating the electronic properties of an uncompressed crystal, i.e. we find the real ground electronic state within the limits of a particular model. On the other hand, it is not evident that the real ground state of a model corresponds better to the ground state of the real crystal. For example, in our case the performed optimization leads to lattice parameters which are slightly larger than the experimental ones: a_0=3.23Å (experimental value for GaN is 3.189Å) and c_0=5.28Å (experimental value for GaN is 5.185Å). Such an optimization changes not only the volume of the crystal, but also the anisotropy of the crystal: in the optimized GaN we have one nearest neighbor N atom which is more distant from a Ga

atom than 3 other N atoms (d_{1N}=1.980Å and d_{3N}=1.978Å), d_{1N}>d_{3N}. In the real wurtzite GaN crystal the anisotropy is opposite: d_{1N}=1.944Å and d_{3N}=1.952Å, d_{1N}<d_{3N}. Therefore we should use the experimental lattice parameters to investigate problems related to the crystal anisotropy, such as the linear dichroism. Problems related to the anisotropy were not considered in this work and the optimized GaN crystal structure will be used.
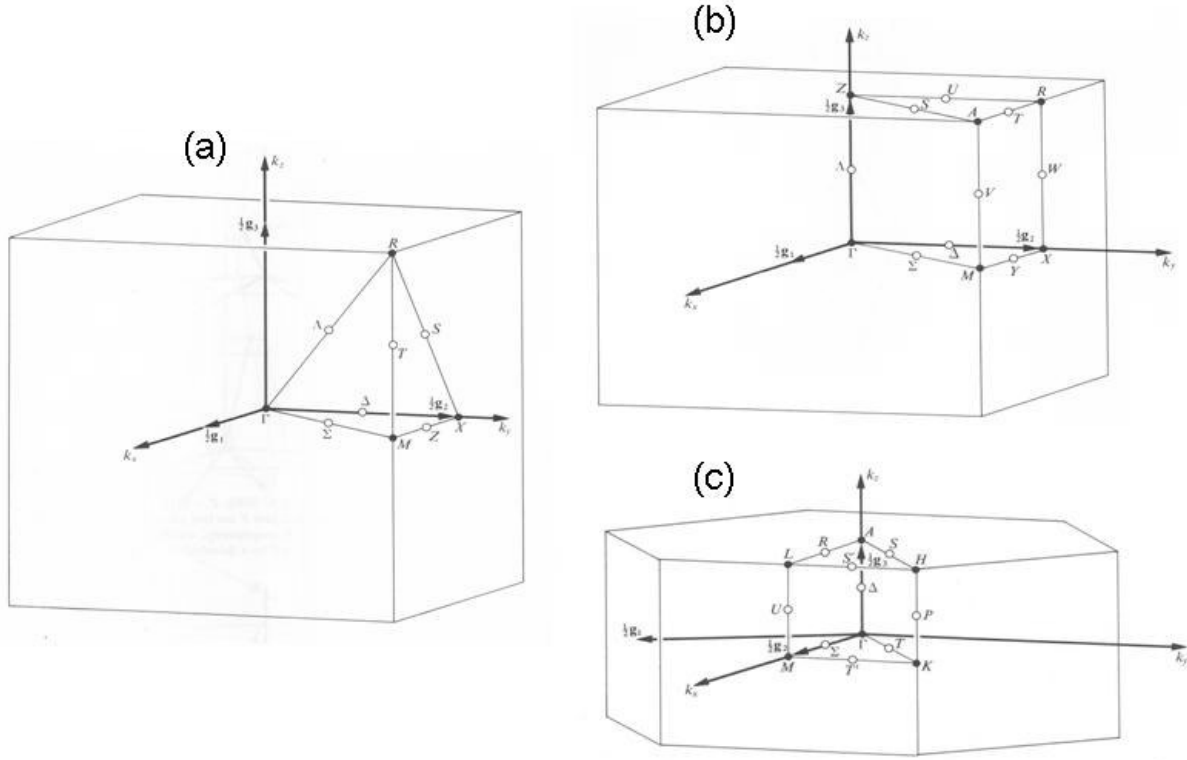
Fig. 3.5. First Brillouin zones for cubic primitive, tetragonal primitive and hexagonal primitive lattices. High symmetry points for every Brillouin zone are shown [7].

Incorporation of Mn in GaN distorts the lattice of GaN in the vicinity of the Mn atoms. In particular, experimental EXAFS studies have shown that the Mn-N distance between an Mn atom and its nearest neighbor N atoms is 2.7% longer than the Ga-N distance in bulk GaN, with no measurable variations of the other distances [5]. The Mn atoms in (Ga,Mn)N "push away" the nearest-neighbor N atoms. This experimental result agrees with the conclusions of a band structure calculation [6]: an optimal value of Mn-N distance was found in this calculation, where the Mn-N distance have being changed and the total energy of the

(Ga,Mn)N crystal have being calculated. This optimal value of the Mn-N distance corresponds to the minimum of the total energy as a function of the Mn-N distance. It was found that the Mn-N distance should be 3% longer than the Ga-N distance in bulk GaN, in agreement with the result of EXAFS experiments [5]. The second conclusion of the calculation is that the relaxation has no effect on the band structure of (Ga,Mn)N. For this reason the relaxation is not taken into account in our band structure calculations for (Ga,Mn)N.

Dispersion curves $E(\mathbf{k})$ for different crystal lattices will be presented in this chapter. Therefore it is worth to remind the notation for high symmetry points in the first Brillouin zones of the primitive cubic, primitive tetragonal and hexagonal lattices (fig. 3.5, [7]). This notation will be used to indicate the paths in $\mathbf{k}$-space along which the eigenvalues of energy are calculated.

3.3.1 Zinc-blende (Ga,Mn)N

Fig. 3.6. Band structure of zinc-blende $Ga_{1-x}Mn_xN$ (x=0.0625) in the ferromagnetic state calculated in [4]: (a) bands of electrons with spin up, (b) bands of electrons with spin down. The 3d-bands of Mn are shown by fat lines. The Fermi level is denoted by a horizontal line at 0 eV.
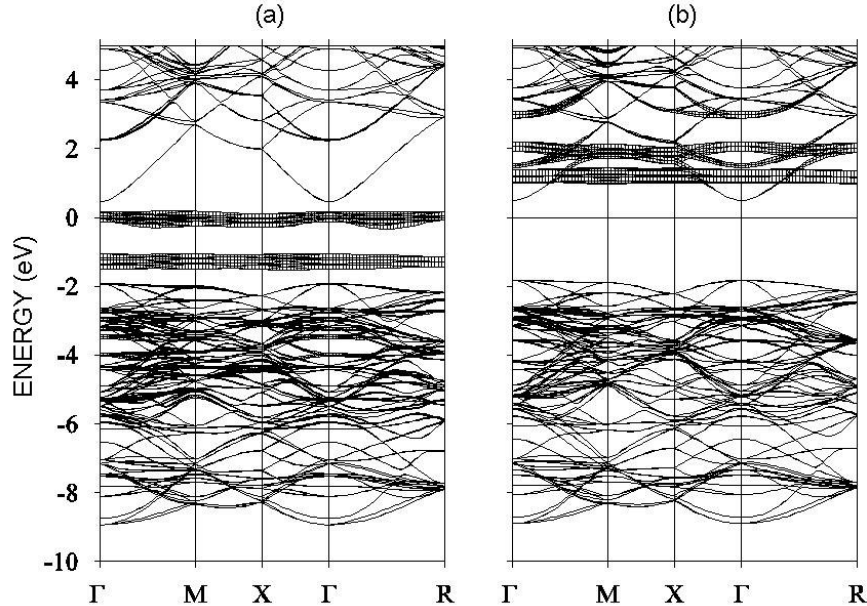
The band structure of zinc-blende $Ga_{1-x}Mn_xN$ (x=0.0625) was calculated using the LMTO method [8] by E. Kulatov et al. [4]. The local spin density approximation was used for the exchange-correlation potential. Other parameters of this calculation can be found in the original article. The band structure and some results of the calculation are of great importance because they will be used in following analysis of experimental results.

The band structure of zinc-blende $Ga_{1-x}Mn_xN$ (x=0.0625) in the ferromagnetic state is shown in fig. 3.6. There are two different band structures for different types of electrons. The first band structure (fig. 3.6a) corresponds to the electrons which spin magnetic moment points to the direction of magnetization. The electrons of this type will be called as "electrons with spin up". The second band structure (fig. 3.6b) corresponds to the electrons which spin magnetic moment is opposite to the direction of magnetization. The electrons of this type will be further called as "electrons with spin down". The valence band of (Ga,Mn)N is below -2 eV. The Fermi level has 0 eV position, therefore all the bands under 0 eV are filled by electrons. The states of the conduction band are above 0.5 eV and they are empty. The $3d$-bands of Mn with spin up are very narrow and they are situated in the gap. These bands are not hybridized with the valence band and the $3d$-orbitals are localized near Mn atoms. The effective mass of these electrons should be large because the bands are narrow. Therefore the electrons are hardly moved by external electric fields and they remain localized near the Mn atoms. The calculated gap width is approximately 2.3 eV, while the experimental value of the gap is higher and equals 3.3 eV (tab. 3.1). Such an underestimation of the band gap is typical of *ab-initio* calculations based on density functional theory [6]. This underestimation can be corrected describing the exchange-correlation effects by the self-energy operator within the GW approximation [9].

Total and partial densities of states of $Ga_{1-x}Mn_xN$ (x=0.25, 0.0125, 0.0625, 0.03125) are presented in fig. 3.7. The states of electrons with spin up and spin down are shown in upper and lower parts of every figure. Now let us consider the $3d$-states of Mn situated in the gap of (Ga,Mn)N. The $3d$-states of Mn are split by exchange interaction between $3d$-electrons of Mn: the $3d$-states of Mn with spin up have a lower energy than the $3d$-states with spin down. This relative position of $3d$-states insures the maximum of the total spin moment when the population of the $3d$-states increases, in agreement with the Hund's rule for free atoms. The size of the exchange splitting remains essentially the same (~2 eV) for all concentrations of Mn (fig. 3.7). Therefore the splitting does not depend on the distance between Mn atoms.

This means that the splitting is essentially due to internal exchange interactions between $3d$-electrons of the same Mn atom. Hence the exchange splitting of $3d$-states of Mn should be present not only in ferromagnetic (Ga,Mn)N, but in paramagnetic and antiferromagnetic (Ga,Mn)N crystals also. As we will see late the exchange splitting can be obtained from the x-ray absorption spectra of Mn in (Ga,Mn)N and the experimental value of the splitting (~1.8 eV) agrees well with the calculated one (~2 eV).
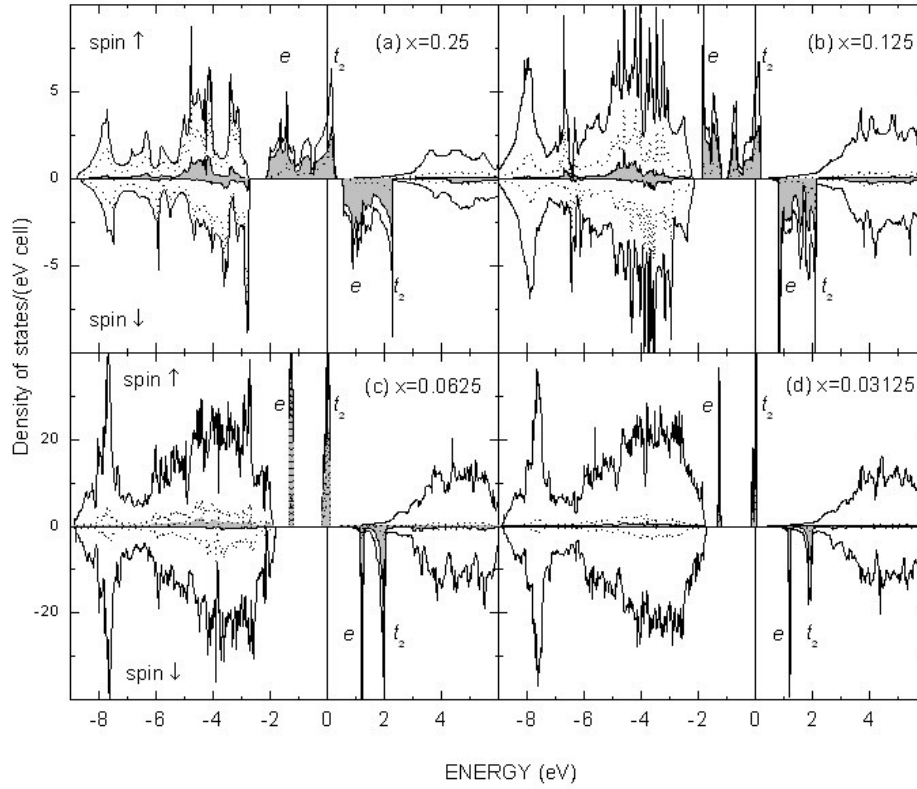
Fig. 3.7. Total and partial densities of states (DOS) in zinc-blende $Ga_{1-x}Mn_xN$ (x=0.25, 0.0125, 0.0625, 0.03125) [4]. Electronic states with spin up (upper part) and spin down (lower part of each figure) are shown. The total DOS is denoted by a solid line, $3d$-states of Mn by a filled area, $2p$-states of N by a dash line. The vertical solid line at 0 eV denotes the Fermi level.

The crystal field caused by the four nearest-neighbor N atoms (fig. 3.1) additionally splits the $3d$-states of Mn into a doubly degenerate e and a triply degenerate t_2 bands. The t_2 band consist of d-orbitals which have the xy, yz, xz symmetries, while the e band is composed by $3d$-orbitals which have the x^2-y^2, $2z^2$-x^2-y^2 symmetries (fig. 3.8). Geometrically the $d(xy$,

yz, xz)-orbitals are closer to the nearest-neighbor N atoms than $d(x^2-y^2, 2z^2- x^2-y^2)$-orbitals of Mn. The strong interaction of the $3d(t_2)$ states of Mn with the $2p$ states of N splits the t_2 band into bonding (below -2 eV) and anti-bonding (above -1 eV) parts and push up the anti-bonding part of the $d(t_2)$ band above the $d(e)$ band [10]. As a result the $3d(e$, spin up) band is filled by electrons, while the $3d(t_2$, spin up) is partially empty. The experimental value of the splitting between the t_2 (spin up) and e (spin up) bands (that is the crystal field splitting) can be obtained from the optical absorption measurement (see the section "Optical absorption spectra modeling").
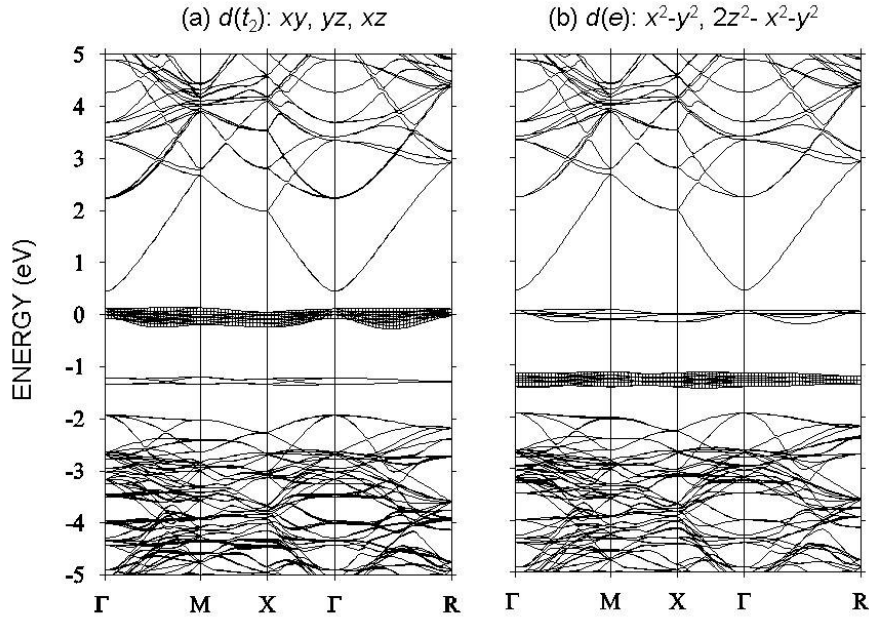
Fig. 3.8. Band structure of zinc-blende $Ga_{1-x}Mn_xN$ (x=0.0625) in ferromagnetic state, spin up [4]: (a) $3d(xy, yz, xz)$-electrons of Mn, (b) $3d(x^2-y^2, 2z^2-x^2-y^2)$-electrons of Mn. The $3d$-bands of Mn a shown by fat lines. The Fermi level is denoted by a horizontal line at 0 eV.

It is worth to mention here that the *x, y* and *z* axes have the same directions as the three orthogonal edges of the cubic supercell (fig. 3.2b). If we change direction of the axes, the orientation of Mn $d(xy, yz, xz, x^2-y^2, 2z^2- x^2-y^2)$ orbitals relative the four N atoms will also change. And the distribution of $3d$-orbitals between e and t_2 bands will differ from the distribution described above. Therefore the distribution of the $d(xy, yz, xz, x^2-y^2, 2z^2- x^2-y^2)$ orbitals between the e and t_2 bands depends on the direction of the *x, y* and *z* axes. The *z* axis is usually chosen to be parallel to the *c* axis in the wurtzite (Ga,Mn)N. However we will rotate the axes to obtain the same orientation of the axes relatively to the four N atoms as in the

zinc-blende (Ga,Mn)N. This rotation allows obtaining the described above distribution of the $d(xy, yz, xz, x^2-y^2, 2z^2- x^2-y^2)$ orbitals between the e and t_2 bands in the wurtzite (Ga,Mn)N (see also the discussion in the section "Wurtzite (Ga,Mn)N").

Electrical, optical, magnetic and other properties of materials essentially depend on the position of the Fermi level: the electrons which energy is close to the Fermi energy determine the transport properties of a crystal; the optical and magnetic properties of semiconductors doped with a transition metal depend on the valence state of the transition metal in the semiconductor. The Fermi level falls in the t_2(spin up) band of Mn in (Ga,Mn)N. It divides the t_2 band on two parts – filled and empty, with a ratio close to 2:1 (fig. 3.7). Therefore according to this calculation the Mn atoms have $3d^4$ electronic configuration in (Ga,Mn)N.

The calculated total magnetic moment of (Ga,Mn)N crystal per a Mn atom is $4\mu_B$ and this value does not depend on the concentration of Mn in (Ga,Mn)N (tab. 3.5). The main part of this moment is localized near the Mn atoms. A small contribution to the total magnetic moment arises from the nearest-neighbor N atoms (tab. 3.5). Besides that, these magnetic moments have the same direction as the Mn magnetic moment.

Tab. 3.5. Calculated magnetic moments in zinc-blende $Ga_{1-x}Mn_xN$ [4]: total magnetic moment per one Mn atom ($Mn_{tot}/1Mn$), magnetic moment of Mn (M_{Mn}), magnetic moment of nearest-neighbor N atom (M_N).

magnetic moment	concentration of Mn atoms, x			
	0.03125	0.0625	0.125	0.25
$M_{tot}/1Mn$ (μ_B)	4.0	4.0	4.0	4.0
M_{Mn} (μ_B)	3.32	3.34	3.39	3.38
M_N (μ_B)	0.044	0.039	0.038	0.043

Now let us consider the $3d$ bands of Mn and their dependence on the concentration of Mn in (Ga,Mn)N. As it was mentioned above the exchange splitting between d bands with spin up and spin down does not depend on the concentration of Mn and is essentially due to internal exchange interactions of $3d$ electrons. At the same time the width of Mn $3d$ bands is determined by interactions between $3d$ orbitals of nearest-neighbor Mn atoms. When the Mn atoms are well separated, the interaction between the $3d$ orbitals of neighbor atoms is weak and the $3d$ bands of Mn in (Ga,Mn)N are narrow (fig. 3.7d). At high concentration of Mn the overlap of the $3d$ electrons of neighbor Mn atoms increases and the $3d$ bands of Mn become

wider (fig. 3.7a). This increase of the band width arises from the stronger electrostatic interaction between the 3d electrons of different atoms when the distance between the Mn atoms decreases. The same type of broadening of atomic orbitals is observed when we form a solid from atoms: the narrow atomic orbitals are transformed to the energy bands.
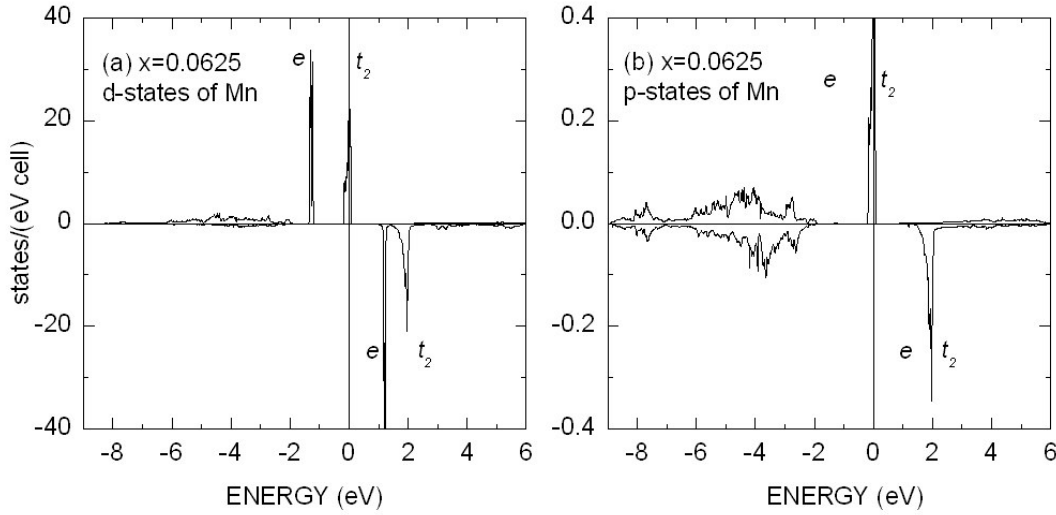
Fig. 3.9. Density of (a) 3d states and (b) 4p states of Mn in zinc-blende Ga$_{1-x}$Mn$_x$N (x=0.0625) [4]. Electron states with spin up (upper part) and spin down (lower part of each figure) are shown. The vertical solid line at 0 eV denotes the Fermi level.

Four nearest-neighbor N atoms form a tetrahedron around a Mn atom in (Ga,Mn)N. The tetrahedral crystal field splits the 3d bands of Mn into e and t_2 bands. In the same tetrahedral field, the 4p orbitals of Mn acquire the t_2 symmetry. Therefore the matrix element is not zero

$$\left\langle 3d_{t_2} \left| H_{cryst} \right| 4p \right\rangle \neq 0 , \qquad (3.2)$$

and 4p-3d hybridization of Mn orbitals is possible. The densities of 3d and 4p states of Mn are shown in fig. 3.9. A high intensity of p states is observed in the t_2 bands with spins up and down. This is a result of the p-d hybridization mentioned above. A small amount of p states also appears in the e bands at high concentration of Mn (fig. 3.10). Although a direct hybridization of p and d_e states is not permitted, these p states could arise from the overlap of 3d orbitals of neighbor Mn atoms. The contribution of the overlap to the density of p states is

essential if the distances between neighbor Mn atoms are small. Just as in the case of $3d$ states, the width of the p states of Mn in the gap increases together with Mn concentration in (Ga,Mn)N.
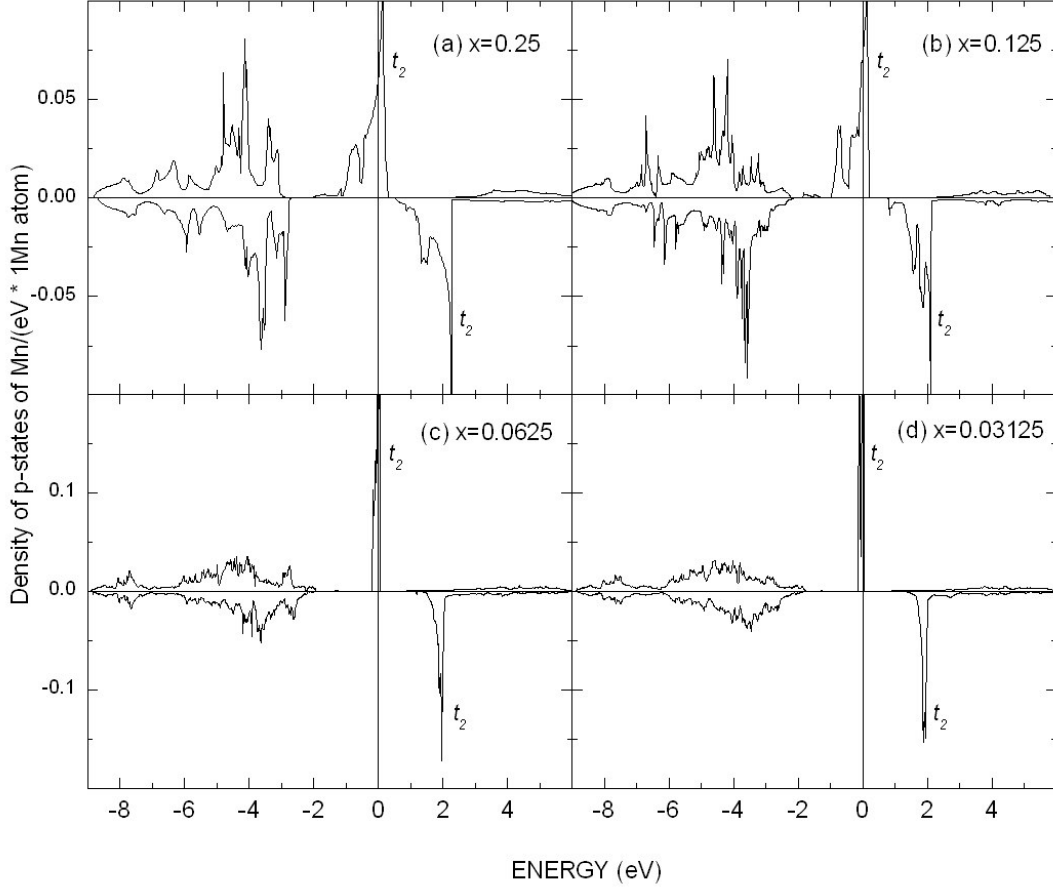
Fig. 3.10. Density of $4p$ states of Mn in zinc-blende $Ga_{1-x}Mn_xN$ (x=0.25, 0.125, 0.0625, 0.0315) [4]. Electron states with spin up (upper part) and spin down (lower part of each figure) are shown. The vertical solid line at 0 eV denotes the Fermi level.

One can estimate the relative contributions of the p-d hybridization and of the overlap of $3d$ orbitals to the density of Mn p states in the gap of (Ga,Mn)N. For this purpose, the total number of p states with spin up (N_p^{up}) and spin down (N_p^{down}) were calculated for different concentrations of Mn in (Ga,Mn)N, i.e. an integration of Mn p states with spins up and down was performed for (Ga,Mn)N crystals with different distances between the Mn atoms. The functions $N_p^{up}(x)$ and $N_p^{down}(x)$ are shown in fig. 3.11. As we see, the number of p states in the

gap decrease when the overlap of the $3d$ orbitals of Mn decrease. At a certain concentration of Mn the overlap becomes too small to influence the number of p states. In other words the derivatives of the functions $N_p^{up}(x)$ and $N_p^{down}(x)$ should be close to 0 when the concentration x of Mn is close to 0:

$$\frac{dN_p}{dx}(x \to 0) \to 0. \tag{3.3}$$

Let us find the functions $N_p^{up}(x)$ and $N_p^{down}(x)$ which correspond to the calculated values shown in fig. 3.11 by symbols, and which satisfy the requirement (3.3). These functions are shown by solid lines in fig. 3.11. The p states of Mn which total number is $N_p^{up}(0)$ and $N_p^{down}(0)$ are not related to the overlap of Mn d orbitals. These states arise from the p-d hybridization of Mn states induced by the tetrahedral crystal field. Contribution to the p states from the overlap of Mn d orbitals is smaller, but it becomes considerable at high concentration of Mn.
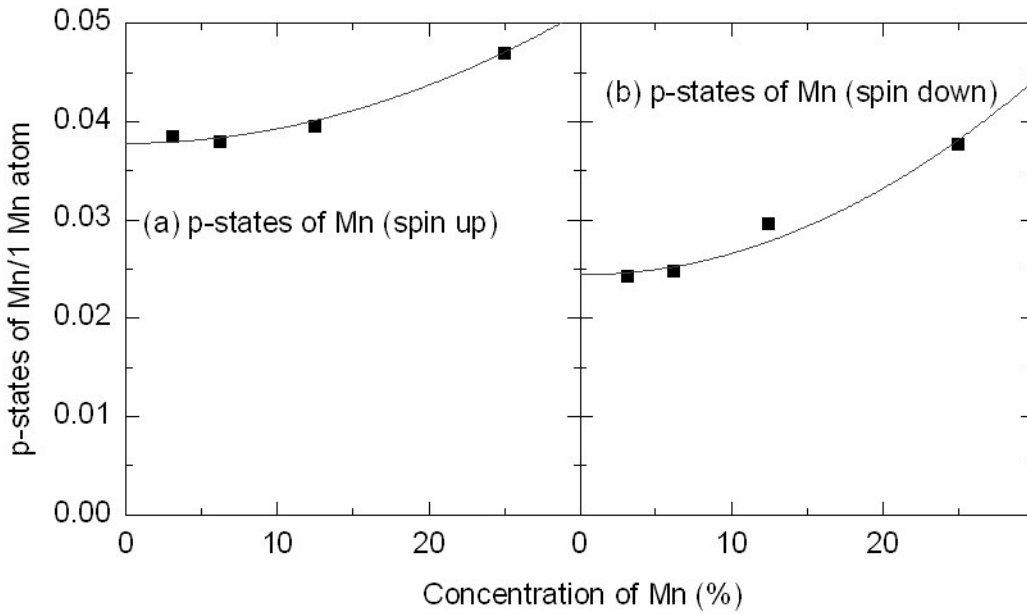
Fig. 3.11. Total number of Mn $4p$ states with (a) spin up and (b) spin down in zinc-blende Ga$_{1-x}$Mn$_x$N as function of Mn concentration. The calculated values are shown by symbols [4]; interpolated values by a polynomial third power are shown by solid lines.

3.3.2 Wurtzite (Ga,Mn)N
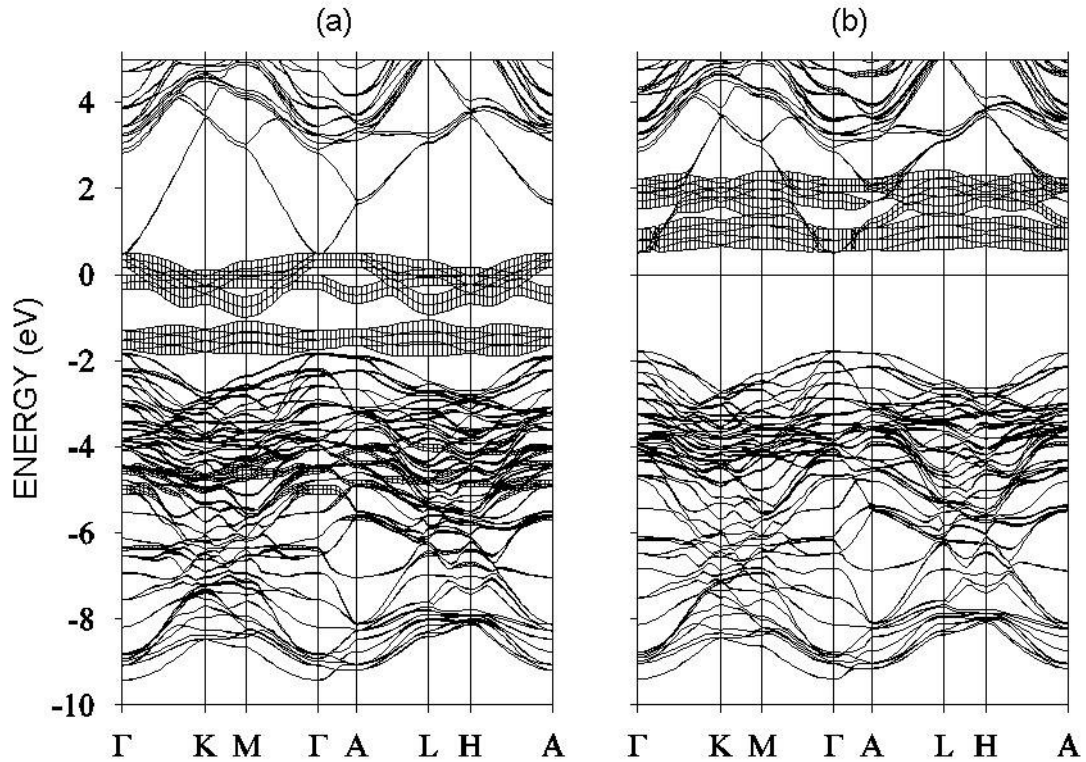
Fig. 3.12. Band structure of wurtzite $Ga_{1-x}Mn_xN$ (x=0.0625) in ferromagnetic state [11]: (a) bands of electrons with spin up, (b) bands of electrons with spin down. The $3d$-bands of Mn are shown by fat lines. The Fermi level is denoted by a horizontal line at 0 eV.

The band structure (energy dispersion curves) of $Ga_{1-x}Mn_xN$ (x=0.0625) was calculated by the LMTO method [11]. The local spin density approximation was used to take into account exchange interaction and correlation between electrons. The band structure is similar to the band structure of zinc-blende (Ga,Mn)N (compare fig. 3.12 and fig. 3.6). Calculated value of the gap at Γ point is approximately 2.4 eV which is a bit higher than the calculated gap width in zinc-blende (Ga,Mn)N (2.3 eV) and considerably less than the experimental value of the gap width in wurtzite (Ga,Mn)N (3.5 eV, see tab. 3.2). As it was mentioned above, such an underestimation of the gap is typical of density functional calculations.

The $3d$ bands (spin up) of Mn are situated in the gap of GaN. They are split by the exchange interaction and crystal field. The exchange interaction splits the $3d$ bands according to the direction of electron spin: electrons which spin magnetic moment points to the same direction as the magnetization of (Ga,Mn)N crystal have smaller total energy than electrons which have an opposite spin moment. Energy splitting between the $3d$ bands with spin up and

spin down is approximately 2 eV, the same splitting was found in the zinc-blende (Ga,Mn)N. As it was mentioned above in the case of zinc-blende (Ga,Mn)N, this splitting does not depend on the Mn concentration and it arises from the exchange interaction between the $3d$ electrons of the same Mn atoms. Thus this splitting does not depend on macroscopic magnetic properties of (Ga,Mn)N, i.e. it is present in ferromagnetic and paramagnetic (Ga,Mn)N crystals.

In addition the $3d$ states of Mn are split by the tetrahedral crystal field induced by the four nearest neighbor N atoms. Although the distances between the four N atoms and the Mn atom are not the same in wurtzite (Ga,Mn)N, the distortion of the tetrahedron formed by the four N atoms is small. This distortion does not alter the tetrahedral symmetry of the crystal field. The tetrahedral crystal field splits the $3d$ states of Mn into a doubly degenerate e and a triply degenerate t_2 bands. The distribution of $3d$ orbitals between these two bands are the same as in zinc-blende (Ga,Mn)N: the e band consist of x^2-y^2, $2z^2-x^2-y^2$ orbitals, while the t_2 band is formed by xy, yz and xz orbitals (fig. 3.13, the $3d$ bands of Mn are shown by fat lines).

(a) $d(t_2)$: xy, yz, xz (b) $d(e)$: x^2-y^2, $2z^2-x^2-y^2$
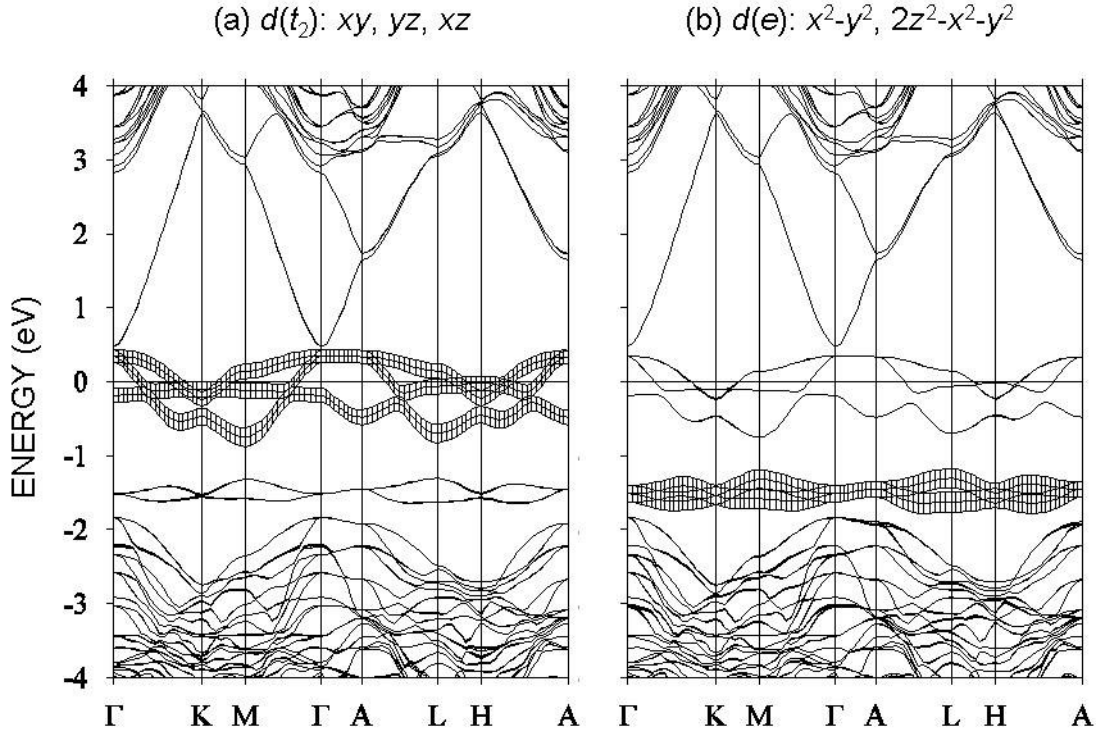
Fig. 3.13. Band structure of wurtzite $Ga_{1-x}Mn_xN$ ($x=0.0625$) in ferromagnetic state, spin up [11]: (a) $3d(xy$, yz, $xz)$-electrons of Mn, (b) $3d(x^2-y^2$, $2z^2-x^2-y^2)$-electrons of Mn. The $3d$-bands of Mn a shown by fat lines. The Fermi level is denoted by a horizontal line at 0 eV.

It is worth to mention here that the axes *x*, *y* and *z* have the same orientation relative to the four N atoms as in zinc-blende (Ga,Mn)N. This allows us to affirm that the distribution of 3*d* orbitals between *e* and t_2 bands in wurtzite (Ga,Mn)N is essentially the same in wurtzite and in zinc-blende (Ga,Mn)N. If we change orientation of the axes (for example, we put the *z* axis to be parallel to the *c*-axis of the crystal), then the content of the 3*d* bands will change. But it does not mean that the 3*d* states at the Fermi level have other nature in wurtzite (Ga,Mn)N, as it was erroneously mentioned in [12].

Total and partial densities of states in wurtzite (Ga,Mn)N shown in fig. 3.14 were calculated by the LAPW method implemented in the Wien2k package [13] using the generalized gradient approximation [14]. The Wien2k package also allows calculating the x-ray absorption spectra. Therefore we apply this method now to obtain the band structure parameters which will be further used in interpretation of our x-ray absorption spectra of Mn in (Ga,Mn)N.

Two wurtzite supercells (fig. 3.3a,b) with a Ga atom substituted by a Mn atom were used to simulate an uniformly doped $Ga_{1-x}Mn_xN$ with 6.25% and 12.5% of Mn. The ratio of muffin tin radii R(Mn)/R(N) = R(Ga)/R(N) was determined from the position of the minimum of the electron density between Mn and N atoms in zinc-blende (Ga,Mn)N [4]. The wave function in the muffin tin spheres was expanded using the spherical harmonics Y^l_m and l_{max} was chosen to be 10. The same wave function was represented as series of plane waves [15]

$$\phi^{\bar{k}}_{\bar{K}} = \frac{1}{\sqrt{V}} e^{i(\bar{k}+\bar{K})\bar{r}} \tag{3.4}$$

out of the muffin tin spheres, and the $R_{min} \cdot K_{max}$ were chosen to be 7 (here R_{min} is the least muffin tin radius, *V* is the volume of the supercell). Actually, the values of $R_{min} \cdot K_{max}$ and l_{max} should be determined for each material: these parameters should be large enough, so that the total energy should be stable when the parameters are increased. Comparison with results of other calculations performed by different methods shows that the chosen values of the parameters allow us to obtain good results. Convergence to self-consistency was achieved on a 9×9×4 and a 7×7×8 **k**-points mesh for 6.25% and 12.5% concentrations of Mn respectively. The total energy and the total charge in the Mn sphere were stable within 10^{-5} Ry and 10^{-5} *e* respectively for the last few iterations.
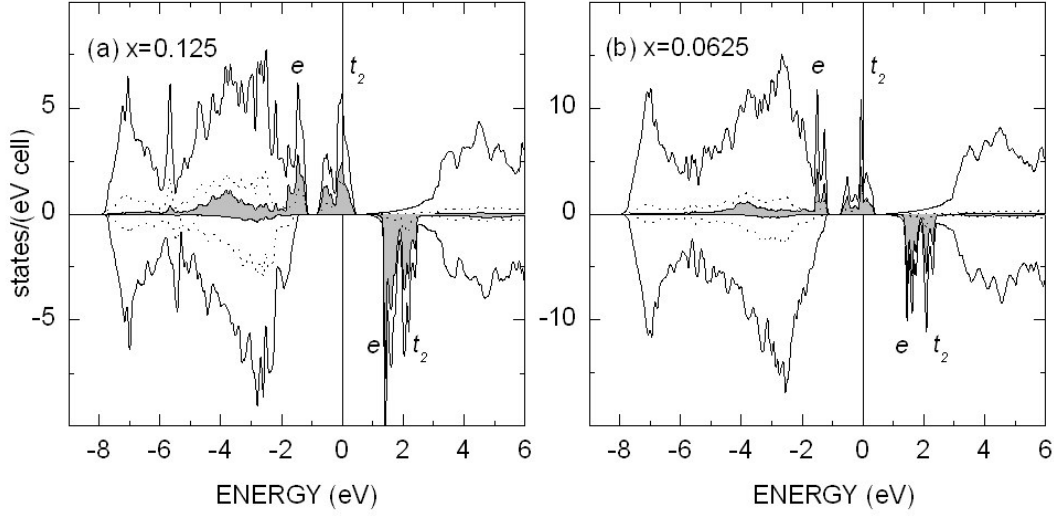
Fig. 3.14. Total and partial densities of states (DOS) in wurtzite $Ga_{1-x}Mn_xN$ (x=0.125, 0.0625). Electronic states with spin up (upper part) and spin down (lower part of each figure) are shown. The total DOS is denoted by a solid line, $3d$-states of Mn by a filled area, $2p$-states of N by a dash line. The vertical solid line at 0 eV denotes the Fermi level.

Just as in the zinc-blende (Ga,Mn)N, in wurtzite (Ga,Mn)N the $t_2(xy, yz, xz)$ orbitals of Mn interact stronger with the nearest-neighbor N atoms, and as a result the anti-bonding $t_2(xy, yz, xz)$ states are situated above the $e(x^2-y^2, 2z^2-x^2-y^2)$ states [10]. Thus the e band (spin up) is filled by two electrons, while the t_2 band (spin up) is partially empty. The Fermi level falls in the t_2(spin up) band and it divides the band into filled and empty parts with the ratio approximately 2:1 (the calculated ratio is 1.90:1). Thus according to this simple reasoning the electronic configuration of Mn in (Ga,Mn)N should be $3d^4$. This is confirmed by a direct calculation of the number of $3d$ electrons in the muffin tin sphere of Mn: the calculated population of $3d$ electrons is 4.29, this population is close to 4. Of course, the calculated value of electrons depends on the radius of muffin tin sphere of Mn. But as we will see later a reasonable choice of muffin tin radii (touching and not overlapping muffin tin spheres, the radii ratio should be quite natural and correspond to the minimum of charge density) allows us to obtain a good estimation for the valence state of transition elements.

Tab. 3.6. Calculated magnetic moments in wurtzite $Ga_{1-x}Mn_xN$ (x=0.125, 0.0625): total magnetic moment per one Mn atom (Mn_{tot}/1Mn), magnetic moment of Mn (M_{Mn}), magnetic moment of nearest-neighbor N atom (M_N).

magnetic moment	concentration of Mn, x	
	0.0625	0.125
M_{tot}/1Mn(μ_B)	4.0	4.0
M_{Mn}(μ_B)	3.21	3.22
M_N(μ_B)	3N 1N -0.02 0.06	3N 1N -0.01 0.05

The calculated total magnetic moment per 1 Mn atom does not depend on the concentration of Mn in $Ga_{1-x}Mn_xN$ (x=0.0625, 0.125) and it equals to $4\mu_B$. Contributions from different atoms to the total magnetic moment are listed in tab. 3.6. The greatest part of total magnetic moment is localized in the muffin tin sphere of Mn. This confirms the conclusion about localization of $3d$ orbitals near Mn atoms. Magnetic moments of nearest-neighbor N atoms are not very large and they do not contribute essentially in the total magnetic moment.

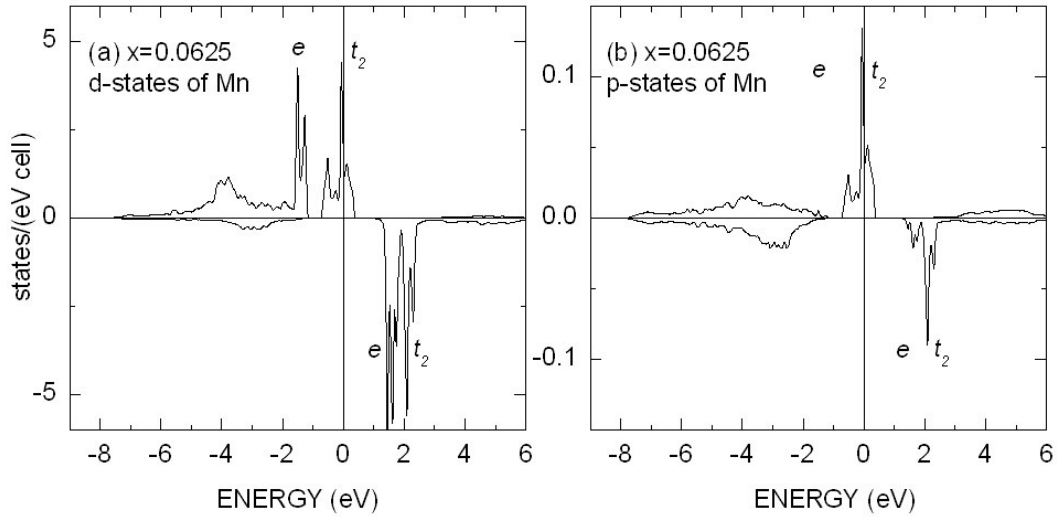Fig. 3.15. Density of (a) $3d$ states and (b) $4p$ states of Mn in wurtzite $Ga_{1-x}Mn_xN$ (x=0.0625). Electron states with spin up (upper part) and spin down (lower part of each figure) are shown. The vertical solid line at 0 eV denotes the Fermi level.

In wurtzite (Ga,Mn)N, Mn atoms have the same tetrahedral local environment just as in zinc-blende (Ga,Mn)N and $4p$ orbitals of Mn acquire the t_2 symmetry. Therefore the $4p$-$3d$ (t_2) hybridization is permitted and a high intensity of p states appears in t_2 bands with spins up and down. As it was shown above in the case of zinc-blende (Ga,Mn)N, this high density of p states in the gap is essentially due to the $4p$-$3d$ hybridization. Another contribution to the density arises from the overlap of $3d$ orbitals of nearest Mn atoms, but this contribution becomes essential only at high concentration of Mn (in order of 25%). The width of Mn $3d$ bands in the gap depends on the distance between nearest-neighbor Mn atoms: when the distance is more than $2a_0$ (a_0 – is the lattice parameter of GaN), the $3d$ bands are very narrow. The bands become very wide when the distance is less than a_0.

Before turning to modeling of experimental spectra of (Ga,Mn)N, let us outline the main results obtained from the band structure calculations which are common for wurtzite and zinc-blende (Ga,Mn)N.

1.   The $3d$ states of Mn are situated in the band gap of (Ga,Mn)N; the $3d$ orbitals of Mn atoms are localized near the Mn atoms.

2.   The $3d$ states of Mn are split by the exchange interaction and crystal field. The exchange splitting ($\Delta E_{exc}\sim 2$ eV) does not depend on the concentration of Mn in (Ga,Mn)N and it is due to the exchange interaction between the $3d$ electrons inside a Mn atom. This splitting therefore is present in the band structure of (Ga,Mn)N independently of macroscopic magnetic structure of the crystal. The crystal field caused by the four nearest-neighbor N atoms splits the $3d$ states of Mn into a doubly degenerate e band and a triply degenerate t_2 band. The t_2 band is placed above the e band.

3.   The Fermi level falls into the t_2 band (spin up), the e band (spin up) is completely filled by 2 electrons, while the t_2 band (spin up) is partially filled by 2 electrons. Thus the electronic configuration of Mn is $3d^4$ in (Ga,Mn)N.

4.   The $4p$-$3d$ hybridization of Mn orbitals results in a high density of empty p states in the t_2 bands with spins up and down in the gap of (Ga,Mn)N. A small contribution to the density arises from nearest-neighbor Mn atoms.

3.4 X-ray absorption spectra modeling

Experimental x-ray absorption spectra of Mn in wurtzite $Ga_{1-x}Mn_xN$ are shown in fig. 1.3 (the Mn content is indicated in the figure). The spectra were measured at the K-edge of Mn (~6539 eV) and x-ray absorption near-edge structure is shown only. An investigation of the extended x-ray absorption near-edge structure confirmed that Mn atoms substitute Ga atoms in the studied samples of wurtzite $Ga_{1-x}Mn_xN$ [5]. Therefore the results of band structure calculations described in this chapter can be used in an interpretation of experimental absorption spectra.

The x-ray absorption near-edge structure (fig. 1.3) corresponds to transitions of $1s$ electrons of Mn to empty states above the Fermi level. Although there are other possible transitions in this energy range (for example transitions of $2s$ electrons) these transitions give only a very smooth contribution to the absorption spectrum while absorption caused by transitions of $1s$ electrons changes very much near the absorption K-edge. That is why the structure of the K-edge absorption spectra is determined by transitions of $1s$ electrons. Taking into account these transitions we can calculate the absorption coefficient $\mu(E)$ using the dipole approximation:

$$\mu(E) \propto \left| \left\langle \psi_{1s} \left| \mathbf{e}\nabla \right| \psi_{4p} \right\rangle \right|^2 \cdot n_{4p}(\hbar\omega - E_F + E_{1s}), \tag{3.5}$$

here ψ_{1s} is the wave function of a $1s$ electron, ψ_{4p} is the wave function of a $4p$ empty state, n_{4p} is the density of $4p$ states above the Fermi level, $\mathbf{e}$ is the light polarization. The x-ray absorption spectra of Mn in wurtzite $Ga_{1-x}Mn_xN$ (x=0.0625, 0.125) calculated using the formula (3.5) and the Wien2k code [13] are shown in fig. 3.16.

The calculated spectra include transitions of $1s$ electrons to empty p states of Mn. As it was found above there are two bands of empty p states in the gap: t_2 (spin up) and t_2 (spin down). The two bands give rise to two intense absorption lines in the calculated spectra: line A_2 (at 0 eV) corresponds to transitions to the band t_2 (spin up) and line A_3 (at 2 eV) is related to transition to the band t_2 (spin down). The absorption lines are split by an energy interval ~2 eV and actually this is the exchange splitting of $3d$ states described above. Two absorption lines separated by an interval ~2 eV are also present in the experimental x-ray absorption

spectra (fig. 1.3, a double line at 6540 eV). It is quite natural to attribute the double line in the experimental spectra to the transitions $1s$-$d(t_2$, spin up) and $1s$-$d(t_2$, spin down) described above.
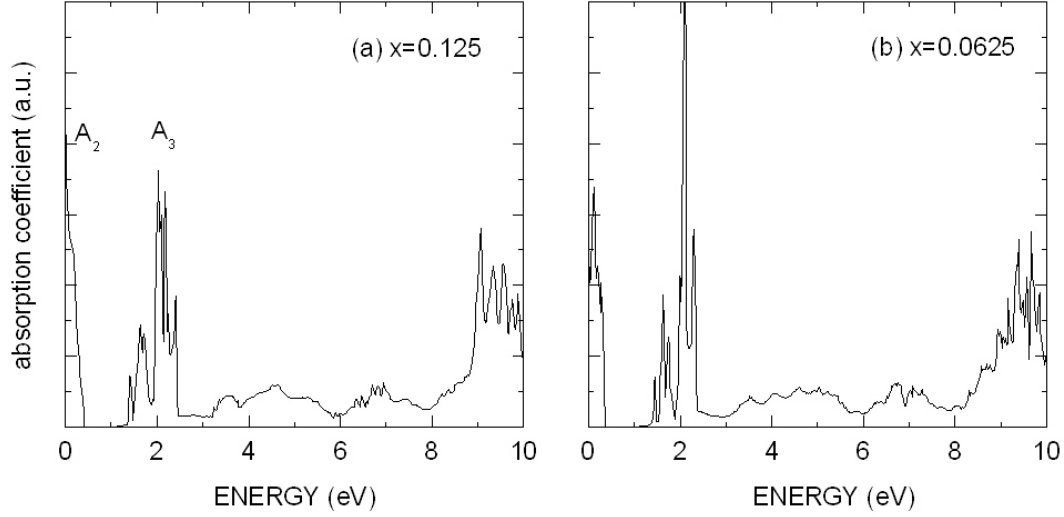
Fig. 3.16. Calculated x-ray absorption near-edge structure of Mn in wurtzite $Ga_{1-x}Mn_xN$ (x=0.0625, 0.125).

To compare the theoretical and experimental results, the calculated spectra have to be broadened. The broadening of experimental spectra is related to finite widths of the $1s$ and final levels, as well as to the finite resolution of the monochromator. These factors can be taken into account by a convolution of the calculated spectra with Lorentz or Gauss functions. If the broadening of experimental spectrum is essentially related to finite widths of $1s$ and final states, the calculated spectrum has to be convoluted with the Lorentz function:

$$L(E) = \frac{2}{\pi} \frac{\Gamma}{(2E)^2 + \Gamma^2}, \tag{3.6}$$

where Γ is the full width at half maximum. The parameter Γ should be calculated according to the formula:

$$\Gamma = \frac{\hbar}{\tau_h} + \frac{\hbar}{\tau_e},$$

(3.7)

where h is the Plank's constant, τ_h and τ_e are the lifetime of the 1s hole, which is left after excitation of 1s electron, and lifetime of exited electron correspondingly. Usually the lifetime of core hole is smaller for a deep level and greater for a shallow level. However this is not a rule without exceptions. For example the natural width ($\hbar/\tau_h$) of Mn 1s level is 1.16 eV, while the natural width of Mn 2s level is 2.62 eV [16]. This means that the lifetime of the 1s hole is greater than the lifetime of the 2s hole.

While the lifetime of the core hole is independent on the photon energy, the lifetime of the excited electron changes very rapidly with the energy of the electron. If the photon energy is close to the absorption edge, the kinetic energy of the excited electron is small and such an electron has a long lifetime. Therefore the width of pre-edge features in x-ray absorption near edge structure is determined by the core hole lifetime and by resolution of the monochromator. The lifetime of the excited electron decreases very quickly when the photon energy increase [17]. This increases the broadening of x-ray absorption spectrum at higher energy because the second term in formula (3.7) becomes considerable as compared to the first one. For example, according to the energy dependence of the electron free path in solids [18], the lifetime of the excited electron (E_e=30 eV) is $1.7 \cdot 10^{-16}$ sec, this lifetime corresponds to $\Gamma_e = \hbar/\tau_e$=3.9 eV.

If the broadening of experimental spectrum is essentially related to finite resolution of the monochromator, the calculated spectrum should be convoluted with the Gauss function:

$$G(E) = \sqrt{\frac{\ln 2}{\pi}} \frac{2}{\Gamma} \exp(-\frac{E^2}{\Gamma^2} 4 \ln 2),$$

(3.8)

where Γ is the full width at half maximum.

In the present case the natural width of the Mn 1s level is 1.16 eV, while the resolution of the monochromator is only 0.45 eV. Therefore the main contribution to the broadening arises from the natural width of 1s level and the calculated x-ray absorption spectra should be convoluted with the Lorentz function. Actually these two factors (natural width of core level and finite resolution of monochromator) should be taken into account to reproduce the

experimental broadening precisely. For this purpose the calculated spectra should be convoluted with the Voigt function, this function is a result of convolution the Lorentz function with the Gauss function. We will apply the Voigt function later in the study of distribution of Mn in (Ga,Mn)N where a careful description of the x-ray pre-edge features is necessary.

The calculated x-ray absorption spectrum of Mn in wurtzite $Ga_{1-x}Mn_xN$ (x=0.0625) was convoluted with the Lorentz function (fig. 3.17):

$$\mu^{\Gamma}(E) = \int \mu(E - \varepsilon)L(\varepsilon)d\varepsilon ,$$ (3.9)

where μ^{Γ} is the absorption coefficient after the broadening.

The broadening parameter Γ was adjusted to fit well the pre-edge features of the experimental spectrum. The obtained value of Γ is 1.44 eV. Actually the value of broadening changes with the photoelectron energy and it should be greater at higher energy.
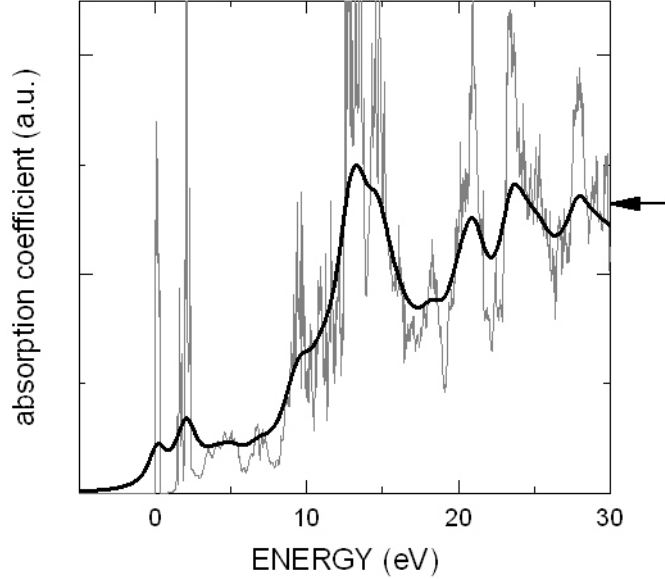
Fig. 3.17. Calculated x-ray absorption spectrum at the K-edge of Mn in wurtzite $Ga_{1-x}Mn_xN$ (x=0.0625): before (gray line) and after (solid black line) broadening. The arrow marks the intensity assigned to unity in the comparison to normalized experimental spectra.

In order to compare the theoretical and experimental spectra with different concentrations of Mn the spectra should be normalized. The init intensity position for the spectrum is shown by an arrow in fig. 3.17. Finally a comparison of theoretical and experimental results can be performed. The calculated and experimental x-ray absorption spectra at the K-edge of Mn in wurtzite $Ga_{1-x}Mn_xN$ for $x=0.0625$ and 0.057 are shown in fig. 3.18. The two spectra have the same structure: the absorption lines A_2 and A_3 are separated by ~2 eV and the main absorption peak (B in fig. 3.18) is present in the both spectra.
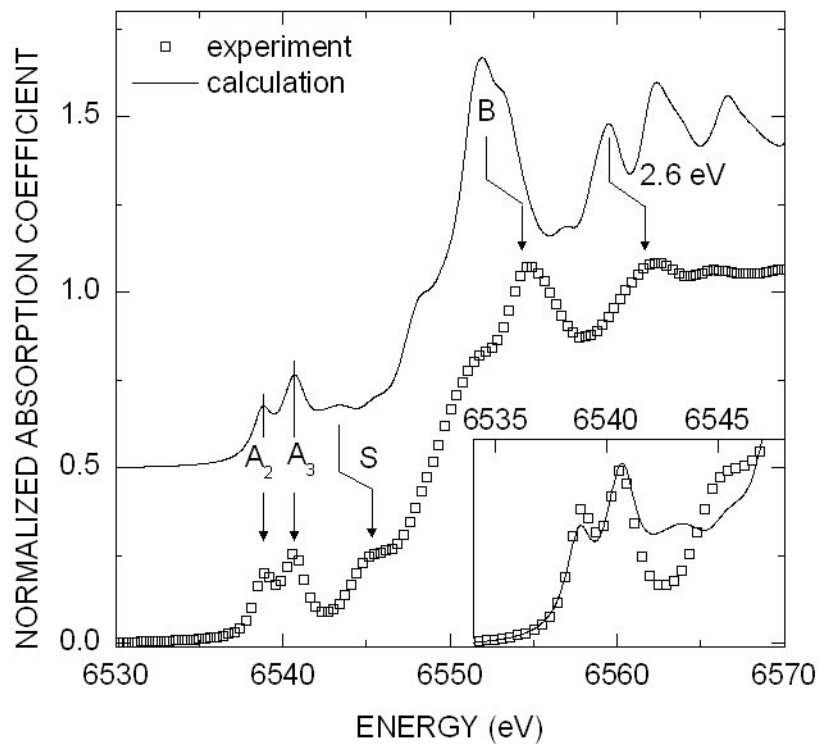
Fig. 3.18. K-edge x-ray absorption spectrum of Mn in wurtzite $Ga_{1-x}Mn_xN$ calculated for $x=0.0625$ (solid line), compared with the experimental spectrum for $x=0.057$ (symbols). The inset shows the pre-edge structure.

However there are several differences between the experimental and theoretical spectra. The main differences are:

> *i.* the calculation predicts absorption at 6543 eV (S line in fig. 3.18) which is not
> observed experimentally;

ii. an oscillatory structure above 6550 eV seems to be shifted down in energy in the calculated spectrum.

Let us consider these discrepancies in detail. The absorption at 6543 eV (S line in fig. 3.18) in the calculated x-ray absorption spectrum corresponds to transitions of $1s$ electrons of Mn into $4p$ states of the conduction band; it is clear from a comparison of fig. 3.15 and fig. 3.16. The experimental absorption coefficient equals to 0 at this energy (6543 eV) and therefore there are no really empty $4p$ states to the right of the double absorption line A_2-A_3. Thus the experimental results show that the $3d$ states (spin down) of Mn are deep in the gap, while according to the calculation $3d$ states (spin down) are near the top of the conduction band. This discrepancy may result from the underestimation of the width of the gap in the present calculation. The calculated gap is only 1.9 eV in the Γ point (the LAPW method implemented in the Wien2k package), while the experimental gap width is almost two times greater (3.5 eV). An additional contribution to the underestimation of energy interval between the Mn $3d$ states (spin down) and the conduction band could arise from formation of the $1s$ core hole. This core hole is left behind exited $1s$ electron and the hole attractive potential can change the position of $3d$ states as compared to the conduction band: the influence of the potential can be different on localized $3d$ states and delocalized states of the conduction band and the energy shift to a low energy can be more significant for $3d$ states of Mn as compared to the shift for p states of the conduction band. As a result the energy interval between the $3d$ states and conduction band increases.

The fundamental electronic state of (Ga,Mn)N was calculated in this work and multi-electronic effects were not taken into account. However influence of the core hole partially can be taken into account if one introduces a rigid shift of about 2.6 eV between the $3d$ states of Mn and the conduction band. This translation shifts the absorption structure at 6543 eV (S field in fig. 3.18) to the position at 6545 eV where absorption is observed experimentally. In addition the calculated absorption coefficient has a minimum at 6543 eV in agreement with the experimental x-ray absorption spectra. Finally, this translation shifts the most intense peak of oscillatory structure (B in fig. 3.18) to the position where such a peak is observed at 6555 eV.

There is a very high density of $3d$-states in the gap of (Ga,Mn)N (fig. 3.15). Therefore quadrupole transitions can contribute to the x-ray absorption in the gap. The intensity of the

quadrupole transitions can not be calculated using the same Wien2k package (this code does not support the calculation of the quadrupole transitions today), therefore a multiple-scattering approach was used to evaluate the quadrupole contribution to the K-edge absorption spectrum of Mn in (Ga,Mn)N (FDMNES package [19]). The FDMNES code allows calculating the x-ray spectra. However the *p-d* hybridization of the Mn orbitals which is very important in our case can be treated more accurately using the LAPW method. In addition, the position of the Fermi level in the FDMNES method is an adjustable parameter. The position of the Fermi level changes significantly the pre-edge structure of the x-ray absorption spectrum. Arbitrary choice of the position of the Fermi level may lead to an erroneous interpretation of the pre-edge features. However the Fermi level position is naturally obtained in the band structure methods (like the LAPW method): the total number of electrons in a crystal is fixed, so the position of the Fermi level can be calculated precisely after the band structure calculation.

The matrix elements of the dipole and quadrupole transitions in (3.5) were calculated using the FDMNES package, while the ratio of Mn-3*d* and Mn-4*p* densities of states was calculated using the Wien2k package. The obtained ratio of intensities of the quadrupole and dipole transitions is:

$$\frac{I_{quadrupole}}{I_{dipole}} \approx 0.1 \qquad (3.10)$$

Thus the x-ray pre-edge structure is mainly of dipole origin and the quadrupole transitions lead only to a small correction of the pre-edge structure.

It is interesting to compare the x-ray absorption spectrum of Mn^{3+} in (Ga,Mn)N with the spectrum of Mn^{2+} in other diluted magnetic semiconductors where the valence state of Mn is 2+. It is well known that Mn atoms have valence 2+ in (Zn,Mn)Te. This semiconductor crystallizes in the zinc-blende crystal structure and therefore substitutional Mn atoms have tetrahedral atomic environment like in wurtzite (Ga,Mn)N. Also the band structure of (Zn,Mn)Te is very similar to the band structure of (Ga,Mn)N: the 3*d* states of Mn are split by the exchange interaction (fig. 3.19), there is a 4*p*-3*d* hybridization of Mn states [20]. However there is an important difference in the position of 3*d* states: in the case of (Zn,Mn)Te the states are in the valence band and they are filled by electrons (electronic configuration $3d^5$). According to the proposed interpretation of the Mn pre-edge absorption structure the line A_2

arises from transitions to the t_2 band (spin up) of Mn. However this band is filled in (Zn,Mn)Te and transitions into this band are not possible. Thus the line A_2 should disappear in x-ray absorption spectra of (Zn,Mn)Te. Indeed, the line A_2 is not present in the x-ray absorption near-edge structure of Mn in (Zn,Mn)Te (fig. 3.20). Therefore it is possible to "see" experimentally whether the $3d$ states (spin up) of Mn are filled or not. This permits us to determine the valence state of Mn in diluted magnetic semiconductors.
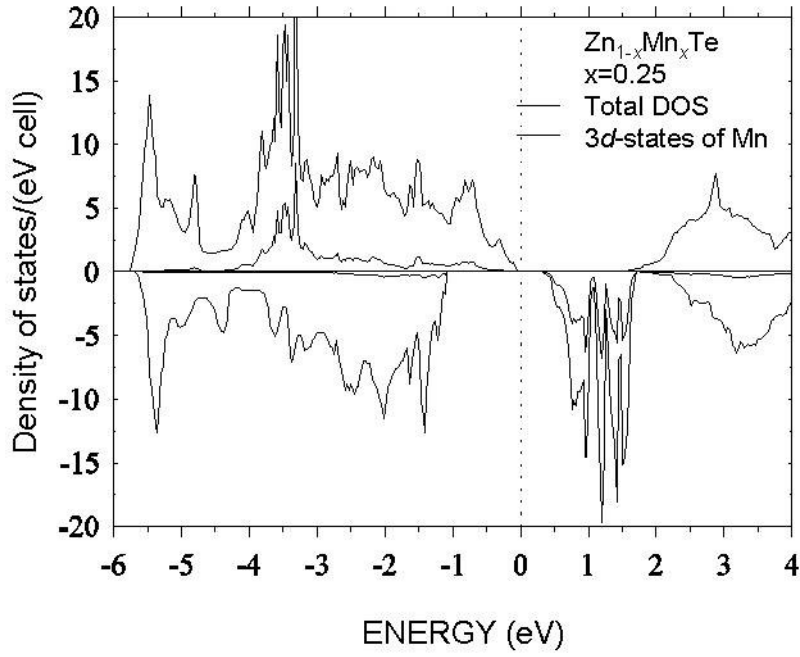
Fig. 3.19. Total density of states and density of Mn $3d$ states in $Zn_{1-x}Mn_xTe$ (x=0.25) [20]. The Fermi level is denoted by a vertical solid line at 0 eV.

Not only structure but the absorption edge position also depends on valence state of Mn. The absorption edge in x-ray absorption spectra is defined as the energy where the absorption coefficient accounts for 50% of its value at high energy, where the absorption coefficient saturates (see E_1 and E_2 in fig. 3.20). Of course this definition does not allow us to calculate precisely the absorption edge position because the absorption coefficient does not saturate and a fine structure remains at high energy. However this definition allows us to calculate approximately the edge position and the precision of this approach is sufficient to distinguish different electronic states of transition metals in semiconductors.
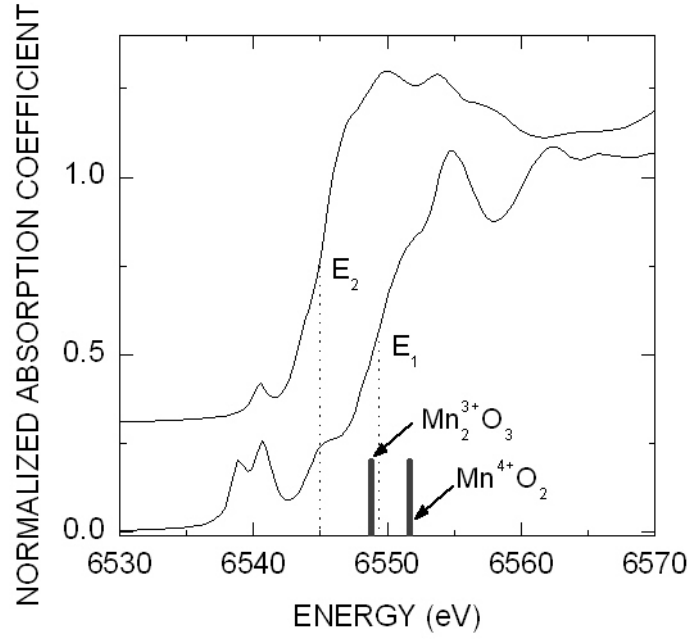
Fig. 3.20. X-ray absorption near-edge structure of Mn in (upward): $Ga_{1-x}Mn_xN$ ($x=0.057$, n type), $Zn_{1-x}Mn_xTe:N$ ($x=0.038$, p type). The x-ray absorption spectra were recorded by X. Biquard et al. [5]. The edge positions of Mn in Mn_2O_3 and MnO_2 from [5] are also shown.

It was observed for many compounds that the absorption edge shifts down to low energy when the valence of a transition metal decreases (see for example [5] where x-ray absorption spectra of Mn oxides are shown). Such a shift is observed in x-ray absorption spectrum of Mn in (Zn,Mn)Te: the absorption edge of Mn in (Zn,Mn)Te is shifted down as compared to the edge of Mn in (Ga,Mn)N (fig. 3.20). This implies a higher valence state of Mn in (Ga,Mn)N while the valence state of Mn in (Zn,Mn)Te is known to be 2+. A comparison absorption edge positions in different materials (edge positions of Mn in Mn_2O_3 and in MnO_2 are shown in fig. 3.20) confirms the 3+ valence state of Mn in (Ga,Mn)N [5].

In that way the calculated band structure agrees well with experimental data obtained on wurtzite (Ga,Mn)N epilayers. The calculation allow us to obtain a link between the band structure parameters and x-ray absorption near-edge structure of (Ga,Mn)N crystal. In particular, according to the interpretation of x-ray absorption near-edge structure of Mn, the first pre-edge line (A_2 in fig. 3.18) is due to transitions of $1s$ electrons to the t_2 band (spin up) of Mn, while the second pre-edge line (A_3 in fig. 3.18) is due to transitions to the t_2 band (spin

down). The presence of the line A_2 in x-ray absorption spectrum means that the $3d$ states (spin up) are not completely filled. The calculated population of $3d$ electrons near a Mn atom in (Ga,Mn)N is 4.29 e. This value points to the $3d^4$ electronic configuration and 3+ valence state of Mn in (Ga,Mn)N. The exchange splitting of the $3d$ states of Mn can be determined from the x-ray absorption spectra: it is 1.8 eV, it equals to the energy splitting between the absorption line A_2 and A_3.

3.5 Optical absorption spectra modeling

The valence state of Mn in (Ga,Mn)N can be also determined from optical absorption spectra of the semiconductor. An optical method has a number of important advantages as compared to x-ray absorption measurements and the method is very useful in studies of electronic properties of materials. Relatively low cost and high speed are two among the advantages. Another important advantage is a very high resolution that can be achieved in optical measurements which can be of the order of 0.5 meV [21]. This value has to be compared to the resolution obtained in x-ray absorption spectra (~1.5 eV for K-edge of Mn). Thus optical absorption allows a much more precise investigation of the electronic structure. However there is also an important shortcoming of optical methods: optical spectra are generally quite difficult to interpret. The hole which is left behind an excited electron is very close (in energy and in space) to the final state of the electron and the influence of the hole on the final state is not taken into account in modern *ab-initio* methods. At the same time this is not a critical problem in the case of x-ray absorption spectra since the core hole is very deep and often its influence can be taken partially into account (for example the FDMNES code [19] permits to treat the core hole).

So each method has its advantages and shortcomings and as usual the best is to use different methods which are more appropriate to solve a particular problem. Here I describe briefly an "optical" approach to solve the problem of the valence state and distribution of Mn in (Ga,Mn)N. As it will be shown later, optical absorption measurements also allow to study distribution of Mn in (Ga,Mn)N.

Optical absorption spectra of ions in different electronic configurations are quite different: absorption spectrum of Mn^{3+} ions contains a set of characteristic lines which are absent in the spectrum of Mn^{2+} ions. One of these characteristic lines of Mn^{3+} ions was theoretically found in [4]. The presence of this line in optical absorption spectra of (Ga,Mn)N was confirmed experimentally by several research groups [21,22,23]. According to the interpretation of the spectra proposed in [4], the absorption line is due to electronic transitions from the e band (spin up) to the t_2 band (spin up) of Mn. These transitions are only possible if the t_2 band (spin up) is not filled by electrons. Therefore the absorption line is indeed a characteristic line of Mn^{3+} ions (in the case of Mn^{2+} the t_2 band is filled). Let us consider the optical spectra modeling in detail.

Optical absorption of a solid can be described using the imaginary part of permittivity:

$$\varepsilon(\omega) = \varepsilon_1(\omega) + i\varepsilon_2(\omega). \tag{3.11}$$

Actually the permittivity is not a scalar quantity but a symmetric tensor of second order $\varepsilon_{ij}(\omega)$ and as every symmetric tensor of second order it can be diagonalized by an appropriate choice of the coordinate system [24]:

$$\varepsilon^{TENSOR} = \begin{pmatrix} \varepsilon_{xx} & 0 & 0 \\ 0 & \varepsilon_{yy} & 0 \\ 0 & 0 & \varepsilon_{zz} \end{pmatrix}. \tag{3.12}$$

The diagonal components of permittivity are equal each to other in cubic crystals

$$\varepsilon_{xx} = \varepsilon_{yy} = \varepsilon_{zz} = \varepsilon. \tag{3.13}$$

Therefore optical absorption in cubic crystals can be described by one quantity – the imaginary part of the diagonal matrix element (ε_2). The imaginary part of permittivity as a function of photon energy calculated for zinc-blende $Ga_{1-x}Mn_xN$ (x=0.0625, homogeneous distribution of Mn) [25] is shown in fig. 3.21.
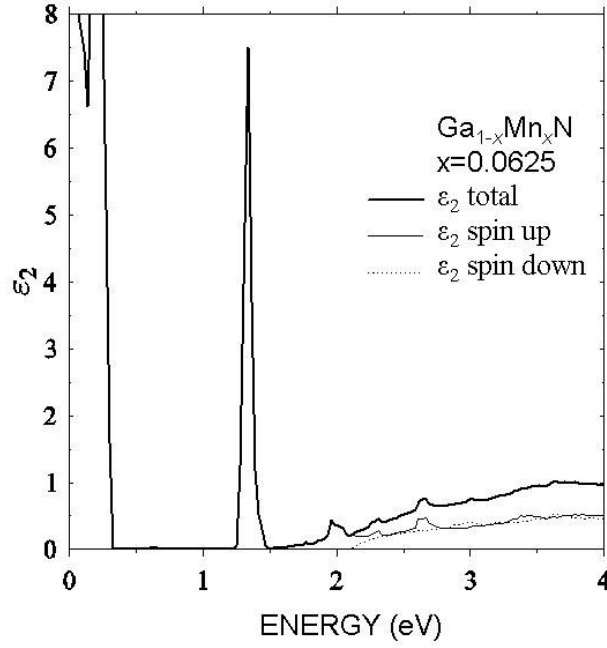
Fig. 3.21. Calculated imaginary part of the permittivity as a function of photon energy for zinc-blende $Ga_{1-x}Mn_xN$ ($x=0.0625$, homogeneous distribution of Mn) [25]. The intense absorption line at 1.3 eV is caused by internal electronic transitions of Mn from e band to t_2 band.

A very intense absorption line should be observed at 1.3 eV according to the calculation. An analysis performed in [4] shows that 95% of absorption at this energy are related to electronic transitions from the e band (spin up) to t_2 band (spin up). As we know the density of $4p$ states in e band (spin up) is close to 0. At the same time $4p$ orbitals of Mn are hybridized with $3d$ (t_2, spin up) orbitals in tetrahedral crystal field. Because of this hybridization electronic transitions from e band (spin up) to t_2 band (spin up) are permitted by the dipole selection rule:

$$\Delta l = \pm 1. \tag{3.14}$$

Therefore the absorption line at 1.3 eV could be very intense and it should be observed in experimental optical absorption spectra.

The crystal field has the tetrahedral symmetry in wurtzite (Ga,Mn)N and the $4p$-$3d$ hybridization of Mn orbitals results in a high intensity of p states in t_2 bands. Therefore the

intense absorption line at 1.3 eV should be observed in both zinc-blende and wurtzite (Ga,Mn)N.

Experimental investigations confirmed the presence of the intensive absorption line in optical spectra of wurtzite (Ga,Mn)N [21,22,23]. The optical absorption measurements show that this line is actually at 1.4 eV. Also it was shown that the absorption line is characteristic of Mn^{3+} ions. To prove it, Si atoms were incorporated in (Ga,Mn)N layers [23]. It is well known that Si has four valence electrons and it is an effective donor in (Ga,Si)N. Therefore incorporation of Si atoms in (Ga,Mn)N results in a raise of Fermi level and a change of Mn valence state from 3+ to 2+. If Mn has 2+ valence state in (Ga,Mn)N the t_2 band (spin up) is filled and electronic transitions to this band are impossible. In this case the absorption line is not observed in experimental spectra of (Ga,Mn,Si)N [23]. Thus presence of the absorption line in experimental optical absorption spectra of (Ga,Mn)N points to a high concentration of Mn^{3+} in investigated (Ga,Mn)N samples.

The crystal splitting between the e and t_2 bands (spin up) obtained from the *ab-initio* calculation can be checked using the optical absorption spectra: the position of the absorption line in the experimental optical absorption spectra (1.4 eV) equals to the crystal splitting between the e and t_2 bands (spin up). According to the *ab-initio* calculation [25], the splitting is 1.3 eV, close to the experimental value 1.4 eV.

X-ray absorption near-edge structure at the K-edge of Mn in (Ga,Mn)N was presented in the chapter I. It was shown that the double structure in the spectra points to 3+ valence state of Mn atoms. Optical absorption measurements performed on the same samples confirm this conclusion [21]: the intensive absorption line is observed in optical absorption spectra implying a high concentration of Mn^{3+} ions.

3.6 Transport properties (Ga,Mn)N

Important information about donor and acceptor impurities in a crystal can be obtained from transport measurements. Hall voltage measurements allow determining the concentration of carriers in a crystal. The mobility of the carriers can be calculated using the

carrier concentration and the conductivity of the crystal. Additional information can be deduced from Hall measurements at different temperatures. Such measurements permit to distinguish metals from semiconductors. For semiconductors the impurity activation energy can be determined from the temperature dependence of the carrier concentration $n(T)$.

Epitaxial layers of wurtzite GaN have n type conductivity. In pure GaN crystals the valence band should be filled and the conduction band separated by the gap from valence band should be empty. Therefore no conductivity is expected in this case and the GaN crystals should be insulating. The observed conductivity of n type can be related to donor defects which form shallow levels near the top of the conduction band. Atoms of Si [26], O [27] and N vacancies [26] are considered as possible donors in GaN. At room temperature these defects are ionized and the liberated electrons pass to the conduction band. The electrons become free and they can contribute to electrical conductivity.

At the same time Mg is an usual acceptor in (Ga,Mg)N. Incorporation of Mg in $Ga_{1-x}Mg_xN$, with the concentration $x=0.0005$ only, results in a change of conductivity type and the (Ga,Mg)N layers have p type conductivity [28]. A completely different behavior is observed when Ga atoms are replaced by Mn atoms in (Ga,Mn)N: wurtzite (Ga,Mn)N layers have n type conductivity just as wurtzite GaN layers. Our transport measurement show that the electron concentration in such (Ga,Mn)N layer is $\sim 10^{18}$ cm^{-3} and it does not correlate to the Mn concentration. The Mn concentration range in these samples was very wide: from $x=0.003$ to 0.057. Therefore it is quite difficult to explain such an independence of electrical properties of the (Ga,Mn)N layers if Mn is an acceptor or a donor in (Ga,Mn)N. It is interesting to note that co-doping of the (Ga,Mn)N samples by Mg changes significantly their properties: the samples became insulating [27]. Thus the performed transport measurements of (Ga,Mn)N layers confirm results of x-ray and optical investigations: Mn impurity is neither acceptor (Mn^{2+}) nor donor (Mn^{4+}) in (Ga,Mn)N; therefore the Mn has the neutral electronic configuration Mn^{3+} in (Ga,Mn)N.

Experimental investigations show that the electronic state of Mn changes under donor co-doping: Mn ions capture the extra electrons and become Mn^{2+} [23]. As it was shown previously (fig. 3.14) the $3d$ states of Mn^{3+} are localized near Mn ions and do not contribute to electrical conductivity. An experimental demonstration of this statement can be found in [22] where the 3+ valence state of Mn was found in $Ga_{1-x-y}Mn_xMg_yN$ samples and the samples were insulating. So if the Mn^{2+} ions also do not participate in electrical conductivity then it is

quite difficult to explain the residual *n* type conductivity observed in (Ga,Mn)N samples [22,29]. Thus it is quite natural to suppose that "excited" Mn^{2+} ions participate in the *n* type conductivity. Actually the specific mechanism of the conductivity is still unknown.

3.7 Distribution of Mn atoms in (Ga,Mn)N

Magnetic properties of (III,Mn)V diluted magnetic semiconductors strongly depend on the valence state of the magnetic impurity because the strength of magnetic interactions between magnetic ions depends on the concentration of holes (or electrons). Such a dependence is observed in (Ga,Mn)As crystals: *p* type (Ga,Mn)As layers are ferromagnetic while electrically compensated (Ga,Mn)As layers exhibit antiferromagnetic properties [30].

Another important factor influences magnetic properties of DMSs – it is the specific distribution of magnetic impurities in the crystal lattice. Semiconductors can be ferromagnetic or antiferromagnetic depending on the distances between neighbor Mn atoms. For example, it was shown that neighboring interstitial and substitutional Mn atoms may be antiferromagnetically coupled in (Ga,Mn)As [31] while (Ga,Mn)As epitaxial layers with a homogeneous distribution of Mn are ferromagnetic.

In (Ga,Mn)N epitaxial layers, Mn atoms substitute Ga atoms. The substitutional position of Mn in (Ga,Mn)N was confirmed be extended x-ray absorption fine structure measurements at K-edge of Mn [5]: high energy oscillations in x-ray absorption spectra of Mn caused by photoelectron wave reflections from neighbor atoms. Simulation of the spectra permits to determine the number of neighbor atoms and the distances to them. Thus a crystal can be locally reconstructed around the Mn atoms using the x-ray absorption measurements. However different adjustable parameters are used in such a simulation: numbers of first and second neighbors, distances to them and etc. Therefore it is difficult to state from the simulation that Mn atoms do not form closest substitutional pairs in (Ga,Mn)N. To "see" a neighbor Mn atom one needs to distinguish the contribution to EXAFS oscillations of a Mn atom from the contribution of other 11 neighbor Ga atoms.

It is interesting to note that the information about Mn-Mn closest pairs formation in (Ga,Mn)N can be obtained from near-edge part of x-ray absorption spectra. The EXAFS oscillations are not sensitive to the occurrence of one Mn atom among other 11 neighbor Ga atoms because of the significant contribution of the Ga atoms to the EXAFS oscillations. The density of $3d$ states in the gap of GaN is determined by Mn atoms only, neighbor Ga atoms do not contribute to the density. Therefore the pre-edge double line in x-ray absorption spectra of Mn described in previous sections should be sensitive to the occurrence of a neighbor Mn atom.

As it was mentioned above, the width of $3d$ bands in the gap depends on the concentration of Mn in (Ga,Mn)N, i.e. it depends on the distance between nearest neighbor Mn atoms. When the distance is very large (a few lattice parameters), the $3d$ bands are narrow. The width of $3d$ bands increases together with the concentration of Mn. If Mn atoms form closest substitutional pairs (or chains) in (Ga,Mn)N the $3d$ bands should be very wide. The bands of p states in the gap also become wider together with the $3d$ bands.

These effects were confirmed by a band structure calculation performed for zinc-blende (Ga,Mn)N in [25]. An orthorhombic supercell $2\sqrt{2}a_0 \cdot \sqrt{2}a_0 \cdot 2a_0$ was used in the calculation; here a_0 is the lattice parameter of GaN. Two Ga atoms were replaced by Mn atoms in the supercell, hence this supercell corresponds to a $Ga_{1-x}Mn_xN$ crystal with a Mn concentration $x=0.0625$, the ferromagnetic alignment of spins of the atoms was assumed. The distance between the two nearest neighbor Mn atoms in the supercell is $a_0/\sqrt{2}$. This is the smallest possible distance between two substitutional Mn atoms in zinc-blende (and in wurtzite) (Ga,Mn)N.

The density of Mn $4p$ states in zinc-blende $Ga_{1-x}Mn_xN$ ($x=0.0625$) with a homogeneous distribution of Mn is shown in fig. 3.22a (the same density was shown in fig. 3.10c). In this case the overlap of $3d$ orbitals of neighbor Mn atoms is small. The $3d$ bands are very narrow and they are in the band gap. The $4p$ orbitals of Mn are hybridized with the $3d$ orbitals and there is a high density of empty p states in the t_2 bands with spins up and down. Electronic transitions to the narrow $3d$ bands are present in x-ray absorption spectra as the double pre-edge line (fig. 3.22c).

The picture described above changes significantly when Mn atoms form close pairs in (Ga,Mn)N (fig. 3.22b). Overlap between $3d$ orbitals of nearest neighbor Mn atoms is more important in this case and the t_2 bands of Mn becomes wider. Electronic transitions to the

bands are possible but they should result in a single wide absorption line in x-ray absorption spectra (fig. 3.22d). Therefore one should observe one broad pre-edge line in x-ray absorption spectra of Mn if all Mn atoms form close pairs (or chains). This permits us to determine the distribution of Mn in (Ga,Mn)N using x-ray absorption spectra.
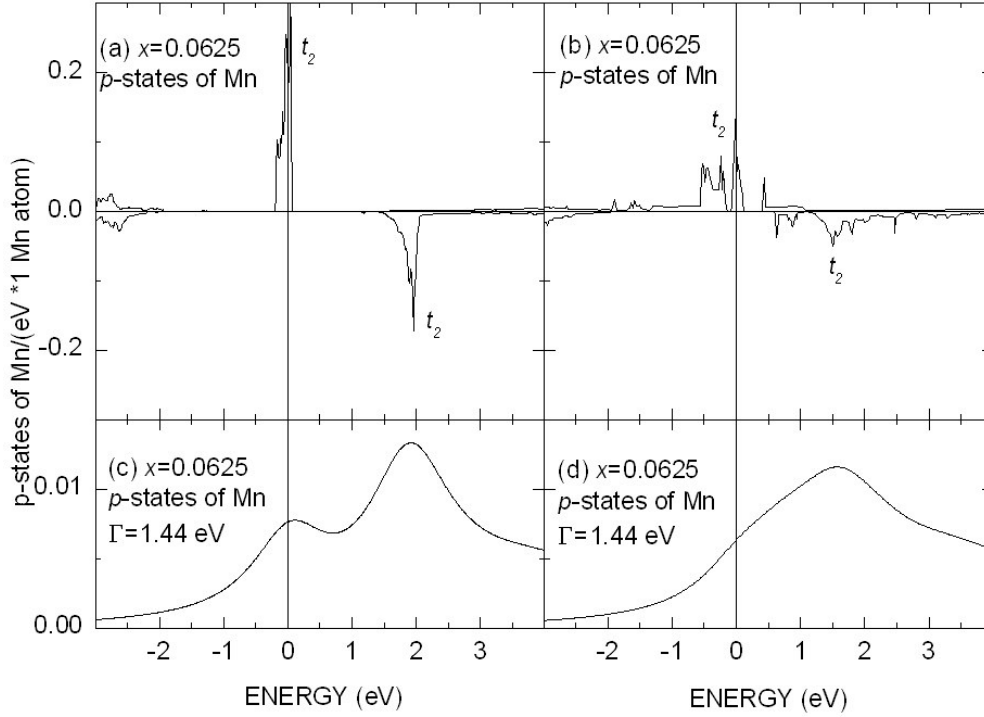
Fig. 3.22. Density of $4p$ states of Mn in zinc-blende $Ga_{1-x}Mn_xN$ (x=0.0625): (a) homogeneous distribution of Mn [4]; (b) Mn atoms forming close pairs (the distance between two Mn is $a_0/\sqrt{2}$) [25]; (c) sum of densities (spins up and down) of p states shown in the fig. a convoluted with the Lorentz function (parameter Γ=1.44 eV); (d) sum of densities (spins up and down) of p states shown in the fig. b convoluted with the Lorentz function (parameter Γ=1.44 eV).

Let us estimate the precision of the method when some Mn atoms are distributed homogeneously in (Ga,Mn)N but other Mn atoms form close pairs. In this case the pre-edge absorption structure in fig. 3.22c is superimposed to the pre-edge structure in fig. 3.22d. To perform this estimation it is very important to obtain a good fit of the pre-edge absorption double lines in experimental x-ray absorption spectra, therefore the core lifetime and the finite resolution of the monochromator will be taken into account (the pre-edge structure was fitted

using the Lorentz function only in the previous figures). Thus the calculated x-ray absorption spectrum is broadened now by the Voigt function [32]:

$$V(E,\Gamma_G,\Gamma_L) = \int G(\varepsilon,\Gamma_G)L(E-\varepsilon,\Gamma_L)d\varepsilon, \qquad (3.15)$$

here Γ_L and Γ_G are natural the width of $1s$ level and resolution of the monochromator correspondingly (see formulas 3.6 and 3.8).

The resolution of the monochromator was estimated from a fit of pre-edge structure of Mn in $Ga_{1-x}Mn_xN$ (x=0.003). The Mn concentration in the sample is very low and the width of $3d$ bands was chosen to be 0.01 eV. The natural width of $1s$ core hole (Γ_L) was fixed to 1.16 eV [17], it is expected that this value does not depend on the host semiconductor. The lifetime of exited photoelectron with small energy is expected to be very long and therefore the broadening caused by the photoelectron is very small. That is why this broadening was neglected in the fit. Then there is only one broadening parameter to be found – the resolution of the monochromator (Γ_G). A good fit of the pre-edge structure was obtained using Γ_G=0.50 eV (fig. 3.23a). Energy positions and intensities of the two absorption line (A_2 and A_3) were adjusted.

The obtained broadening parameter Γ_G=0.50 eV was further used to fit experimental pre-edge structure of Mn in $Ga_{1-x}Mn_xN$ (x=0.057). Now interaction between neighbor Mn atoms should be taken into account, so the calculated pre-edge structure for $Ga_{1-x}Mn_xN$ (x=0.0625, fig. 3.16) was used to fit the experimental spectrum. The obtained fit is shown in fig. 3.23b. Energy positions and intensities of the two absorption line (A_2 and A_3) were adjusted. It is worth to remember that the pre-edge structure was calculated using a supercell with a homogeneous distribution of Mn. The good fit of experimental pre-edge structure indicates a homogeneous distribution of Mn in $Ga_{1-x}Mn_xN$ (x=0.057) sample.

Let us consider a mixed distribution of Mn: 50% of Mn atoms are distributed homogeneously and other 50% of Mn atoms form close pairs. Superposition of the two x-ray absorption spectra shown in fig. 3.22d and 3.23b results in the spectrum presented in fig. 3.24a. The spectrum differs from the x-ray absorption spectrum of homogeneously distributed Mn atoms (fig. 3.23b). And this mixed distribution of Mn in (Ga,Mn)N can be distinguished from the homogeneous distribution. However the low resolution of x-ray absorption spectra (cased by the natural width of $1s$ level – 1.16 eV) limits the precision of the method. For

example x-ray absorption spectrum of (Ga,Mn)N with 70% homogeneously distributed Mn atoms will be
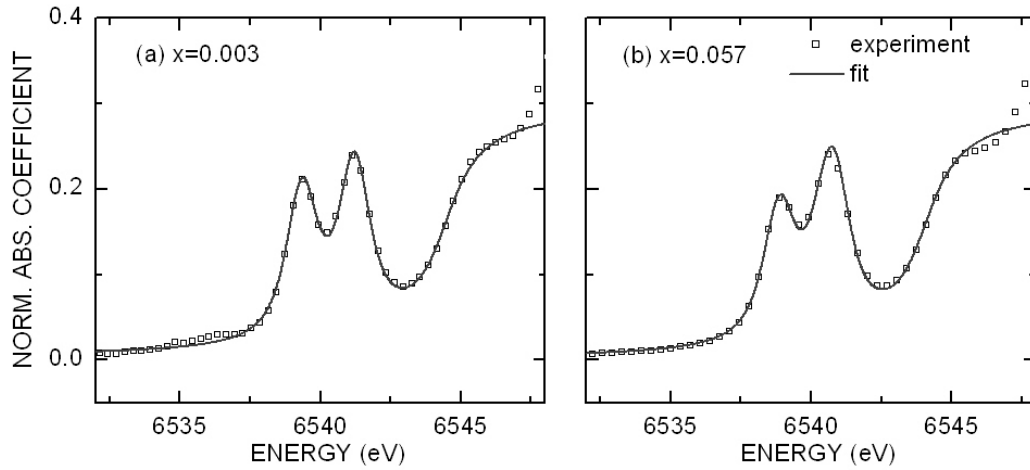
Fig. 3.23. (a) Experimental x-ray absorption structure of Mn in $Ga_{1-x}Mn_xN$ (x=0.003, symbols) and a fit of the spectrum (solid line), the resolution of monochromator is found to be 0.50 eV from this fit, the natural width of $1s$ core hole is assumed to be 1.16 eV; (b) experimental x-ray absorption structure of Mn in $Ga_{1-x}Mn_xN$ (x=0.057) and a fit of the spectrum using calculated widths of the $3d$ bands of Mn in $Ga_{1-x}Mn_xN$ (x=0.0625). The same values of the monochromator resolution (0.50 eV) and of the natural width of $1s$ level (1.16 eV) were used.
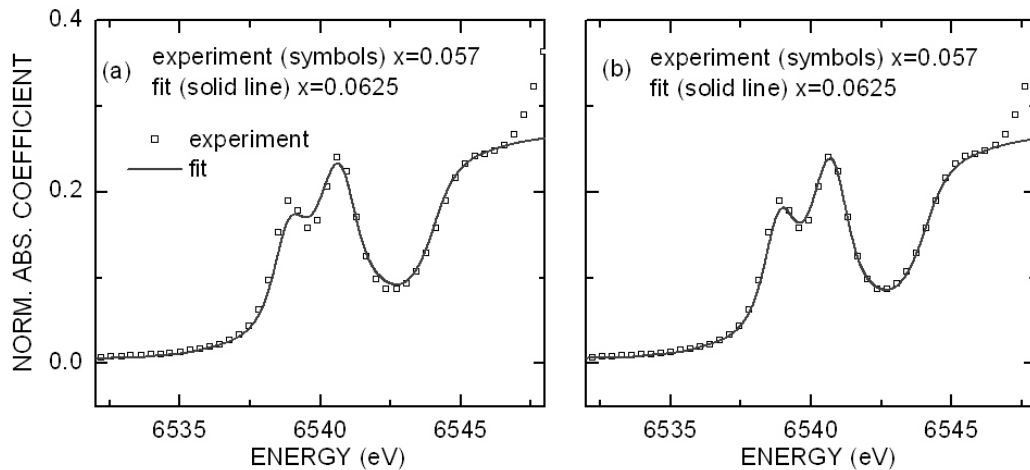
Fig. 3.24. Superposition of the fit in fig. 3.23b (homogeneous distribution of Mn) and calculated x-ray absorption spectrum of Mn in $Ga_{1-x}Mn_xN$ (x=0.0625) where pairs of Mn are formed (fig. 3.22d): (a) 50% and (b) 70% of Mn atoms are distributed homogeneously. The superposition is denoted by a solid line. Experimental pre-edge absorption structure of Mn in $Ga_{1-x}Mn_xN$ (x=0.057) is shown by symbols.

hardly distinguished from the spectrum of (Ga,Mn)N with 100% homogeneously distributed Mn atoms (fig. 3.24b).

Information about the distribution of Mn in (Ga,Mn)N can be also obtained from optical absorption spectra. The optical method has an advantage over the x-ray absorption method because of a higher resolution of optical spectra. The absorption line at 1.3 eV (fig. 3.21) corresponds to electronic transitions from e (spin up) to t_2 bands (spin up) in (Ga,Mn)N. In (Ga,Mn)N with a homogeneous distribution of Mn, the e and t_2 bands are situated in the band gap. The e and t_2 bands are very narrow in $Ga_{1-x}Mn_xN$ with a low concentration of Mn ($x<0.001$). However in $Ga_{1-x}Mn_xN$ ($x=0.0625$) with a homogeneous distribution of Mn the e and t_2 bands are wider and the calculated width of the absorption line at 1.3 eV is 0.25 eV [25], this width is determined by the overlap of the $3d$ orbitals of nearest neighbor Mn atoms. In experimental optical absorption spectra measured on a $Ga_{1-x}Mn_xN$ ($x=0.06$) sample at low temperature (fig 3.3 in [33], T=5K, the sample is similar to other (Ga,Mn)N samples studied by the x-ray absorption spectroscopy in precedent chapters) the width of the absorption line is also 0.25 eV, this value coincide with the calculated width of the absorption line in $Ga_{1-x}Mn_xN$ ($x=0.0625$) with homogeneous distribution of Mn. Therefore the experimental measurements confirm a homogeneous distribution of Mn in (Ga,Mn)N epilayers.

The band structure of (Ga,Mn)N crystals where Mn atoms form close pairs differs from the band structure of (Ga,Mn)N with a homogeneous distribution of Mn. The main differences are: (*i*) the density of states decreases in the center and increases in the sides of the t_2 band (spin up) [34]; (*ii*) the e band (spin up) is shifted to the valence band and it become wider [25]. The first change of band structure leads to occurrence of an intensive absorption line at 0.5 eV (fig. 3.25) which arises from internal transitions in the t_2 band (spin up) [34]. This absorption line was not observed experimentally. The second change leads to a broadening and a shift of the absorption line from 1.3 eV to 1.5 eV. The broadening is caused by hybridization the e band (spin up) with the valence band. The calculated width of the absorption line at 1.5 eV is about 0.4 eV. This broadening is not observed in experimental optical spectra: as it was mentioned above the experimentally observed line width is only 0.25 eV.

Thus one can conclude that the distribution of Mn in (Ga,Mn)N samples is essentially homogeneous. This result is confirmed by x-ray absorption as well as optical absorption measurements.
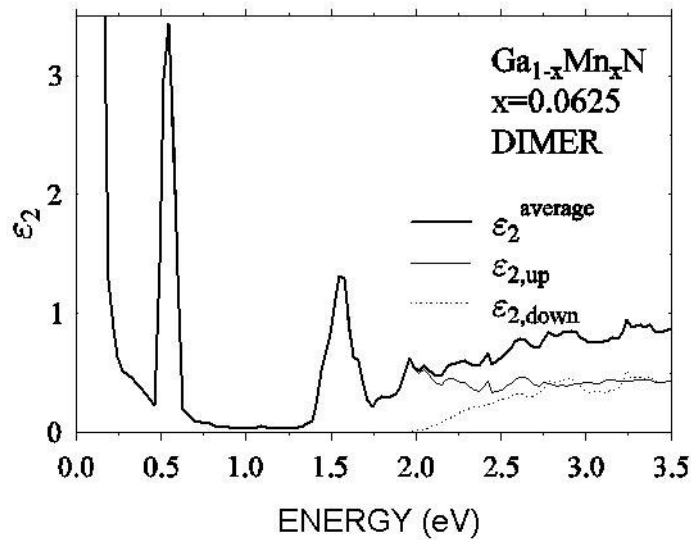
Fig. 3.25. Imaginary part of permittivity as a function of photon energy calculated for zinc-blende $Ga_{1-x}Mn_xN$ (x=0.0625, Mn atoms form close pairs) [25]. The intensive absorption line at 1.5 eV is caused by internal electronic transitions of Mn from e band to t_2 band.

3.8 Electronic properties of (Ga,Mn)As

The (Ga,Mn)As semiconductor is intensively studied during last years and a lot of experimental results obtained on (Ga,Mn)As samples are available now. These results will be useful for the study of (Ga,Mn)N. Also the band structures of (Ga,Mn)As and (Ge,Mn) semiconductors are similar. Therefore these results allow us to predict electronic properties of (Ge,Mn). In addition some limitations of the *ab-initio* calculations will be shown: an *ab-initio* calculation of (Ga,Mn)As properties predicts an absorption line in x-ray absorption spectra which is not observed experimentally. That is why I present here my results of *ab-initio* calculations performed for (Ga,Mn)As semiconductor.

The diluted magnetic semiconductor (Ga,Mn)As crystallizes in the zinc-blende structure shown in fig. 3.1 where N atoms have to be replaced by As atoms. Every Ga atom has four nearest neighbor As atoms which form a regular tetrahedron around the Ga atom. The second

neighbors of every Ga atom are twelve other Ga atoms which are placed at the same distance from the central Ga atom (tab. 3.7).

Tab. 3.7. Crystal structure and band parameters of zinc-blende GaAs.

parameter	value	reference
band gap at T=300K (eV)	1.420 – 1.435	[2]
lattice parameters at T=300K (Å)	5.65	[2]
crystal volume per 1 atom ($Å^3$)	22.58	calculation
number of nearest neighbors for a Ga atom distance to the atoms (Å)	4 atoms of As 2.45	calculation
number of second neighbors for a Ga atom distance to the atoms (Å)	12 atoms of Ga 4.00	calculation

The gap of GaAs (E_G=1.4 eV) is smaller than the gap of GaN (E_G=4.3 – 4.5 eV). This difference between the gap widths leads to a complete merging of Mn $3d$ bands (spin up) with the valence band. The Fermi level is pinned in the top of the valence band and the $3d$ bands (spin up) of Mn are filled by 5 electrons. Such a change of electronic state of Mn (Mn atoms have $3d^4$ electronic configuration in GaN) leads to a change in electrical, optical and magnetic properties of (Ga,Mn)As. Let us consider the electronic structure of (Ga,Mn)As in detail.
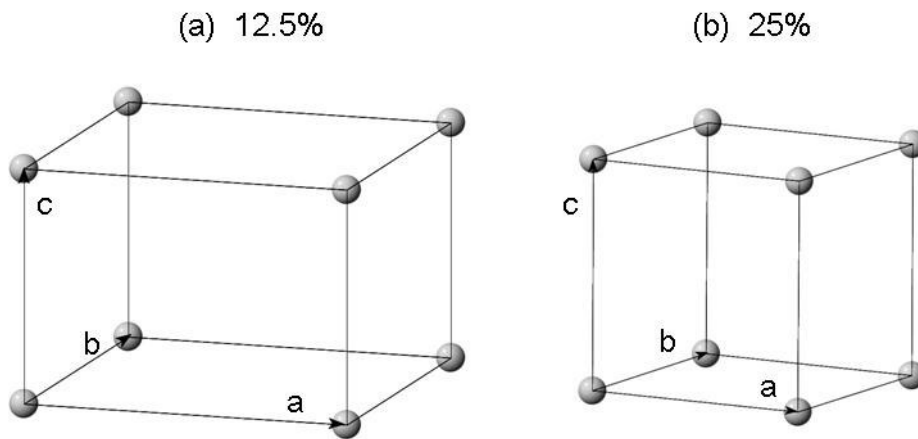

Fig. 3.26. Supercells of zinc-blende $Ga_{1-x}Mn_xAs$ with Mn concentration (a) x=0.125 and (b) x=0.25 were used in the band structure calculation. Only Mn atoms are shown in the supercells.

Tab. 3.8. Lengths of primitive translation vectors for the tetragonal and cubic supercells of (Ga,Mn)As (fig. 3.26), a_0 – lattice parameter of GaAs.

concentration of Mn atoms, x	a	b	c
0.125	$\sqrt{2}a_0$	$\sqrt{2}a_0$	a_0
0.25	a_0	a_0	a_0

The tetragonal supercell of (Ga,Mn)As were used in band structure calculation of $Ga_{1-x}Mn_xAs$ (fig. 3.26a). Primitive translation vectors for the supercell are listed in tab. 3.8. This cell maintains 1 Mn atom, 7 Ga and 8 As atoms. Therefore the concentration of Mn in $Ga_{1-x}Mn_xAs$ crystal based on the supercell is 0.125.

A smaller supercell was used to optimize the lattice parameter and the distances Mn-As between Mn atoms and nearest neighbor As atoms (fig. 3.26b). The supercell maintains 1 Mn atom, 3 Ga and 4 As atoms, so the concentration of Mn is 0.25. The total energy as a function of supercell volume was calculated to optimize the lattice parameter a_0 (fig. 3.27). A minimum of the $E(V)$ function corresponds to the optimal value of lattice parameter. The $E(V)$ function calculated by LAPW method [13] using the generalized gradient approximation [14] is shown in fig. 3.27. In addition several grids in reciprocal **k**-space were used to estimate necessary number of **k**-points to obtain a parabolic like dependence of the $E(V)$ function.
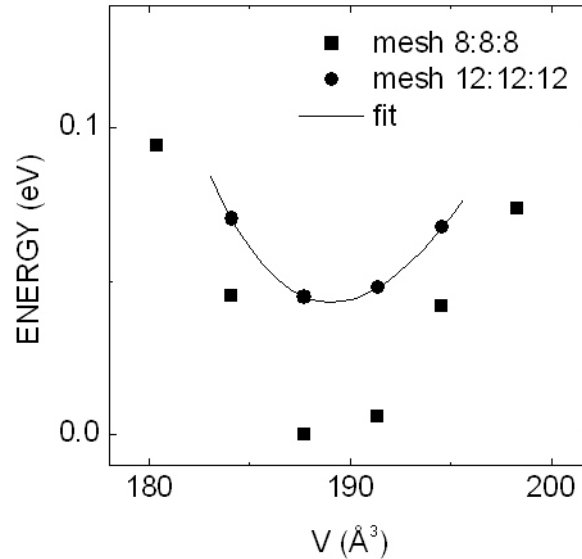

Fig. 3.27. Total energy of $Ga_{1-x}Mn_xAs$ ($x=0.25$) supercell as a function of the cell volume calculated on 8:8:8 (squares) and 12:12:12 (circles) meshes in reciprocal **k**-space. Solid line denotes a fit of the $E(V)$ function by a polynomial of third degree.

The $E(V)$ function calculated on the 8:8:8 mesh is shown by squares in fig. 3.27. This mesh was constructed in the following way. The first Brillouin zone of a cubic primitive lattice is a cube. Each from the three orthogonal cube edges (along the $\mathbf{k}_x$, $\mathbf{k}_y$ and $\mathbf{k}_z$ axes) are divided by 8 $\mathbf{k}$-points with an equal distance between two neighbor points. All combinations of these $\mathbf{k}$-coordinates (k_x, k_y, k_z) constitute the mesh 8:8:8. It is clear from fig. 3.27 that the mesh is not sufficiently fine to reproduce the parabolic like dependence of E(V) function. A better result for $E(V)$ function an be obtained on a 12:12:12 mesh. The Brillouin zone of $Ga_{1-x}Mn_xAs$ (x=0.125) crystal is two times smaller than the Brillouin zone of $Ga_{1-x}Mn_xAs$ (x=0.25), therefore less $\mathbf{k}$-points are necessary to perform a good calculation.

The calculated value of lattice parameter which corresponds to the minimum of total energy is a_0=5.744Å. This value is 1.7% greater than the experimental lattice parameter of GaAs (see tab. 3.7). Actually, the optimal value of lattice parameter obtained using the generalized gradient approximation is usually greater than experimental value of the parameter [29]. However such an increase of lattice parameter usually does not lead to a significant change in the band structure.

The Mn atoms incorporated in (Ga,Mn)As locally distort the crystal lattice. An EXAFS simulation of the K-edge absorption spectra of Mn shows, that Mn-As distance between a Mn atom and its nearest neighbor As atoms in (Ga,Mn)As is 2.2% greater than Ga-As distance in GaAs [35]: Mn atoms push away neighbor As atoms. At the same time the distance from Mn to second neighbors (Ga atoms) remains essentially the same. To take into account this distortion an optimization of As positions around a Mn atom was performed. The Mn-As was changed and the force $F(d_{\text{Mn-As}})$ acting to the As atoms was calculated. The optimal distance $d_{\text{Mn-As}}$ should be a root of the equation:

$$F(d_{Mn-As}) = 0 \,. \tag{3.16}$$

This optimization shows that the $d_{\text{Mn-As}}$ distance is 0.4% greater than the experimental value of $d_{\text{Ga-As}}$ distance in GaAs (the optimized $d_{\text{Mn-As}}$ distance was calculated using the optimized value of the lattice parameter a_0=5.744Å). However according to EXAFS measurement the $d_{\text{Mn-As}}$ distance in (Ga,Mn)As is 2.5% greater than the $d_{\text{Ga-As}}$ distance in bulk GaAs (a_0=5.65Å of bulk GaAs). According to the Vegard's law the lattice parameter of $Ga_{1-x}Mn_xAs$ (x=0.125) should be a_0=5.68Å [30]. Therefore we used an underestimated lattice parameter of

$Ga_{1-x}Mn_xAs$ (x=0.125) to obtain the theoretical value of the d_{Mn-As} distance and this may explain the huge difference between the theoretical and experimental d_{Mn-As} distances. Thus we conclude that the experimental lattice parameter of a crystal should be used to obtain real values for local distortions by impurity atoms.

The band structure of $Ga_{1-x}Mn_xAs$ (x=0.125) was calculated by the LAPW method [13] using the generalized gradient approximation [14] and the tetragonal supercell (fig. 3.26a). The wave function in the muffin tin spheres was expanded using the spherical harmonics Y^l_m and l_{max} was chosen to be 10. The same wave function was represented as series of plane waves out of the muffin tin spheres, and the $R_{min}·K_{max}$ were chosen to be 7 (here R_{min} – is the least muffin tin radius). Convergence to self-consistency was achieved on a 8×8×12 k-points mesh. The total energy was stable to within 10^{-5} Ry last a few iterations. Dispersion curves of energy with spin up and down are shown in fig. 3.28a and 3.28b correspondingly. The $3d$ states of Mn are shown by fat lines.
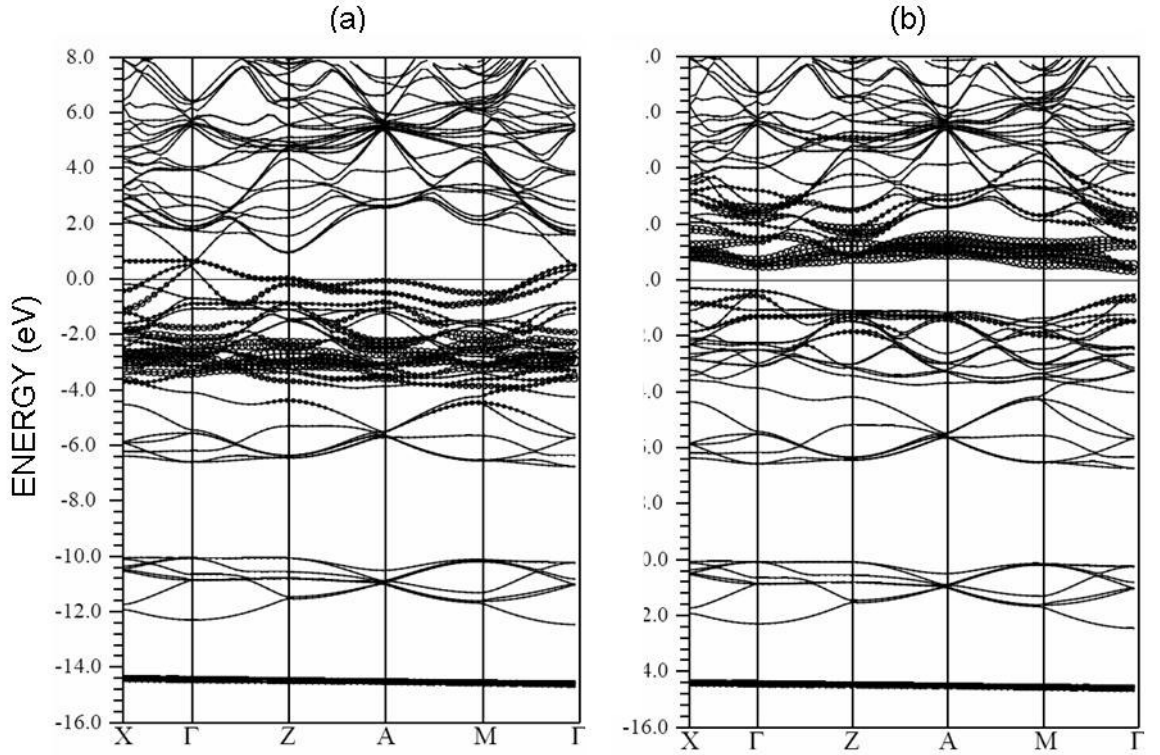
Fig. 3.28. The band structure of zinc-blende $Ga_{1-x}Mn_xAs$ (x=0.125) in ferromagnetic state. Electronic states (a) spin up and (b) spin down are shown. The $3d$ states of Mn are denoted by fat line. The Fermi level is shown by a horizontal line at 0 eV.

The gap is very narrow in GaAs and the wide $3d$ bands of Mn cover the gap field in this calculation. The effective mass of Mn $3d$ electrons should be smaller in (Ga,Mn)As than in (Ga,Mn)N because the $3d$ bands are wider in (Ga,Mn)As. In addition the width of the $3d$ bands points to a delocalization of $3d$ electrons with spin up in (Ga,Mn)As.

The exchange interaction of $3d$ electrons splits the $3d$ states of Mn with different direction of spin: the electrons whose spin points to the direction of magnetization (spin up) have smaller energy. In addition the $3d$ states are split by the crystal field caused by the four nearest neighbor As atoms. Just as in (Ga,Mn)N, the Mn atoms in (Ga,Mn)As are surrounded by four As atoms which form a tetrahedron around a Mn atom. The crystal field splits the $3d$ states into e and t_2 bands. Total and partial densities of states in ferromagnetic $Ga_{1-x}Mn_xAs$ ($x=0.125$) are shown in fig. 3.29. The $3d$ states (spin up) are situated in the valence band; they are filled and hybridized with the valence states. The Fermi level falls in the valence band leaving a hole in the top of the valence band.
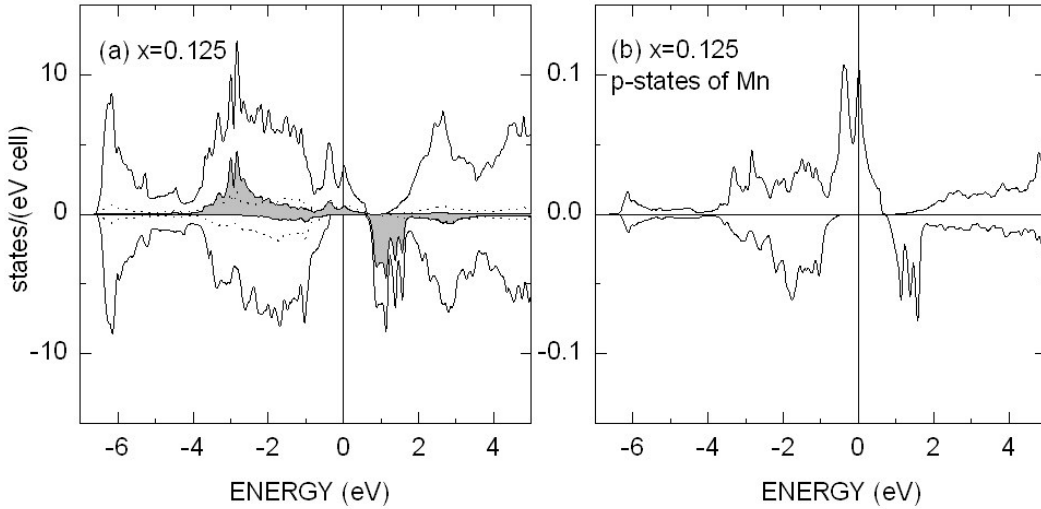
Fig. 3.29. (a) Total and partial densities of Mn states in ferromagnetic zinc-blende $Ga_{1-x}Mn_xAs$ ($x=0.125$). Electron states with spin up (upper part) and spin down (lower part of each figure) are shown. Total density of states is denoted by a solid line, $3d$ states of Mn shown by a filled area, $4p$ states of As shown by a dash line; (b) density of $4p$ states of Mn in $Ga_{1-x}Mn_xAs$ ($x=0.125$). The Fermi level is denoted by a vertical solid line at 0 eV.

The calculated number of $3d$ electrons in the muffin tin sphere of Mn is 4.9. The radius of the sphere was chosen according to the minimum of charge density between Mn and nearest neighbor As atoms [4]. This population of $3d$ states points to a d^5 configuration (2+ valence state) of Mn in (Ga,Mn)As. Early experimental works revealed the acceptor character of the Mn impurity in (Ga,Mn)As: samples with a high concentration of Mn have metallic conductivity of p type [30]. This agrees well with the calculated configuration d^5 of Mn in (Ga,Mn)As.
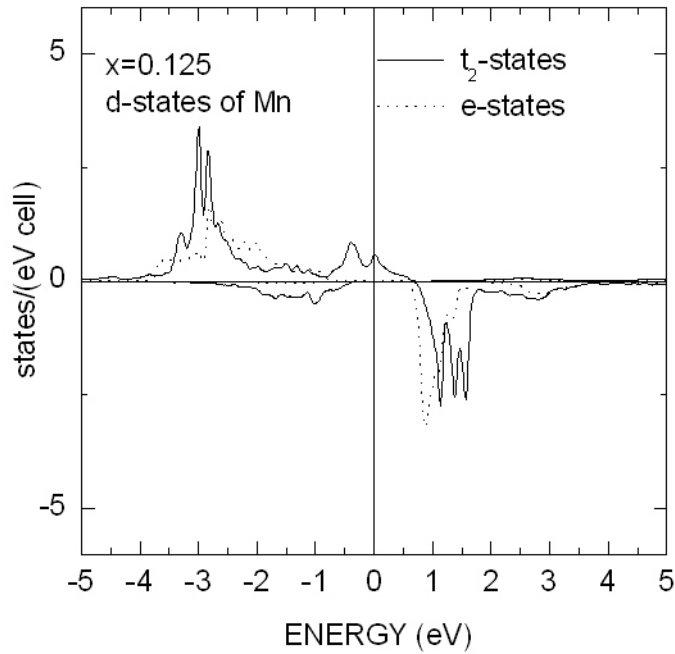
Fig. 3.30. Density of Mn $3d$ states in ferromagnetic zinc-blende $Ga_{1-x}Mn_xAs$ (x=0.125). Electron states with spin up (upper part) and spin down (lower part of each figure) are shown. The $3d$ states of t_2 and e symmetries are denoted by a solid and a dash lines correspondingly.

The energy distribution of e and t_2 bands is shown in fig. 3.30. The e band is formed by $2z^2$-x^2-y^2 and x^2-y^2 orbitals which weakly interact with nearest neighbor As atoms. The t_2 band is formed by xy, yz and xz orbitals. Quite to the contrary, these orbitals interact with the four neighbor As atoms and this interaction splits the t_2 band into a bonding part (under -1 eV) and an anti-bonding part (above -1 eV). This splitting of t_2 band into bonding and anti-bonding parts was also observed in (Ga,Mn)N (fig. 3.14), however in the case of (Ga,Mn)As

no gap is present between the bonding and anti-bonding parts. Therefore the density of states at the Fermi level is formed mainly by $2p$ states of N and anti-bonding t_2 states of Mn.

Calculated magnetic moments of atoms in (Ga,Mn)As are listed in tab. 3.9. The total magnetic moment of (Ga,Mn)As crystal ($4\mu_B$/Mn) is essentially concentrated near Mn atoms, the magnetic moment of Mn ($3.6\mu_B$) does not depend on the concentration of Mn. Magnetic moments of nearest neighbor As atoms are anti-parallel to the total and to Mn magnetic moments. As a result the total magnetic moment of (Ga,Mn)As crystal per one Mn atom is $4\mu_B$ in spite of $3d^5$ electronic configuration of Mn atoms.

Tab. 3.9. Calculated magnetic moments of different atoms in zinc-blende $Ga_{1-x}Mn_xAs$: total magnetic moment per one Mn atom (M_{tot}/1Mn), magnetic moment of Mn atom (M_{Mn}) and magnetic moment of nearest neighbor As atoms (M_{As}). Sign "-" means anti-parallel direction of magnetic moment relative to the total moment.

magnetic moment	concentration of Mn atoms, x	
	0.125	0.25
M_{tot}/1Mn (μ_B)	4.0	4.0
M_{Mn} (μ_B)	3.60	3.60
M_{As} (μ_B)	-0.05	-0.05

The $4p$ orbitals of Mn are hybridized with $3d$ orbitals of the same Mn atom. Just as in (Ga,Mn)N this hybridization is caused by tetrahedral arrangement of ligands (As atoms) around Mn atoms. The $4p$ orbitals acquire t_2 symmetry in the crystal field and hybridize the $3d$ states in t_2 bands (spins up and down). Thus there are two bands of high density of empty p states: t_2 (spin up) and t_2 (spin down) (fig. 3.29b).

It is interesting to compare the results of the band structure calculation with an experimental x-ray absorption spectrum of Mn in (Ga,Mn)As. A sample of $Ga_{1-x}Mn_xAs$ (x=0.08) was grown by low-temperature molecular-beam epitaxy in Nottingham (UK) [36]. X-ray absorption measurement at the K-edge of Mn in (Ga,Mn)As sample was performed by X. Biquard et al. [5]. The K-edge absorption spectrum of Mn is shown in fig. 3.31. According to the dipole selection rule only transitions of $1s$ electrons to empty p states are possible. According to our calculation the probability of transition of $1s$ electrons to Mn p (spin up) and Mn p (spin down) are similar. Therefore two absorption peaks (to the bands t_2 with spins up and down) should be observed in the K-edge absorption spectrum according to the band

structure calculation (fig. 3.29b). Experimental measurements show the presence of only the second peak while the first one is not observed (fig. 3.31).

We can suggest two reasons of this disagreement between the experiment and our calculation. (*i*) The t_2 band (spin up) of Mn is not completely filled according to our calculation in spite of the $3d^5$ electronic state of Mn in (Ga,Mn)As; therefore the $3d$-$4p$ hybridization of Mn states is still possible in the t_2 band (spin up). This error of the band calculations can be corrected when one replace the LDA exchange-correlation potential by the LDA+U one. It was shown that the density of $3d$ states at Fermi level decreases when the LDA+U potential is used [37]. (*ii*) A direct hybridization of the $4p$ states of Mn to the valence band is possible. This hybridization may lead to the high density of Mn $4p$ states near the Fermi level obtained in the calculation. But the $4p$ orbitals of Mn in the valence band should be delocalized and the transition probability between the localized $1s$ orbital of Mn and the delocalized $4p$ orbitals of Mn should be small. Therefore electronic transitions to these states are not observed.

These two reasons explain the discrepancy between our experimental and theoretical results: in the first case the correlation effects are not treated properly in our calculation; in the second case the localization of the $4p$ orbitals of Mn in the valence band is overestimated. It was not a problem in the case of (Ga,Mn)N because the two $3d$ bands (spins up and down) were situated in the gap and they were spatially localized. In the case of (Ga,Mn)As the $3d$ band (spin up) is in the valence band and the p states of Mn near the valence band are not described correctly by the *ab-initio* method.

It is interesting to note that the absorption edge of Mn is shifted downward in spectrum of (Ga,Mn)As as compared to the edge of Mn in the spectrum of (Ga,Mn)N (fig. 3.31). As it was mentioned above such a shift is typical of lower valence state of atom-absorber. Thus this shift agrees well with obtained valence states: Mn^{3+} in (Ga,Mn)N and Mn^{2+} in (Ga,Mn)As.

Therefore the x-ray absorption spectra permit to determine the valence state of Mn in different diluted magnetic semiconductors with tetrahedral arrangement of ligands. However a high resolution is necessary to distinguish pre-edge absorption lines associated to $1s$-t_2 (spin up) and $1s$-t_2 (spin down) electronic transitions. This resolution is limited by the natural width of $1s$ level (1.16 eV).
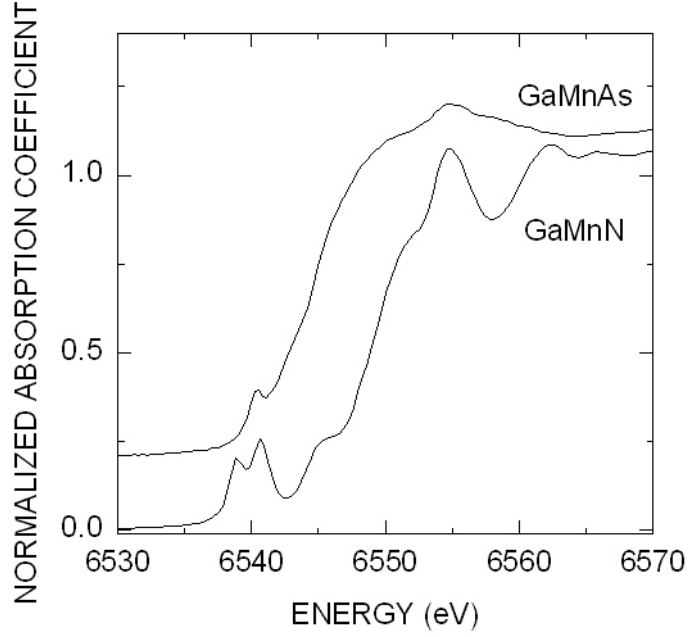
Fig. 3.31. Experimental K-edge x-ray absorption near-edge structure of Mn in (upward): $Ga_{1-x}Mn_xN$ (x=0.057) and $Ga_{1-x}Mn_xAs$ (x=0.08). The (Ga,Mn)As sample was grown in Nottingham [36], the x-ray absorption measurements were performed by X. Biquard et al. [5].

3.9 Electronic properties of (Ge,Mn)

The diluted magnetic semiconductor (Ge,Mn) has the diamond crystal structure. The crystal structure is shown in fig. 3.1a where both Ga and N atoms have to be replaced by Ge atoms. The Ge crystal has the cubic face-centered lattice and the basis of the crystal is formed by two Ge atoms in positions [1]

$$(0,0,0)\ a_0 \qquad (1/4,1/4,1/4)\ a_0,$$

where a_0 – is the lattice parameter of Ge crystal. Every Ge atom in a Ge crystal is surrounded by four Ge atoms placed at the vertices of a regular tetrahedron. The second neighbors of a Ge

atom are twelve other Ge atoms, which are placed at the same distances from the central Ge atom. The distances to the first and second nearest neighbors are listed in tab. 3.10.

Tab. 3.10. Crystal and band parameters of a Ge crystal.

parameter	value	reference
band gap at T=300K (eV)	0.65	[38]
lattice parameter at T=300K (Å)	5.66	[38]
crystal volume per 1 atom (Å^3)	22.61	calculation
number of nearest neighbors for a Ge atom distance to the atoms (Å)	4 Ge atoms 2.45	calculation
number of second neighbors for a Ge atom distance to the atoms (Å)	12 Ge atoms 4.00	calculation

The crystal volume per one atom is two times greater in Ge than the crystal volume in GaN. Another important difference between Ge and GaN is the relatively narrow band gap in Ge. In this case (just as in GaAs) the $3d$ states of Mn (spin up) fall down in the valence band. This position of $3d$ bands determines the electronic properties of (Ge,Mn). Let us consider the band structure of (Ge,Mn) in detail.

A cubic supercell (fig. 3.32) was used to calculate the band structure of Ge$_{1-x}$Mn$_x$ (x=0.125). The lattice parameter a_0 of Ge$_{1-x}$Mn$_x$ (x=0.125) was optimized using the same cubic supercell. With that end in view, the total energy of the cubic supercell was calculated for different lattice parameters. The minimum of the total energy $E(V)$ corresponds to the optimal volume V of the supercell. The $E(V)$ function calculated on different **k**-meshes using the LAPW method [13] is shown in fig. 3.33. The first Brillouin zone of a primitive cubic lattice is a cube. The first calculation was performed using the 2:2:2 **k**-mesh and eigenvalues of energy were calculated in vertices of the cube. It is clear from fig. 3.33 that the mesh is not sufficiently fine to obtain a parabolic like function $E(V)$. A better result for the $E(V)$ function can be obtained using the 4:4:4 **k**-mesh. The best parabolic dependence for $E(V)$ was achieved on 8:8:8 **k**-mesh. Thus the band structure of Ge$_{1-x}$Mn$_x$ (x=0.125) should be calculated on 8:8:8 or a finer **k**-mesh.
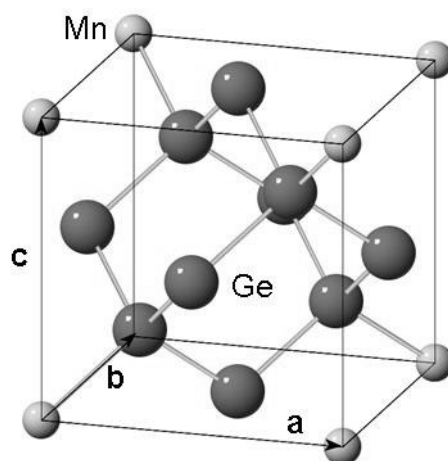
Fig. 3.32. Cubic supercell used for band structure calculation of $Ge_{1-x}Mn_x$ (x=0.125) crystal.
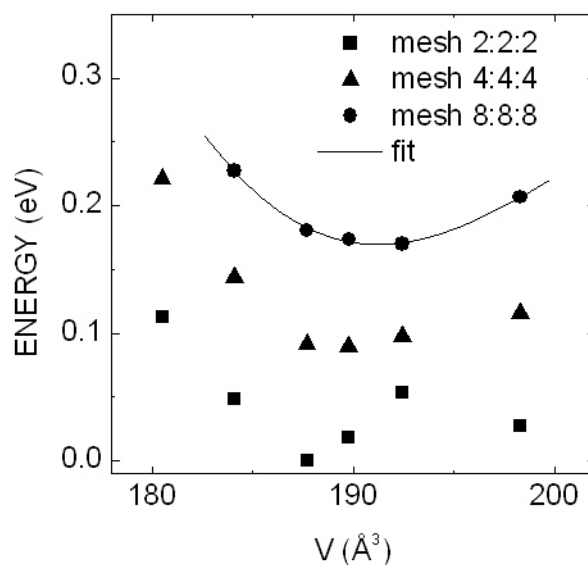
Fig. 3.33. Total energy of cubic supercell $Ge_{1-x}Mn_x$ (x=0.125) calculated on different **k**-meshes. Fit of the calculated $E(V)$ function by a polynomial of third order is shown by a solid line.

The optimized value of the lattice parameter obtained from the minimum of $E(V)$ function is 5.768Å. The experimental value of the lattice parameter for a Ge crystal is 5.66Å (tab. 3.10). Also, experimental investigations show a linear increase of the lattice parameter when the concentration of Mn increases [38]. An extrapolation of this linear dependence to the

concentration x=0.125 gives the value a_0=5.71Å of the lattice parameter for $Ge_{1-x}Mn_x$ (x=0.125). Therefore the value a_0=5.768Å obtained theoretically is compatible with the experimental data. It should be mentioned here that the calculated value was obtained using the generalized gradient approximation [14], usually this approach for the exchange-correlation potential leads to a larger lattice spacing, as it was in the case of GaN.

Atoms of Mn incorporated in a Ge crystal locally distort the crystal lattice. Therefore (Ge,Mn) crystal has not the diamond crystal lattice. To take into account this distortion, the positions of four Ge atoms (nearest neighbors of Mn atoms) in the cubic supercell (fig. 3.32) were optimized. The same optimization method was used as in the case of (Ga,Mn)As: the force $F(d_{Mn-Ge})$ acting to nearest neighbor Ge atoms was calculated as a function of the distance d_{Mn-Ge} between Mn and nearest neighbor Ge atoms. The optimal value of the distance should satisfy equation

$$F(d_{Mn-Ge}) = 0.$$ (3.17)

The optimal value of the d_{Mn-Ge} distance is only 0.1% greater than the undistorted d_{Ge-Ge} distance in Ge crystal. Previous calculations show that such a small distortion does not influence the band structure [6].

The band structure of $Ge_{1-x}Mn_x$ (x=0.125) was calculated using the cubic supercell (fig. 3.32) by the LAPW method [13] and the generalized gradient approximation [14]. Optimized lattice parameter and Ge positions were used. The crystal (Ge,Mn) obtained by translation of the supercell is ferromagnetic because only one Ge atom was replaced by a Mn atom in the supercell and Mn atoms in neighbor supercells have the same direction of magnetic moment. The muffin-tin radii were chosen equal for all atoms. The wave function in the muffin-tin spheres was expanded using the spherical harmonics Y^l_m, and l_{max} was chosen to be 10. The same wave function was represented as series of plane waves out of the muffin-tin spheres, and the $R_{min} \cdot K_{max}$ were chosen to be 7 (here R_{min} – is the least muffin tin radius). Convergence to self-consistency was achieved on a 10×10×10 **k**-mesh. The total energy was stable to within $2 \cdot 10^{-5}$ Ry last a few iterations. The calculated band structure is shown in fig. 3.34.
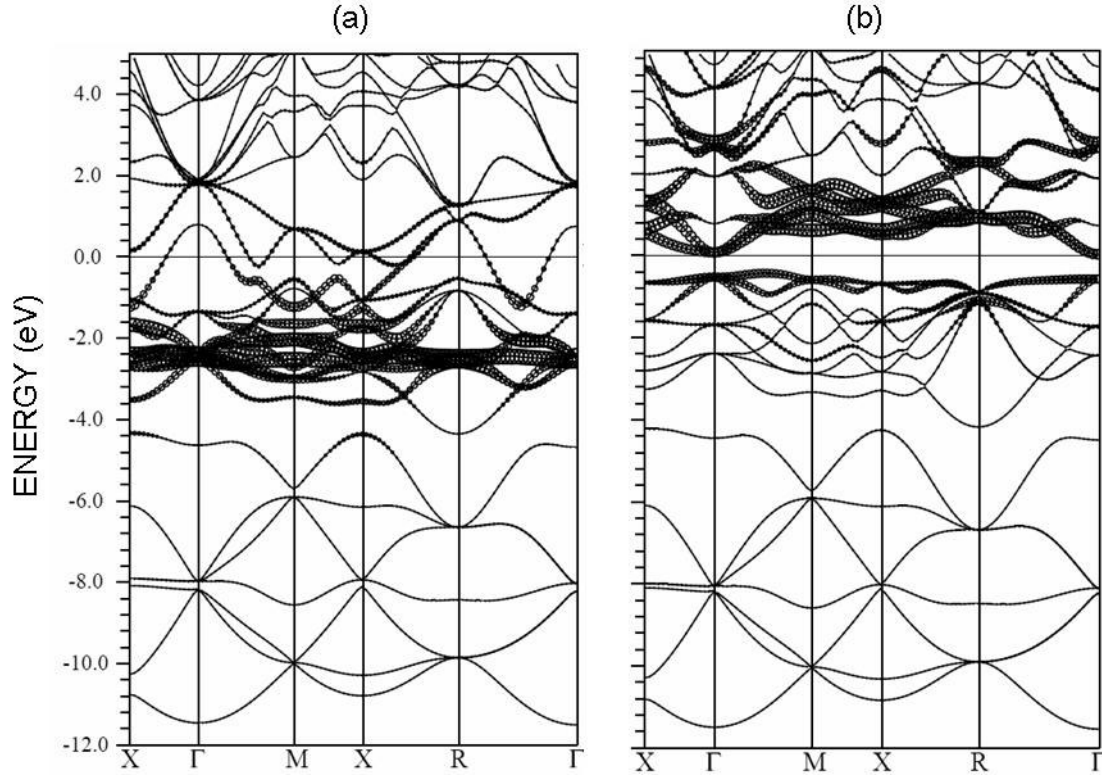
Fig. 3.34. Calculated band structure of ferromagnetic $Ge_{1-x}Mn_x$ (x=0.125). Electronic states with (a) spin up and (b) spin down are shown. The $3d$ states of Mn are marked by circles. The Fermi level is denoted by a solid horizontal line.

A small band gap (about 0.4 eV) is observed only in the band structure of electrons with spin down. The $3d$ states of Mn (spin up) are essentially situated in the valence band under the Fermi level. These states are delocalized and filled. The $3d$ bands in (Ge,Mn) are wider than in (Ga,Mn)N which points to a smaller effective mass and higher mobility of these electrons in (Ge,Mn). The band structure of (Ge,Mn) is quite similar to the band structure of (Ga,Mn)As. This similarity becomes clearer if one compare the partial densities of states in $Ge_{1-x}Mn_x$ (x=0.125) and $Ga_{1-x}Mn_xAs$ (x=0.125) (fig. 3.35).

The calculated population of $3d$ electrons in the muffin-tin sphere of Mn in (Ge,Mn) is 5.01e. This value has to be compared to the population of $3d$ bands in (Ga,Mn)As which is 4.90e. It should be noted that the muffin-tin radii of Mn spheres in (Ge,Mn) and (Ga,Mn)As and lattice parameters of these semiconductors are almost the same (the muffin-tin sphere in Ge is only 1.8% greater). Therefore the calculated population of $3d$ electrons in (Ge,Mn) is compatible to $3d^5$ electronic configuration of Mn atoms.
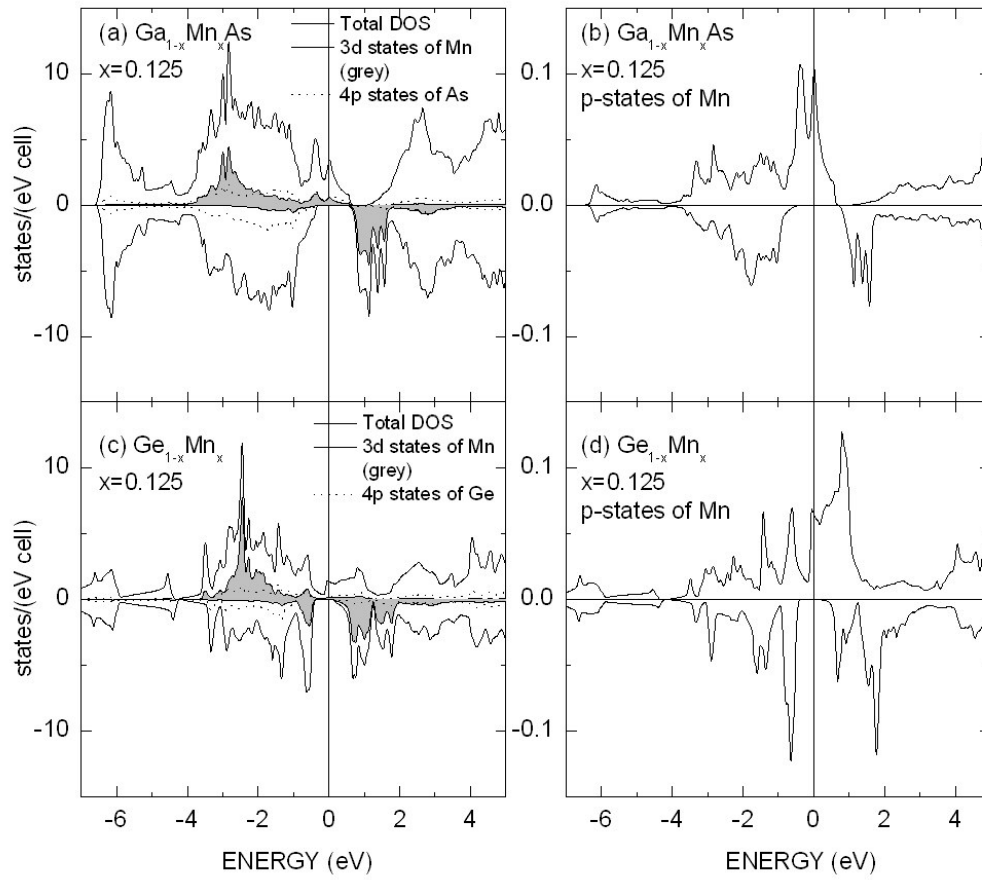
Fig. 3.35. Total and partial densities of Mn in ferromagnetic (a,b) $Ga_{1-x}Mn_xAs$ (x=0.125) and (c,d) $Ge_{1-x}Mn_x$ (x=0.125). Electron states with spin up (upper part) and spin down (lower part of each figure) are shown. Total density is denoted by a solid line, $3d$ states of Mn are shown by a filled area, $4p$ states of (a) As and (c) Ge are shown by a dash line. Density of $4p$ states of Mn in (b) $Ga_{1-x}Mn_xAs$ (x=0.125) and (d) $Ge_{1-x}Mn_x$ (x=0.125). The Fermi level is denoted by a vertical solid line at 0 eV.

Tab. 3.11. Calculated magnetic moments of different atoms in zinc-blende $Ge_{1-x}Mn_x$: total magnetic moment per one Mn atom (M_{tot}/1Mn), magnetic moment of Mn atom (M_{Mn}) and magnetic moment of nearest neighbor Ge atom (M_{Ge}). Sign "-" means anti-parallel direction of magnetic moment relative to the total moment.

magnetic moment	concentration of Mn atoms, x
	0.125
M_{tot}/1Mn (μ_B)	3.0
M_{Mn} (μ_B)	3.22
M_{Ge} (μ_B)	-0.08

The calculated total magnetic moment of the cubic supercell (fig. 3.32) per one Mn atom is $3\mu_B$ (tab. 3.11). Magnetic spin moments of nearest neighbor Ge atoms are opposite to the Mn magnetic moment.

Let us consider the structure of the $3d$ states of Mn in (Ge,Mn). The $3d$ states are split by exchange interaction into two bands: states of electrons with spin up and spin down. The band of electrons with spin up is situated in the valence band and filled by electrons while the band of electrons with spin down is in the gap above the Fermi level. In addition the two bands are split into a doubly degenerate e and a triply degenerate t_2 bands by crystal field caused by the tetrahedral arrangement of nearest neighbor Ge atoms (fig. 3.36). The e band is formed by $2z^2-x^2-y^2$ and x^2-y^2 orbitals while the t_2 band in formed by xy, yz and xz orbitals. These three orbitals interact stronger to $2p$ orbitals of Ge and this interaction splits the t_2 band into bonding (under -0.5eV) and anti-bonding (above -0.5eV) parts (fig. 3.36). Actually the latter splitting is not so sharp as it was in the case of (Ga,Mn)N. But the density of $3d$ states at the Fermi level clearly has t_2 character.
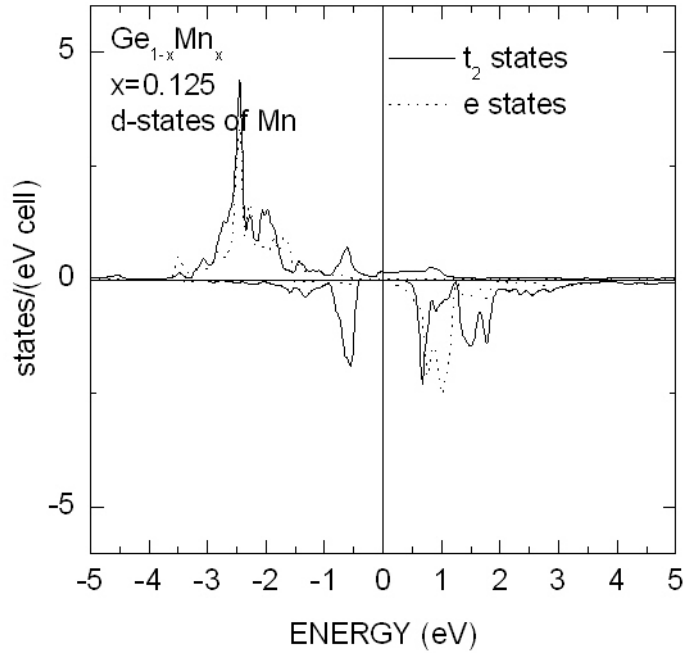
Fig. 3.36. Density of $3d$ states in $Ge_{1-x}Mn_x$ (x=0.125). Electron states with spin up (upper part) and spin down (lower part of each figure) are shown. Solid line shows t_2 states, a dash line shows e states. The Fermi level is denoted by a vertical line at 0 eV.

The position of the Fermi level depends however on the concentration of Mn in (Ge,Mn): a decrease of Mn concentration leads to a shift of the Fermi level downward in energy. Thus the Fermi level in $Ge_{1-x}Mn_x$ ($x=0.0156$) falls in the minimum of density of states (fig. 3.37). This position of the Fermi level agrees well with experimental data which show semiconducting temperature dependence of resistivity of $Ge_{1-x}Mn_x$ ($x=0.006-0.035$) samples in spite of 2+ valence state of Mn (double acceptor) in (Ge,Mn) [39]. Samples of (Ga,Mn)As with the same concentration of Mn per cm^3 exhibit metallic conductivity [30].
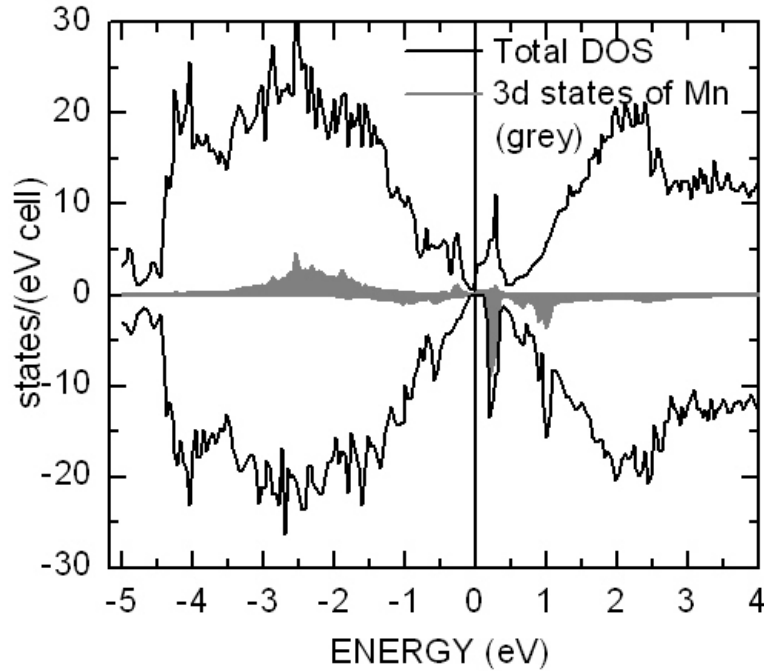
Fig. 3.37. Total and partial densities of Mn states in ferromagnetic $Ge_{1-x}Mn_x$ ($x=0.0156$). The calculation was performed by the LMTO method [8] within the local spin density approximation [40]. Experimental value of lattice parameter was used. Electron states with spin up (upper part) and spin down (lower part of each figure) are shown. Total density is denoted by a solid line, $3d$ states of Mn shown by a filled area. The Fermi level is denoted by a vertical solid line at 0 eV.

The $4p$ orbitals of Mn acquire the t_2 symmetry in the tetrahedral crystal field of four nearest neighbor Ge atoms. Therefore the $4p$ orbitals hybridize with the $3d$ orbitals of Mn in t_2 bands with spins up and down according to the formula (3.2). A high density of empty p states is also observed in e band (spin up). This density arises from the overlap of $3d$ orbitals of

neighbor Mn atoms. In the case of zinc-blende $Ga_{1-x}Mn_xN$ it was shown that this density is comparable to the density of p states in t_2 bands when the concentration of Mn is very high ($x{\sim}0.2$).

A high density of empty p states of Mn was calculated in the energy interval between 0 eV and 2 eV (spin up, fig. 3.35d) in (Ge,Mn). This density could be related to the p-d hybridization of Mn orbitals. However the density of $3d$ states is very low in this energy field. In addition it was shown in the case of (Ga,Mn)As that the density of $3d$ states at the Fermi level become negligible if the exchange-correlation interaction between $3d$ electrons is increased. Another possible contribution to the density of p states between 0 eV and 2 eV (spin up) may arise from hybridization of Mn p states to p states of Ge in the valence band. In this case the p orbitals of Mn should be delocalized because of delocalization of Ge p orbitals close to the valence band. Therefore the matrix element

$$M = \left\langle 1s \left| \nabla e \right| 4p \right\rangle \tag{3.18}$$

is small (overlapping of localized $1s$ and delocalized $4p$ orbitals is small). Thus transitions to Mn p states (spin up) should not be observed in XANES spectra of (Ge,Mn). As we know these transitions are not observed in XANES spectra of (Ga,Mn)As (fig. 3.31).

However this conclusion should be checked experimentally. According to the band structure calculations of (Ge,Mn) the valence state of Mn in (Ge,Mn) is 2+. Only one pre-edge peak (A_3) should be present in the XANES spectra of (Ge,Mn). In general according to the band calculation, the K-edge of Mn should be similar to the K-edge of Mn in (Ga,Mn)As (fig. 3.31).

Summary for chapter III

(Ga,Mn)N

The band structure of the diluted magnetic semiconductor (Ga,Mn)N was calculated. According to the calculation the $3d$ states of Mn are situated in the gap of GaN. The $3d$ states of Mn are split by exchange interaction between $3d$ electrons of the same atom: the $3d$ states (spin up) are placed under the $3d$ states (spin down). In addition, the two $3d$ bands are split by the crystal field caused by the four nearest neighbor N atoms. As a result the $3d$ states of Mn (spin up) are split into a doubly degenerated e and a triply degenerated t_2 bands which are localized in the gap. The Fermi level falls in the t_2 band (spin up); a third part of the band is empty. The calculated electronic configuration of Mn in (Ga,Mn)N is $3d^4$ (valence state of Mn is 3+).

An interpretation of the K-edge x-ray absorption near-edge structure of Mn in (Ga,Mn)N was proposed. This interpretation allows to link the experimental x-ray absorption spectra to electronic properties of real (Ga,Mn)N crystals. In particular, it was experimentally shown that the valence state of Mn in (Ga,Mn)N is 3+. Furthermore, the interpretation allows us to study the distribution of Mn in crystal lattice of diluted magnetic semiconductors: it was shown that the majority of Mn atoms are distributed homogeneously in (Ga,Mn)N epilayers.

Optical absorption experiments allow to obtain an important information about the electronic structure of (Ga,Mn)N. An intense absorption line at 1.4 eV is present in optical absorption spectra of Mn in (Ga,Mn)N [21,22,23]. This absorption line is characteristic of Mn^{3+} ions, it is not observed in the spectra of Mn^{2+} ions [23]. Therefore the optical absorption measurements confirm 3+ valence state of Mn in (Ga,Mn)N. According to *ab-initio* calculations, formation of close Mn-Mn pairs in (Ga,Mn)N would change the optical absorption spectra: the absorption line would shift to 1.55 eV, another intensive absorption line would appear at 0.5 eV [25,34].

Our electric transport measurements show that Mn is neither acceptor nor donor but present as a neutral impurity center in (Ga,Mn)N crystals.

(Ga,Mn)As

The band structure of (Ga,Mn)As was calculated by the LAPW method. According to the calculation the $3d$ states of Mn (spin up) are mainly situated in the valence band under the Fermi level. These states are filled by electrons and they are strongly hybridized with the valence band. The Fermi level falls into the valence band and the top of the valence band is empty.

The total magnetic moment of (Ga,Mn)As crystal ($4\mu_B$ per one Mn atom) is localized near Mn atoms. Calculated magnetic moments of nearest neighbor As atoms are oppositely directed to the Mn moment.

Calculated number of $3d$ electrons in the muffin-tin sphere of Mn is 4.90. This value corresponds to the $3d^5$ electronic configuration (2+ valence state) of Mn in (Ga,Mn)As. Experimental measurements show that epitaxial films of (Ga,Mn)As have metallic conductivity of p type [30]. Thus Mn is acceptor in (Ga,Mn)As.

Only one pre-edge line (A_3) is observed in the K-edge x-ray absorption spectra of Mn in (Ga,Mn)As. According to the proposed interpretation of the K-edge x-ray absorption spectra of Mn, the $3d$ states of Mn (spin up) are filled (valence state of Mn is 2+). Thus the x-ray absorption spectra allow determining the valence state of Mn in diluted magnetic semiconductors.

(Ge,Mn)

The band structure of (Ge,Mn) was calculated. This calculation shows that the $3d$ states of Mn (spin up) are placed in the valence band, they are filled and delocalized. The $3d$ states of Mn (spin down) are empty and localized near Mn atoms. Calculated number of $3d$ electrons in the muffin-tin sphere of Mn is 5.01, this value points to 2+ valence state of Mn in (Ge,Mn).

The total magnetic moment of (Ge,Mn) crystal ($3\mu_B$ per one Mn atom) is mainly concentrated near the Mn atoms. Magnetic moments of nearest neighbor Ge atoms of Mn are oppositely directed to the Mn moments.

According to the band structure calculation, only one line A_3 should be observed in the K-edge x-ray absorption spectrum of Mn in (Ge,Mn). However experimental measurements are necessary to confirm this suggestion.

Chapitre IV. Propriétés magnétiques de DMS

Les propriétés magnétiques des semiconducteurs (Ga,Mn)N, (Ga,Mn)As et (Ge,Mn) sont décrites dans cette chapitre. Cette description est basée sur des résultats obtenus dans notre et dans d'autres laboratoires. Le but de cette description c'est de relier les propriétés électroniques qui ont été étudiées dans la chapitre III aux propriétés magnétiques. Ce lien nous faciliterait notre recherche de nouveaux semiconducteurs magnétiques à température élevée.

Chapter IV. Magnetic properties of DMS

Magnetic properties of the diluted magnetic semiconductors (Ga,Mn)N, (Ga,Mn)As and (Ge,Mn) are described in this chapter. The description is based on experimental results published by different research groups. The aim of this revue is to link the study of the electronic structure presented in the chapter III to observed magnetic properties of the same semiconductors. Such a link between the electronic and magnetic properties would facilitate our search of new high temperature magnetic materials.

4.1 Ferromagnetism in DMS

The magnetization of a ferromagnetic material is not zero even if there is no external magnetic field. Such a behavior of the materials can be explained if we accept two assumptions. The first assumption states that there are uncompensated magnetic moments in the ferromagnetic materials. In diluted magnetic semiconductors, such magnetic moments are provided by ions of a transition metal (for example by Mn in GaAs or GaN). The ions have unfilled 3*d* shells, and because of strong intra-atomic electronic correlations the 3*d* electrons are not distributed homogeneously between two possible spin orientations (spins up and down) but form an uncompensated magnetic spin moment. The second assumption states that there is a strong interaction between these magnetic moments which leads to ferromagnetic alignment of the magnetic moments. In paramagnetic materials (several compounds of transition metals, see for example [1]) the localized magnetic moments are present but there is no interaction. That is why the permanent magnetization is not observed in paramagnetic materials.

There are two different types of interaction between magnetic moments: the dipole magnetic interaction and exchange interaction [2]. The dipole interaction between magnetic

moments is similar to the dipole interaction between electrical dipoles: one magnetic moment creates a magnetic field at the position of the second magnetic moment, and the field acts on the second moment. However the dipole interaction is not sufficiently strong to align magnetic moments at room temperature. On the contrary the exchange interaction is strong and it can lead to the ferromagnetic order in materials. Several mechanisms of the exchange interaction between electrons are known today.

Direct exchange between electrons leads to a spin order in the $3d$ shells of transition metals and in the hydrogen molecule. Let us consider a Mn^{2+} ion in (Ga,Mn)As. The total energy of the five $3d$ electrons includes the positive repulsion energy. The repulsion energy decreases when distances between the electrons increase. The parallel alignment of electron spins insures the greatest distances because two electrons with the same spin can not have the same coordinate. Therefore Mn^{2+} ions have the lowest energy when the five d electrons have parallel spin moments. In hydrogen molecule, $1s$ electrons of H atoms are not localized and they interact not only with each other, but with hydrogen nuclei. That is why the lowest energy of hydrogen molecule corresponds to a maximum of electronic density between the two hydrogen nuclei and anti-parallel spin orientation. Thus the total energy of the electron system depends on the orientation of electron spins. This dependence corresponds to exchange interaction in Mn^{2+} ion and hydrogen molecule.

The direct exchange interaction leads to a magnetic order in transition metals (such as Mn, Fe, Ni), where atoms are very close to each other and the direct interaction of $3d$ orbitals is possible. In contrast to the metals, the distances between magnetic impurities in diluted magnetic semiconductors are much bigger. Therefore, the ferromagnetic properties of DMS at high temperature can not be explained by the direct exchange interaction of impurity atoms.

A long range exchange mechanism was suggested by Vonsovskii [3] and Zener [4] to explain ferromagnetism in materials co-doped with transition metals. It was proposed that ferromagnetic order in such dilute systems can result from exchange interaction between impurities via free charge carriers. The Curie temperature of diluted magnetic metals was calculated by Abrikosov and Gor'kov [5].

Later the same method (but free holes were considered as charge carriers) was independently developed to describe the magnetic properties of diluted magnetic semiconductors [6]. Two exchange mechanisms were taken into consideration: the exchange via free holes and the superexchange via intermediate nonmagnetic atoms. According to the

description while the first long range mechanism insures ferromagnetic order, the second one aligns spin moments of impurity atoms antiferromagnetically. Including these two mechanisms in the model allows to explain ferromagnetism in *p* type (Ga,Mn)As and antiferromagnetic properties of electrically compensated (Ga,Mn)As samples. Quantitative estimation of the Curie temperature for (Ga,Mn)As and (Zn,Mn)Te:N were performed in [6]. The obtained values of T_C agree well with experimental values. For example, the calculated T_C of $Ga_{1-x}Mn_xAs$ (*x*=0.053) is 120K that is very close to experimental values 110K [7] and 120K [8]. The Curie temperature was calculated for other diluted magnetic semiconductor using the same model. The T_C values for several semiconductors are listed in tab. 4.1. However all the calculated values of T_C were obtained using the mean-field approximation, assuming a high concentration of free holes (3.5×10^{20} cm^{-3}) and the 2+ valence state of Mn in the semiconductors.

Tab. 4.1. Curie temperatures of different diluted magnetic semiconductors calculated in [6].

semiconductor	Curie temperature (K)
$Ga_{1-x}Mn_xN$ (*x*=0.05)	410
$Ga_{1-x}Mn_xAs$ (*x*=0.053)	120
$Ge_{1-x}Mn_x$ (*x*=0.05)	75

According to the calculation, T_C=300K would be achieved in $Ga_{1-x}Mn_xAs$ for *x*=0.1. This conclusion seems to be confirmed by experiment: if we extrapolate the experimental dependence $T_C(x_{eff})$ to x_{eff}=0.1 (x_{eff} – concentration of substitutional Mn atoms which participate in ferromagnetic ordering, for details see [8]) we obtain T_C near room temperature. Furthermore according to the calculation, $Ga_{1-x}Mn_xN$ is another semiconductor which would be ferromagnetic at room temperature when the concentration of Mn (*x*) is only 0.05. Therefore the (Ga,Mn)N semiconductor would be promising in practical applications.

The Curie temperature of a diluted magnetic semiconductor can be calculated using the first-principles (*ab-initio*) calculation methods described in chapter II. Usually the computational scheme consists of two steps. First of all, the Heisenberg exchange parameter J_{ij} which describes interaction between magnetic impurities is calculated by different methods [9,10,11]:

$$H = -\sum_{i \neq j} J_{ij} \mathbf{S}_i \mathbf{S}_j \ . \tag{4.1}$$

This parameter is further used for Curie temperature calculation. Usually the Curie temperature is calculated using the mean-field approximation [1,9,11]. However there are other calculation methods which take into account disordered distribution of magnetic impurities in crystal lattice and the quantum nature of spin moments [12,13].

The *ab-initio* methods have one important advantage as compared to other calculation methods: only the crystal structure of investigated material has to be known to calculate the magnetic properties of the material. Although other experimental parameters of the semiconductor are often used in *ab-initio* calculations (such as the lattice parameter or the lattice deformation around impurity atoms), in principle these parameters can be found from the *ab-initio* calculation. Therefore, *ab-initio* calculations allow us to estimate the magnetic properties of a magnetic semiconductor and we do not need real crystals of the semiconductor to perform such estimation. Experience shows that several years are required to develop a new semiconductor technology; therefore this advantage of *ab-initio* methods is not negligible.

The *ab-initio* methods (like all other methods) have also drawbacks: practically it is quite difficult to take into account strong correlation of $3d$ electrons in magnetic impurity atoms, change of crystal structure around impurity atoms, other defects which could change electronic structure and etc. In addition *ab-initio* calculations performed by different methods give quite different values of the Curie temperature for the same material (for example, the Curie temperature of $Ga_{1-x}Mn_xN$ (x=0.06) is ~350K, the mean field approximation is used in [11], and ~30K, a Monte-Carlo simulation was performed in [14]). However the *ab-initio* methods are constantly improved and it seems they will be very useful in predicting the magnetic properties of different materials.

4.2 Magnetic properties of (Ga,Mn)N, (Ga,Mn)As and (Ge,Mn)

4.2.1 (Ga,Mn)N

The active investigation of $Ga_{1-x}Mn_xN$ started in 2000, and it was stimulated by a prediction of room temperature ferromagnetism in the semiconductor at a relatively low concentration of Mn (x~0.05) [6]. This prediction is based on the assumption that the Mn impurity acts as an acceptor in (Ga,Mn)N (the valence of Mn was supposed to be 2+), and that ferromagnetic interactions are mediated by free holes. According to this prediction the Curie temperature should be 410K in zinc-blende $Ga_{1-x}Mn_xN$ (x=0.05) and it should be slightly lower (~390K) in wurtzite $Ga_{1-x}Mn_xN$ (x=0.05).

Early experimental works following this prediction did not give any clearcut conclusion about the magnetic properties of (Ga,Mn)N: paramagnetic [15] and ferromagnetic properties at low temperature (T_C~10K [16], T_C~8K [17]), as well as room temperature ferromagnetism [18,19] in (Ga,Mn)N were reported by several groups. The highest Curie temperature (T_C~940K) was deduced from magnetization measurements of (Ga,Mn)N layers [20]. Such a variety of contradictory results can be explained by different types of distribution of the Mn impurity and additional impurities in different (Ga,Mn)N samples. As it will be discussed later, the Curie temperature can change upon co-doping with a donor or an acceptor. Therefore, the presence of unexpected impurities in (Ga,Mn)N samples which are found to be ferromagnetic at room temperature can not be excluded.

It was found in chapter III that Mn atoms have the 3+ valence state in (Ga,Mn)N. Therefore, substituting Ga atoms by Mn atoms does not lead to a high concentration of free holes. Furthermore, (Ga,Mn)N remains *n* type because of additional co-doping by a donor (it may be oxygen, silicon or N vacancies). Thus the main exchange mechanism (via free holes), supposed in [6], is absent in (Ga,Mn)N. In this case one could not expect ferromagnetic properties in (Ga,Mn)N at high temperature: this semiconductor may be ferromagnetic at low temperature, or it is not ferromagnetic at all (paramagnetic). This conclusion is supported by experimental measurements performed on wurtzite (Ga,Mn)N samples. Previously the crystal structure of these samples was studied by x-ray diffraction and possible inclusions or clusters were not detected [20,21]. The electronic structure of the samples was studied using x-ray

absorption and optical absorption measurements (see chapter III, [22,23]). Further, the magnetization of the same samples was measured. According to the measurements a $Ga_{1-x}Mn_xN$ (x=0.017) sample is paramagnetic at 2K [15]. Another sample but with a higher concentration of Mn (x=0.063) exhibit ferromagnetism till T_C=8K [17].

The measured magnetization of paramagnetic wurtzite (Ga,Mn)N samples as a function of magnetic field $M(B)$ depends on the direction of the magnetic field with respect to the c axis (R.M.Galera in [24]). Such an anisotropy is typical of Mn^{3+} ions, while an isotropic character of the $M(B)$ dependence is expected for Mn^{2+} ions [25]. Therefore the magnetization measurements imply a high concentration of Mn^{3+} ions in (Ga,Mn)N.

Thus the $Ga_{1-x}Mn_xN$ (x=0.06) semiconductor is not ferromagnetic at high temperature. However this conclusion is valid for a pure (Ga,Mn)N semiconductor. Additional co-doping of the semiconductor with an acceptor or a donor could increase the concentration of free charge carriers and therefore the Curie temperature. In the first case (co-doping with an acceptor) free holes can mediate exchange interactions between impurity atoms. However there is no efficient acceptor today to create a very high concentration of holes especially if the double co-doping should be performed (with Mn and Mg). Another possibility to increase the Curie temperature it is co-doping with a donor. In this case exchange interactions between Mn impurities appear via the double exchange mechanism proposed by Zener for the manganese compounds with perovskite structure [26]. This exchange mechanism leads to ferromagnetic order in compounds where equivalent Mn atoms have different valence states. In (Ga,Mn)N this situation could be achieved by co-doping with a donor: one part of Mn ions capture additional electrons and become Mn^{2+} while other part of Mn ions rest in 3+ valence state. According to the Zener's double-exchange mechanism the additional electrons can move from Mn^{2+} to Mn^{3+} ions and these electron jumps decrease the total energy of the crystal. It is assumed that the oscillations are only possible when the spins of the Mn ions are parallel. If spin moments of neighbor Mn atoms are antiparallel, then such oscillations of electrons are forbidden because the spin moment should not change direction. Therefore the (Ga,Mn)N crystals should be ferromagnetic if a mixture of Mn^{3+} and Mn^{2+} ions are present in the crystals [27]. An estimation of the Curie temperature for (Ga,Mn)N was performed which takes into account the double-exchange mechanism. According to the calculation, very high Curie temperatures (T_C=1000K for $Ga_{0.95}Mn_{0.05}N$) upon co-doping (Ga,Mn)N by a donor (the

concentration of the donor impurity should be two times smaller than the concentration of Mn) would be achieved [27].

4.2.2 (Ga,Mn)As

This diluted magnetic semiconductor has been intensively studied during the 90-s of the last century, and a great progress was achieved thanks to the development the low temperature molecular beam epitaxy [7]. This technology allows us to incorporate a high concentration of Mn impurities (x~0.05) in $Ga_{1-x}Mn_xAs$ crystals and at the same time to avoid segregation of the Mn impurity in the surface and cluster formation. Today it well established that this semiconductor is ferromagnetic and the highest Curie temperature was achieved to be 173K [8].

Band structure calculations performed for (Ga,Mn)As show that the $3d$ states (spin up) of Mn are filled and located in the band gap (2+ valence state of Mn). Transport measurements performed on $Ga_{1-x}Mn_xAs$ (x=0.053) samples confirm the acceptor character of the Mn impurity: the samples exhibit metallic p-type conductivity [7]. Therefore the observed ferromagnetic interactions between Mn atoms in (Ga,Mn)As can be mediated by free holes [7]. This statement is confirmed by the fact that electrically compensated (Ga,Mn)As samples are antiferromagnetic [7]. In addition, magnetization measurements of (Ga,Mn)As layers reveal a link between the hole concentration and magnetic properties of (Ga,Mn)As. The magnetization contains two components: ferromagnetic and paramagnetic [7]. The paramagnetic component is weaker in samples with a high concentration of holes.

The Curie temperature of $Ga_{1-x}Mn_xAs$ (x=0.053) was calculated in [6] using the model of carrier induced ferromagnetic interactions. The calculated value T_C=120K for $Ga_{1-x}Mn_xAs$ (x=0.053) agrees well with experimental data: T_C=110K for $Ga_{1-x}Mn_xAs$ (x=0.053) [7] and T_C=120K for $Ga_{1-x}Mn_xAs$ (x=0.056) [8].

The Curie temperature of $Ga_{1-x}Mn_xAs$ samples can be changed by annealing. It was shown that a significant fraction of Mn impurity occupies interstitial positions and these Mn_I ions (donor in an interstitial position) compensate substitutional Mn_S atoms (acceptor in a substitutional position) [28]. In addition, Mn atoms in such (Mn_S-Mn_I) pairs are coupled

antiferromagnetically according to magnetization measurements [28] and *ab-initio* calculations [29], and these atoms do not participate in the ferromagnetic ordering. Annealing of $Ga_{1-x}Mn_xAs$ samples allows us to reduce the concentration of interstitial Mn impurities and this annealing increases considerably the Curie temperature [8,28].

Ab-initio calculations were also used to investigate magnetic properties of (Ga,Mn)As. Early calculations predicted overestimated T_C values of $Ga_{1-x}Mn_xAs$: 260K [11], 290K [30] for $x=0.05$. The overestimation was explained for example by a small content of antisites in real samples (As atoms in positions of Ga atoms). Such anti-sites should decrease the concentration of holes and by consequence the Curie temperature [9]. According to more recent calculations the main cause of the overestimation is neglecting the disorder in calculations. Good results (close to experimental values) were obtained in different works which take into account the disorder [12,14,30,31] (the local spin density approximation was used). In addition, it was suggested that the influence of the spin-orbit coupling is not very strong: the Curie temperature of $Ga_{1-x}Mn_xAs$ ($x=0.08$) decreases by 10% after including the spin-orbit coupling in a calculation [30].

Although the experimentally achieved values of the Curie temperature of (Ga,Mn)As are lower than 300K, this semiconductor could be made ferromagnetic at room temperature in the future. Extrapolation of experimental function $T_C(x)$ gives $T_C=300$ when $x\sim0.1$ for a perfect $Ga_{1-x}Mn_xAs$ crystal [8]. The lattice parameter of GaAs is sufficiently large to incorporate a high concentration of Mn impurity. Therefore incorporation of 10% Mn impurity is not an insurmountable problem. However a higher concentration of Mn is necessary to achieve $T_C=300$ in a real crystal.

4.2.3 (Ge,Mn)

Observation of high temperature ferromagnetism in (Ge,Mn) crystals has stimulated an active research [32,33]. In particular, a Curie temperature as high as 285K was reported for a $Ge_{1-x}Mn_x$ ($x=0.06$) epitaxial layer. However, more recent investigations of (Ge,Mn) epilayers show that the ferromagnetism observed at 285K arises from Mn_5Ge_3 clusters [34,35]. This seems to be reasonable because the Curie temperature of Mn_5Ge_3 is 296K (very close to the

observed value, 285K) and there are (Ge,Mn) samples which do not show considerable magnetization in the temperature region from 110K to 285K in the magnetic field H=0.1T [35]. The (Ge,Mn) samples where the Mn_5Ge_3 clusters are present [34] are superparamagnetic at T<285K and the blocking temperature of the clusters is about 210K.

The (Ge,Mn) layers that are free from the Mn_5Ge_3 clusters also exhibit an interesting magnetic behavior. The magnetization of these samples starts to increase from T_C=110K and it further increases with temperature lowering [32,35]. However the measured magnetization is field induced [35]: it strongly depends on the applied value of the magnetic field, and no ferromagnetic hysteresis was observed till T=20K. It was shown also that the (Ge,Mn) samples are superparamagnetic in this temperature region 20<T<110K and this superparamagnetism can be related to the presence of Mn-rich clusters [34]. The blocking temperature of the Mn-rich clusters determined from field-cooled measurements is T_b~12K [34]. However a hysteresis behavior of the magnetization was observed at 5K in [32,35] and it was supposed that T_b~12K is a ferromagnetic transition temperature. The nature of Mn-rich cluster is still unknown, but it was shown that the T_b transition temperature can be determined from Hall effect measurements [35]. Therefore it was suggested that exchange interactions inside the Mn-rich clusters are mediated by electrons [35].

A very different magnetization behavior was reported in [33]: in 150K<T<285K interval (Ge,Mn) samples exhibit ferromagnetism while at lower temperature (T<150K) the samples are antiferromagnetic. Such a behavior however was not confirmed in other reports.

$Ge_{1-x}Mn_x$ samples show a semiconducting and not metallic behavior of the resistivity in spite of high concentration of Mn atoms (x=0.035 [32], x=0.088 [35]). The $Ga_{1-x}Mn_xAs$ crystals doped with such a high concentration of Mn impurities are metallic (note that Mn is a double acceptor in Ge). The low concentration of holes in (Ge,Mn) can be explained by formation of clusters where Mn atoms are not acceptors. Another possible explanation is a low density of states at the Fermi level (fig. 3.37).

In general, recent investigations conclude that the distribution of Mn in the studied GeMn samples is inhomogeneous and the samples are not ferromagnetic at room temperature [34,35]. However a new germanium rich phase was reported recently [36]. The composition of the clusters is close to Ge_2Mn, and the GeMn samples containing the Ge_2Mn clusters exhibit room temperature ferromagnetism. Therefore the inhomogeneous GeMn alloy may have important practical applications.

While the experimental distribution of Mn in Ge can be hardly changed, theoretically (Ge,Mn) samples with a homogeneous distribution of Mn can be considered. The band structures of (Ge,Mn) and (Ga,Mn)As crystals are similar: $3d$ states of Mn (spin up) are situated deep in the valence band, they are delocalized and free holes are created in the top of the valence band. In this case ferromagnetic exchange interactions in (Ge,Mn) can be mediated by itinerant holes. The Curie temperature of $Ge_{1-x}Mn_x$ (x=0.025, p=3.5·10^{20} holes/cm^3) was calculated in [37]: T_C~80K.

Summary for chapter IV

(Ga,Mn)N

Experimental investigation of wurtzite $Ga_{1-x}Mn_xN$ ($x=0.063$) shows that this diluted magnetic semiconductor exhibit ferromagnetic properties at low temperature ($T_C \sim 8K$ [17]). Absence of high temperature ferromagnetism in this semiconductor can be explained by lack of any exchange mechanism which could lead to ferromagnetic ordering at high temperature. However ferromagnetic ordering mechanisms could appear upon co-doping (Ga,Mn)N with an acceptor or a donor impurity. In the first case ferromagnetic interactions in (Ga,Mn)N can be mediated by free holes. Co-doping with a donor could lead to ferromagnetic exchange interactions between Mn atoms via the double-exchange mechanism [27]. The two co-doping would increase the Curie temperature of (Ga,Mn)N.

(Ga,Mn)As

The diluted magnetic semiconductor (Ga,Mn)As was found to be ferromagnetic at 173K. This ferromagnetism is mediated by free holes and the Curie temperature increases together with concentration of Mn ions [8]. Real GaMnAs crystals contain substitutional and interstitial Mn atoms and the interstitial Mn atoms suppress considerably the Curie temperature. It was shown that the interstitial Mn atoms can be eliminated by annealing [28].

The observed ferromagnetism was described using the mean-field model [6] and obtained value of the Curie temperature agrees well with experimental data. Another models were proposed in [27] and in [38] which also explain well the experimentally observed dependence of the Curie temperature on concentration of Mn in (Ga,Mn)As. *Ab-initio* calculations give values of T_C which are very close to the experimental values [12,13,30,31], these calculations show a very strong dependence of the calculated T_C on distribution of Mn in (Ga,Mn)As: disordered distribution of Mn significantly decrease the Curie temperature. Experimental and theoretical studies suggest that $T_C=300K$ would be achieved at reasonable concentrations of Mn in $Ga_{1-x}Mn_xAs$ ($x_{eff} \sim 0.1$ [8] and $x=0.125$ [37]).

(Ge,Mn)

Ferromagnetic properties of GeMn samples with T_C=285K reported in [33] can be related to presence of Mn_5Ge_3 precipitates in the samples. Samples of GeMn without the Mn_5Ge_3 precipitates were grown as well [35]. They do not exhibit ferromagnetism till to T=20K [35] and it was found that the samples are superparamagnetic in the temperature region 20K<T<150K [34]. At lower temperature (T<15K) GeMn samples show ferromagnetic [32,35] or frozen state [34]. These results also demonstrate inhomogeneous distribution of Mn in GeMn. A new germanium-rich phase was recently found in GeMn [36]. The GeMn samples exhibit ferromagnetism at room temperature, therefore the new phase may have important practical applications.

An estimation of the Curie temperature for $Ge_{1-x}Mn_x$ (x=0.025, hole concentration p=3.5·10^{20} cm^{-3}) with homogeneous distribution of Mn predicts T_C~80K [37]. However additional studies are necessary to clarify magnetic properties of (Ge,Mn) diluted magnetic semiconductor.

Conclusion

Scientific research is traditionally divided onto two basic parts: experimental and theoretical ones. Experimental research is intended to provide us with the real information about the phenomena of the nature. Theoretical research allows us to reveal the main laws of the nature; the laws can be further used to predict unknown phenomena and to construct novel devices. According to this division of the scientific research, scientific groups are also divided onto experimental and theoretical ones. The experimental groups use simple models to explain their experimental results and to extract from the results some useful parameters. In contrast, the theoretical groups use quit sophisticated models, such as *ab-initio* calculations, to predict properties of materials; however experimental investigations are generally not used in the predictions. In this work we try to take advantages of the both experimental and *ab-initio* investigations to optimize our research and, at the same time, to obtain reliable information about properties of diluted magnetic semiconductors.

The main objectives of the work are:

- to evaluate the predictive character of *ab-initio* methods regarding a spectroscopic study, by making a comparison between the experimental x-ray absorption spectra and the spectra calculated using *ab-initio* methods;
- to characterize the main features of experimental x-ray absorption spectra;
- to improve our understanding of DMSs, and in particular of (Ga,Mn)N, and the possibility of carrier induced ferromagnetism in wide band gap semiconductors.

X-ray absorption spectroscopy was chosen for the experimental investigation of diluted magnetic semiconductors. This method has several important advantages as compared to other ones. Firstly, it allows a separate investigation of elements in complex alloys. The electronic state of Mn and the local atomic structure around the Mn atoms were studied in this work using the x-ray absorption spectra at the K-edge of Mn. Secondly, interpretation of the

K-edge absorption spectra is more straightforward as compared to L-edge and optical absorption spectra where the core-hole effects are very important. Thirdly, the K-edge spectra allow a more direct study of bulk properties of materials: surface properties of investigated samples (lattice deformations near the substrate surface, concentration of electrons on a surface) do not influence the K-edge spectra, while they drastically change the L-edge spectra. Finally, this method is accessible in the European Synchrotron Radiation Facility (ESRF) in Grenoble and preliminary results were available in our group.

The linear *ab-initio* methods LAPW and LMTO were used to calculate the band structure and x-ray absorption spectra of (Ga,Mn)N, (Ga,Mn)As and (Ge,Mn). The calculation methods are well developed now and they are very efficient: a relatively small computational cost of the methods allows calculating large supercells which are necessary to describe crystals with a low concentration of impurity. At the same time, the precision of the methods is close to the one of non-linear *ab-initio* methods, such as the APW method.

The experimental and calculated K-edge x-ray absorption spectra of Mn in (Ga,Mn)N were compared. Let us outline the main results of this comparison:

- the tetrahedral environment of Mn in zinc-blende and wurtzite semiconductors leads to the strong $4p$-$3d$ hybridization of Mn orbitals; this hybridization gives rise to intense pre-edge lines in the K-edge x-ray absorption spectra of Mn; the absorption lines are mainly of dipolar origin;

- as a result, two intense pre-edge absorption lines are present in the K-edge x-ray absorption spectrum of Mn in (Ga,Mn)N: the low energy line corresponds to electron transitions to the narrow t_2 band (spin up) and the high energy line reflects transitions to the t_2 band (spin down); the energy splitting between the two t_2 bands is due to internal exchange interaction of $3d$ electrons in Mn atoms, this splitting therefore is present independently on the macroscopic magnetic structure of the (Ga,Mn)N samples;

- the e band (spin down) is empty, however it is not hybridized with the $4p$ orbitals of Mn and therefore its influence on the x-ray absorption spectrum is weak. As a result, the 10Dq parameter, often used in optical spectroscopy, can not be obtained from the K-edge x-ray absorption spectra of Mn;

- according to the band structure calculation the width of the t_2 bands depends on the distances between nearest neighbor Mn atoms: if Mn atoms are distributed homogeneously in $Ga_{1-x}Mn_xN$ (x=0.0625), then the t_2 bands are narrow and the two pre-edge absorption line are well distinguished (the resolution of the monochromator should be better than 0.5 eV); in contrast, if Mn atoms form close pairs, then the two line merge in one wide line;

- the absorption lines at higher energy (S and B lines) reflect $4p$-states of Mn in the conduction band; a good agreement between the experimental and calculated x-ray absorption spectra of Mn can be obtained if we introduce a rigid shift of 2.6 eV between the t_2 bands and the $4p$ states of Mn in the conduction band; this shift may contain two contributions: (*i*) the usual underestimation of the gap in the band structure calculation, and (*ii*) the attractive potential of the core hole shifts the $3d$ bands and the $4p$ states of Mn in the conduction band downward in energy, and the shift is more important for the localized $3d$ bands than for the delocalized $4p$ orbitals; therefore the splitting between the $3d$ bands and the $4p$ states increases.

From the results of the comparison we conclude that:

- the electronic state of Mn in (Ga,Mn)N is Mn^{3+} (electronic configuration $3d^4$): one absorption line is expected in the case of Mn^{2+} (electronic configuration $3d^5$) because the t_2 band (spin up) is filled and where are only transitions to the t_2 band (spin down); but two absorption lines are observed in the x-ray absorption spectra of Mn in (Ga,Mn)N, this means that the t_2 band (spin up) is not completely filled;

- as a result, the Mn is not an acceptor in (Ga,Mn)N; this conclusion is confirmed by our transport measurements: our (Ga,Mn)N samples reveal *n*-type conductivity, we do not observe any correlation between the electron density and the Mn concentration;

- the t_2 bands of Mn in our (Ga,Mn)N samples are narrow, this points to a homogeneous distribution of Mn in the samples; the overlap of $3d$ orbitals of nearest neighbor Mn atoms is small and the interaction between nearest neighbor Mn atoms is weak;

- according to our band structure calculation, the number of $3d$ electrons in the MT-sphere of Mn in (Ge,Mn) is close to 5 (Mn^{2+}); therefore a single absorption line should be observed in the K-edge x-ray absorption spectra of Mn in (Ge,Mn); this conclusion however should be checked experimentally.

We compared also our experimental and calculated K-edge x-ray absorption spectra of Mn in (Ga,Mn)As. The main conclusions of this comparison:

- a single pre-edge absorption line is observed in the K-edge x-ray absorption spectrum of Mn in (Ga,Mn)As in agreement with the 2+ valence state of Mn in (Ga,Mn)As and with the interpretation of the pre-edge x-ray absorption structure described above;

- our band structure calculation predicts a strong intensity of Mn p-states in the top of the valence band in (Ga,Mn)As, however electronic transitions to the p states are not observed in the experimental K-edge x-ray absorption spectrum of Mn. We explain this disagreement by two possible reasons: (*i*) the density of the empty $3d$ states of Mn in the top of the valence band is overestimated, and this leads to an overestimation of the density of Mn p states in the top of the valence band. This hypothesis can be checked using the LDA+U approximation; the U parameter should be chosen sufficiently large to shift the $3d$ bands (spin up) away from the top of the valence band; so the $3d$-$4p$ hybridization would not be possible; (*ii*) the hybridization of the $4p$ states of Mn with the states of the valence band is overestimated. This second cause is more probable: according to our calculation, the hybridization of the $3p$ states of Mg with the states of the valence band is present in (Ga,Mg)N, and a strong pre-edge absorption line is predicted, but there are no $3d$ states of Mg near the top of the valence band.

Optical spectroscopy is another powerful method which allows us to study the electronic properties of crystals. This method has its own advantages and shortcomings as compared to x-ray absorption spectroscopy. An optical approach to solve the same problems (electronic state and distribution of Mn) was briefly described in parallel to the x-ray absorption method. Such a comparison allows us to reveal strong points of the methods and to optimize our research by combining the strongest points of the x-ray spectroscopy, optical spectroscopy and *ab-initio* calculations. Let us outline the main results of this comparison:

- a very sharp line at 1.4 eV is observed in the optical absorption spectra of very diluted $Ga_{1-x}Mn_xN$ ($x<0.001$) samples [1,2,3]; this line was attributed to an internal e-t_2 (spin up) transition of Mn [1,2,4]; the e-t_2 splitting is due to the crystal field induced by the four nearest neighbor N atoms, therefore the optical spectroscopy allows measuring the crystal field splitting (10Dq), while the exchange splitting of the $3d$ states of Mn

can be obtained from the x-ray absorption spectra; the value of the e-t_2 splitting obtained from an *ab-initio* calculation [5] is close to the experimental value 1.4 eV; this value is much lager than the e-t_2 splitting in II-VI semiconductors;

- the resolution of the optical spectra is significantly better than the resolution of the x-ray absorption spectra: the natural width of $1s$ level (1.16 eV for Mn) limits precision of x-ray absorption spectroscopy, only rough features in the electronic structure can be identified by this method. In contrast, optical method allows a much more precise investigation of the electronic structure;

- the calculated width of the absorption line at 1.4 eV in $Ga_{1-x}Mn_xN$ (x=0.0625) with a homogeneous distribution of Mn [5] agrees well with the broadening of the line obtained from optical absorption measurements of a $Ga_{1-x}Mn_xN$ (x=0.06) [6, fig. 3.3]. This points to a homogeneous distribution of Mn in heavy doped (Ga,Mn)N samples; the same conclusion was obtained from the x-ray absorption spectra;

- the intensity of the absorption line at 1.4 eV per one Mn atom decreases when the Mn content x in $Ga_{1-x}Mn_xN$ become larger than 0.01 [6], while the intensity of the line A_2 (transitions to the t_2 band, spin up) in our x-ray absorption spectra of Mn in $Ga_{1-x}Mn_xN$ does not depend on the concentration of Mn. This disagreement between the x-ray and optical measurements can be explained by a stronger influence of the surface and substrate properties on optical absorption spectra. The x-ray absorption spectra are less influenced by interfaces and surfaces, and therefore the x-ray absorption spectra reflect essentially bulk properties of the (Ga,Mn)N layers.

Finally, magnetic properties of our (Ga,Mn)N samples can be explained using the results listed above. Magnetization measurements demonstrate a paramagnetic behavior of $Ga_{1-x}Mn_xN$ (x~0.017) at T=2K [7] and a ferromagnetic behavior of $Ga_{1-x}Mn_xN$ (x~0.063) with T_C~8K [8]. Thus, exchange interaction between Mn atoms in the samples is weak. Strong exchange interaction between the Mn atoms was predicted in p-type (Ga,Mn)N [9], however the valence state of Mn in (Ga,Mn)N is 3+, Mn is not acceptor in (Ga,Mn)N. Therefore the exchange interaction induced by free holes is absent in (Ga,Mn)N and this explains the low Curie temperature of our (Ga,Mn)N samples. However additional doping by acceptor [9] or donor [10] impurities may enhance the exchange interactions between Mn ions and increase the Curie temperature of (Ga,Mn)N.

References

Introduction

1.   G. A. Prinz, "Spin-Polarized Transport", Physics Today, April, p. 58 (1995).

2.   S. A. Solin, "Magnetic field nanosensors", Scientific American, July, p. 71 (2004).

3.   R. Koch, "Morthware", Scientific American, August, p. 57 (2005).

4.   V. A. Ivanov, T. G. Aminov, V. M. Novotortsev, and V. T. Kalinnikov, "Spintronics and spintronics materials", Russian Chemical Bellutin **53**, p. 2357 (2004).

5.   D. Ferrand, J. Cibert, A. Wasiela, C. Bourgognon, S. Tatarenko, G. Fishman, T. Andrearczyk, J. Jaroszynski, S. Kolesnik, T. Dietl, B. Barbara, D. Dufeu, "Carrier-induced ferromagnetism in p-$Zn_{1-x}Mn_xTe$", Physical Review B **63**, 085201 (2001).

6.   T. Dietl, H. Ohno, F. Matsukura, J. Cibert, D. Ferrand, "Zener Model Description of Ferromagnetism in Zinc-Blende Magnetic Semiconductors", Science **287**, 1019 (2000).

7.   H. Hori, S. Sonoda, T. Sasaki, Y. Yamamoto, S. Shimizu, K. Suga, and K. Kindo, "High-T_C ferromagnetism in diluted magnetic semiconducting GaN:Mn films", Physica B 324, 142 (2002); S. Yoshii, S. Sonoda, T. Yamamoto, T. Kashiwagi, M. Hagiwara, Y. Yamamoto, Y. Akasaka, K. Kindo, H. Hori, "Evidence for Carrier-Induced High-T_C Ferromagnetism in Mn-doped GaN film", arXiv:cond-mat/0604647 (2006).

8.   V. A. Chitta, J. A. H. Coaquira, J. R. L. Fernandez, C. A. Duarte, J. R. Leite, D. Schikora, D. J. As, K. Lischka, and E. Abramof, "Room temperature ferromagnetism in

cubic GaN epilayers implanted with Mn^+ ions", Applied Physics Letters **85**, 3777 (2004).

9. R. Giraud, S. Kuroda, S. Marcet, E. Bellet-Amalric, X. Biquard, B. Barbara, D. Fruchart, D. Ferrand, J. Cibert, and H. Mariette, "Structural and magnetic properties of a $Ga_{0,985}Mn_{0,015}N$", Journal of Magnetism and Magnetic Materials, **272-276**, e1557 (2004).

10. Y. L. Soo, G. Kioseoglou, S. Kim, S. Huang, Y. H. Kao, S. Kuwabara, S. Owa, T. Kondo, and H. Munekata, "Local structure and chemical valency of Mn impurities in wide-band-gap III–V magnetic alloy semiconductors $Ga_{1-x}Mn_xN$", Applied Physics Letters **79**, 3926 (2001).

11. A. Wolos, A. Wysmolek, M. Kaminska, A. Twardowski, M. Bockowski, I. Grzegory, S. Porowski, and M. Potemski, "Neutral Mn acceptor in bulk GaN in high magnetic fields", Physical Review B **70**, 245202 (2004).

12. A. Wolos, M. Palczewska, M. Zajac, J. Gosk, M. Kaminska, A. Twardowski, M. Bockowski, I. Grzegory, and S. Porowski, "Optical and magnetic properties of Mn in bulk GaN", Physical Review B **69**, 115210 (2004).

13. B. Han, R. Y. Korotkov, B. W. Wessels, and M. P. Ulmer, "Optical properties of Mn^{4+} ions in GaN:Mn codoped with Mg acceptors", Applied Physics Letters **84**, 5320 (2004).

14. T. Graf, M. Gjukic, M. S. Brandt, M. Stutzmann, and O. Ambacher, "The $Mn^{3+/2+}$ acceptor level in group III nitrides", Applied Physics Letters **81**, 5159 (2002).

15. H. Ohno, "Making Nonmagnetic Semiconductors Ferromagnetic", Science, vol. 281 (1998).

16. K. M. Yu, W. Walukiewicz, T. Wojtowicz, I. Kuryliszyn, X. Liu, Y. Sasaki, and J. K. Furdina, "Effect of the location of Mn sites in ferromagnetic $Ga_{1-x}Mn_xAs$ on its Curie temperature", Physical Review B **65**, 201303(R) (2002).

17. T. Jungwirth, K. Y. Wang, J. Mašek, K. W. Edmonds, J. König, J. Sinova, M. Polini, N. A. Goncharuk, A. H. MacDonald, M. Sawicki, A. W. Rushforth, R. P. Campion, L. X. Zhao, C. T. Foxon, and B. L. Gallagher, "Prospects for high temperature ferromagnetism in (Ga,Mn)As semiconductors", Physical Review B **72**, 165204 (2005).

18. K. W. Edmonds, P. Bogusławski, K.Y.Wang, R. P. Campion, S. N. Novikov, N. R. S. Farley, B. L. Gallagher, C.T. Foxon, M. Sawicki, T. Dietl, M. Buongiorno Nardelli, and J. Bernholc, "Mn Interstitial Diffusion in (Ga,Mn)As", Physical Review Letters **92**, 037201 (2004).

19. Y. D. Park, A. T. Hanbicki, S. C. Erwin, C. S. Hellberg, J. M. Sullivan, J. E. Mattson, T. F. Ambrose, A. Wilson, G. Spanos, B. T. Jonker, "A Group-IV Ferromagnetic Semiconductor: Mn_xGe_{1-x}", Science **295**, 651 (2002).

20. S. Cho, S. Choi, S. Ch. Hong, Y. Kim, J. B. Ketterson, B.-J. Kim, Y. C. Kim, J.-H. Jung, "Ferromagnetism in Mn-doped Ge", Physical Review B **66**, 033303 (2002).

21. A. P. Li, J. F. Wendelken, J. Shen, L. C. Feldman, J. R. Thompson and H. H. Weitering, "Magnetism in Mn_xGe_{1-x} semiconductors mediated by impurity band carriers", Physical Review B **72**, 195205 (2005).

22. C. Jaeger, C. Bihler, T. Vallaitis, S. T. B. Goennenwein, M. Opel, R. Gross, M. S. Brandt, "Spin-glass-like behavior of Ge:Mn", Physical Review B **74**, 045330 (2006).

Chapter I

1. C. Adelmann, J. Brault, D. Jalabert, P. Gentile, H. Mariette, Guido Mula, and B. Daudin, "Dynamically stable gallium surface coverages during plasma-assisted molecular-beam epitaxy of (0001) GaN", Journal of Applied Physics **91**, 9638 (2002).

2. S. Kuroda, E. Bellet-Amalric, R. Giraud, S. Marcet, J. Cibert, and H. Mariette, "Strong influence of Ga/N flux ratio on Mn incorporation into $Ga_{1-x}Mn_xN$ epilayers grown by plasma-assisted molecular beam epitaxy", Applied Physics Letters **83**, 4580 (2003).

3. E. Sarigiannidou, F. Wilhelm, E. Monroy, R. M. Galera, E. Bellet-Amalric, A. Rogalev, J. Goulon, J. Cibert, and H. Mariette, "Intrinsic ferromagnetism in wurtzite (Ga,Mn)N semiconductor", Physical Review B **74**, 041306R (2006).

4. S. C. Jain, M. Willander, J. Narayan, R. Van Overstraeten, "III-nitrides: Growth, characterization, and properties", Journal of Applied Physics 87, 965 (2000).

5. A. Titov, X. Biquard, D. Halley, S. Kuroda, E. Bellet-Amalric, H. Mariette, J. Cibert, A. E. Merad, G. Merad, M. B. Kanoun, E. Kulatov, and Yu. A. Uspenskii "X-ray Absorption Near-Edge Structure and Valence state of Mn in (Ga,Mn)N" Physical Review B **72**, 115209 (2005).

6. E. Z. Kurmaev, V. M. Cherkashenko, L. D. Finkelshtain, "X-ray absorption spectra of solids" [in Russian] Publishing House "Science", Moscow (1988).

7. R. Prinz and D. Koningsberger, editors, "X-ray absorption: principles, applications techniques of EXAFS, SEXAFS and XANES", J. Wiley and Sons, New York, 1988.

8. Web-site http://www.esrf.fr/exp_facilities/BM2/BM2.html

9. Web-site http://www.esrf.fr/exp_facilities/BM30B/BM30Bb-en.html

10. X. Biquard, O. Proux, J. Cibert, D. Ferrand, H. Mariette, R. Giraud, and B. Barbara, "Local Structure and Valence State of Mn in $Ga_{1-x}Mn_xN$ Epilayers", Journal of Superconductivity **16**, 127 (2003).

11. Web-site http://leonardo.phys.washington.edu/feff/

Chapter II

1. S. Cottenier, "Density Functional Theory and the family of (L)APW-methods: a step-by-step introduction", Instituut voor Kern- en Stralingsfysica, K.U.Leuven, Belgium, 2002, ISBN 90-807215-1-4 (to be found at http://www.wien2k.at/reg user/textbooks).

2. P. Hohenberg and W.Kohn, "Inhomogeneous electron gas", Physical Review **136**, B864 (1964).

3. W. Kohn and L. J. Sham, "Self-consistent equations including exchange and correlation effects", Physical Review **140**, A1133 (1965).

4. V. V. Nemoshkalenko, V. N. Antonov, "Methods of computation physics in solid state theory. Band theory of metals" [in Russian], Kiev (1985).

5. P. Blaha, K. Schwarz, G. Madsen, D. Kvasnicka, J. Luitz, "WIEN2k user's guide", Vienna University of Technology Inst. of Physical and Theoretical Chemistry, Austria (2001).

6. O. K. Andersen and O. Jepsen, "Explicit, First-Principles Tight-Binding Theory", Physical Review Letters **53**, 2571 (1984).

7. P. Blaha, K. Schwarz, G. K. H. Madsen, D. Kvasnicka, and J. Luitz, WIEN2k, "An Augmented Plane Wave_Local Orbitals Program for Calculating Crystal Properties", Karlheinz Schwarz, Techn. Universität Wien, Austria, 2001, ISBN 3-9501031-1-2.

8.   O. K. Andersen, "Linear methods in band theory", Physical Review B **12**, 3060 (1975).

Chapter III

1.   Ch. Kittel, "Introduction to solid state physics, fourth edition", J. Wiley&Sons (2005).

2.   I. Vurgaftman, J. R. Meyer, L. R. Ram-Mohan, "Band parameters for III-V compound semiconductors and their alloys", Journal of Applied Physics **89**, 5815 (2001).

3.   S. C. Jain, M. Willander, J. Narayan, R. Van Overstraeten, "III-nitrides: Growth, characterization, and properties", Journal of Applied Physics 87, 965 (2000).

4.   E. Kulatov, H. Nakayama, H. Mariette, H. Ohta, and Yu. A. Uspenskii, "Electronic structure, magnetic ordering, and optical properties of GaN and GaAs doped with Mn", Physical Review B **66**, 045203 (2002).

5.   X. Biquard, O. Proux, J. Cibert, D. Ferrand, H. Mariette, R. Giraud, and B. Barbara, "Local Structure and Valence State of Mn in $Ga_{1-x}Mn_xN$ Epilayers", Journal of Superconductivity **16**, 127 (2003).

6.   L. Kronik, M. Jain, and J. R. Chelikowsky, "Electronic structure and spin polarization of $Mn_xGa_{1-x}N$", Physical Review B **66**, 041203 (2002).

7.   C. J. Bradley and A. P. Cracknell, "The mathematical theory of symmetry in solids", Clarendon Press, Oxford (1972).

8.   O. K. Andersen and O. Jepsen, "Explicit, First-Principles Tight-Binding Theory", Physical Review Letters **53**, 2571 (1984).

9.   A. Rubio, J. L. Corkill, M. L. Cohen, E. L. Shirley, and S. G. Louie, "Quasiparticle band structure of AlN and GaN", Physical Review B **48**, 11810 (1993).

10.   Z. S. Popovic, S. Satpathy, and W. C. Mitchel, "Electronic structure of substitutional versus interstitial manganese in GaN", Physical Review B **70**, 161308 (2004).

11.   E. Kulatov, private communication.

12.   B. Sanyal, O. Bengone, and S. Mirbt, Phys. Rev. B **68**, 205210 (2003).

13.   P. Blaha, K. Schwarz, G. K. H. Madsen, D. Kvasnicka, and J. Luitz, WIEN2k, "An Augmented Plane Wave_Local Orbitals Program for Calculating Crystal Properties", Karlheinz Schwarz, Techn. Universität Wien, Austria, 2001, ISBN 3-9501031-1-2.

14.   J. P. Perdew, K. Burke, and M. Ernzerhof, Physical Review Letters **77**, 3865 (1996).

15.   S. Cottenier, Density Functional Theory and the family of (L)APW-methods: a step-by-step introduction (Instituut voor Kern- en Stralingsfysica, K.U.Leuven, Belgium), 2002, ISBN 90-807215-1-4 (to be found at http://www.wien2k.at/reg user/textbooks).

16.   Web-site: http://www.esrf.fr/exp_facilities/BM30B/BM30Bb-en.html

17.   R. Prinz and D. Koningsberger, editors, "X-ray absorption: principles, applications techniques of EXAFS, SEXAFS and XANES", J. Wiley and Sons, New York, 1988.

18.   J. J. Rehr, R. C. Albers, "Theoretical approaches to x-ray absorption fine structure", Reviews of Modern Physics **72**, 621 (2000).

19.   Y. Joly, "X-ray absorption near-edge structure calculations beyond the muffin-tin approximation", Physical Review B **63**, 125120 (2001).

20. E. Kulatov, Y. Uspenskii, H. Mariette, J. Cibert, D. Ferrand, H. Nakayama, and H. Ohta, "Ab Initio Study of Magnetism in III-V- and II-VI-Based Diluted Magnetic Semiconductors", Journal of Superconductivity, **16**, 123 (2003).

21. S. Marcet, D. Ferrand, D. Halley, S. Kuroda, H. Mariette, E. Gheeraert, F. J. Teran, M. L. Sadowski, R. M. Galera, and J. Cibert, "Magneto-optical spectroscopy of (Ga,Mn)N epilayers", Physical Review **74**, 125201 (2006).

22. A. Wolos, A. Wysmolek, M. Kaminska, A. Twardowski, M. Bockowski, I. Grzegory, S. Porowski, and M. Potemski, "Neutral Mn acceptor in bulk GaN in high magnetic fields", Physical Review B **70**, 245202 (2004).

23. T. Graf, M. Gjukic, M. S. Brandt, M. Stutzmann, and O. Ambacher, "The $Mn^{3+/2+}$ acceptor level in group III nitrides", Applied Physics Letters **81**, 5159 (2002).

24. L. D. Landau and E. M. Lifshitz, "Electrodynamics of continuous media", Pergamon Press, Oxford, New York (1960).

25. E. Kulatov, H. Mariette, J. Cibert, A. Titov, H. Nakayama, Yu. Uspenskii, "Electronic, optical spectra andthe distribution of Mn impurities in GaN and group-IV semiconductors", Journal of Crystal Growth **275**, e2239 (2005).

26. D. C. Look, R. J. Molnar, "Degenerate layer at GaN/sapphire interface: Influence on Hall-effect measurements", Applied Physics Letters 70, 3377 (1997); D. C. Look, D. C. Reynolds, J. W. Hemsky, J. R. Sizelove, R. L. Jones, and R. J. Molnar, "Defect Donor and Acceptor in GaN", Physical Review Letters **79**, 2273 (1997).

27. A. Wolos, M. Palczewska, M. Zajac, J. Gosk, M. Kaminska, A. Twardowski, M. Bockowski, I. Grzegory, and S. Porowski, "Optical and magnetic properties of Mn in bulk GaN", Physical Review B **69**, 115210 (2004).

REFERENCES

28. I. P. Smorchkova, E Haus, B. Heying, P. Kozodoy, P. Fini, J. P. Ibbetson, S. Keller, S. P. DenBaars, J. S. Speck, and U. K. Mishra, "Mg doping of GaN layers grown by plasma-assisted molecular-beam epitaxy", Applied Physics Letters **76**, 718 (2000).

29. A. Titov, X. Biquard, D. Halley, S. Kuroda, E. Bellet-Amalric, H. Mariette, J. Cibert, A. E. Merad, G. Merad, M. B. Kanoun, E. Kulatov, and Yu. A. Uspenskii "X-ray Absorption Near-Edge Structure and Valence state of Mn in (Ga,Mn)N" Physical Review B **72**, 115209 (2005).

30. H. Ohno, "Making Nonmagnetic Semiconductors Ferromagnetic", Science, vol. 281 (1998).

31. J. Masek and F. Maca, "Interstitial Mn in (Ga,Mn)As: Binding energy and exchange coupling", Physical Review B **69**, 165212 (2004).

32. Wikipedia, the free encyclopedia, http://en.wikipedia.org/wiki/Wikipedia

33. S. Marcet, "Thèse de docteur de l'université Joseph Fourier – Grenoble 1", Grenoble (2005).

34. Yu. Uspenskii, E. Kulatov, A. Titov, H. Mariette, J. Cibert, K. Motizuki, H. Nakayama, H. Ohta, "Effect of 3d-transition metal atoms distribution on exchange couplings and optical spectra in the dilute magnetic semiconductors of II-VI, III-V and IV groups", Journal of Magnetism and Magnetic Materials **300**, issue 1, p. 140 (2006).

35. R. Shioda, K. Ando, T. Hayashi, and M. Tanaka, "Local structures of III-V diluted magnetic semiconductors $Ga_{1-x}Mn_xAs$ studied using extended x-ray-absorption fine structure", Physical Review B **58**, 1100 (1998).

36. K. W. Edmonds, P. Bogusławski, K.Y.Wang, R. P. Campion, S. N. Novikov, N. R. S. Farley, B. L. Gallagher, C.T. Foxon, M. Sawicki, T. Dietl, M. Buongiorno Nardelli, and

J. Bernholc, "Mn Interstitial Diffusion in (Ga;Mn)As", Physical Review Letters **92**, 037201 (2004).

37. M. Wierzbowska, D. Sanchez-Portal, and S. Sanvito, Physical Review B **70**, 235209 (2004).

38. S. Cho, S. Choi, S. Ch. Hong, Y. Kim, J. B. Ketterson, B.-J. Kim, Y. C. Kim, J.-H. Jung, "Ferromagnetism in Mn-doped Ge", Physical Review B **66**, 033303 (2002).

39. Y. D. Park, A. T. Hanbicki, S. C. Erwin, C. S. Hellberg, J. M. Sullivan, J. E. Mattson, T. F. Ambrose, A. Wilson, G. Spanos, B. T. Jonker, "A Group-IV Ferromagnetic Semiconductor: Mn_xGe_{1-x}", Science **295**, 651 (2002).

40. U. von Barth, L. Hedin, Journal of Physics C: Solid State Physics **5** (1972) 1629.

Chapter IV

1. Ch. Kittel, "Introduction to solid state physics, fourth edition", J. Wiley&Sons (2005).

2. S. Krupichka, "Physics of ferrites and associated magnetic oxides", vol. 1 (in Russian) Mir, Moscow (1976).

3. S. V. Vonsovskii, Zh. Eksp. Teor. Fiz. **16**, 981 (1946).

4. C. Zener, "Interaction Between the d Shells in the Transition Metals", Physical Review **81**, 440 (1951).

5. A. A. Abrikosov and L. P. Gor'kov, "On the nature of impurity ferromagnetism", Soviet Physics JETP **16**, number 6, 1575 (1963).

REFERENCES

6.   T. Dietl, H. Ohno, F. Matsukura, J. Cibert, D. Ferrand, "Zener Model Description of Ferromagnetism in Zinc-Blende Magnetic Semiconductors", Science **287**, 1019 (2000).

7.   H. Ohno, "Making Nonmagnetic Semiconductors Ferromagnetic", Science, vol. 281 (1998).

8.   T. Jungwirth, K. Y. Wang, J. Mašek, K. W. Edmonds, J. König, J. Sinova, M. Polini, N. A. Goncharuk, A. H. MacDonald, M. Sawicki, A. W. Rushforth, R. P. Campion, L. X. Zhao, C. T. Foxon, and B. L. Gallagher, "Prospects for high temperature ferromagnetism in (Ga,Mn)As semiconductors", Physical Review B **72**, 165204 (2005).

9.   J. Kudrnovsky, I. Turek, V. Drchal, F. Maca, P. Weinberger, and P. Bruno, "Exchange interactions in III-V and group-IV diluted magnetic semiconductors", Physical Review **69**, 115208 (2004).

10.   Y.-J. Zhao, T. Shishidou, and A. J. Freeman, "Ruderman-Kittel-Kasuya-Yosida-like Ferromagnetism in Mn_xGe_{1-x}", Physical Review Letters **90**, 047204 (2003).

11.   K. Sato, P. H. Dederics and H. Katayama-Yoshida, "Curie temperatures of III-V diluted magnetic semiconductors calculated from the first principles", Europhysics Letters **61**, 403 (2003).

12.   G. Bouzerar, T. Ziman and J. Kudrnovsky, "Calculating the Curie temperature reliably in diluted III-V ferromagnetic semiconductors", Europhysics Letters **69**, 812 (2005).

13.   S. Hilbert and W. Nolting, "Magnetism in (III,Mn)-V diluted magnetic semiconductors: Effective Heisenberg model", Physical Review B **71**, 113204 (2005).

14.   K. Sato, W. Schweika, P. H. Dederichs, H. Katayama-Yoshida, "Low-temperature ferromagnetism in (Ga,Mn)N: Ab initio calculations", Physical Review B **70**, 201202R (2004).

15. R. Giraud, S. Kuroda, S. Marcet, E. Bellet-Amalric, X. Biquard, B. Barbara, D. Fruchart, D. Ferrand, J. Cibert, and H. Mariette, "Structural and magnetic properties of a $Ga_{0,985}Mn_{0,015}N$", Journal of Magnetism and Magnetic Materials, **272-276**, e1557 (2004).

16. M. E. Oveberg, C. R. Abernathy, S. J. Pearton, N. A. Theodoropoulou, K. T. McCarthy, A. F. Hebard, "Indication of ferromagnetism in molecular-beam-epitaxy-derived N-type GaMnN", Applied Physics Letters **79**, 1312 (2001).

17. E. Sarigiannidou, F. Wilhelm, E. Monroy, R. M. Galera, E. Bellet-Amalric, A. Rogalev, J. Goulon, J. Cibert, and H. Mariette, "Intrinsic ferromagnetism in wurtzite (Ga,Mn)N semiconductor", Physical Review B **74**, 041306R (2006).

18. V. A. Chitta, J. A. H. Coaquira, J. R. L. Fernandez, C. A. Duarte, J. R. Leite, D. Schikora, D. J. As, K. Lischka, and E. Abramof, "Room temperature ferromagnetism in cubic GaN epilayers implanted with Mn^+ ions", Applied Physics Letters **85**, 3777 (2004).

19. M. L. Reed, N. A. El-Masry, H. H. Stadelmaier, M. K. Ritums, M. J. Reed, C. A. Parker, J. C. Roberts, S. M. Bedair, "Room temperature ferromagnetic properties of (Ga,Mn)N", Applied Physics Letters **79**, 3473 (2001).

20. H. Hori, S. Sonoda, T. Sasaki, Y. Yamamoto, S. Shimizu, K. Suga, and K. Kindo, "High-T_C ferromagnetism in diluted magnetic semiconducting GaN:Mn films", Physica B 324, 142 (2002); S. Yoshii, S. Sonoda, T. Yamamoto, T. Kashiwagi, M. Hagiwara, Y. Yamamoto, Y. Akasaka, K. Kindo, H. Hori, "Evidence for Carrier-Induced High-T_C Ferromagnetism in Mn-doped GaN film", arXiv:cond-mat/0604647 (2006).

21. R. Giraud, S. Kuroda, S. Marcet, E. Bellet-Amalric, X. Biquard, B. Barbara, D. Fruchart, D. Ferrand, J. Cibert and H. Mariette, "Ferromagnetic $Ga_{1-x}Mn_xN$ epilayers vs. antiferromagnetic $GaMn_3N$ clusters", Europhysics Letters **65** (4), 553 (2004).

22. X. Biquard, O. Proux, J. Cibert, D. Ferrand, H. Mariette, R. Giraud, and B. Barbara, "Local Structure and Valence State of Mn in $Ga_{1-x}Mn_xN$ Epilayers", Journal of Superconductivity **16**, 127 (2003).

23. S. Marcet, "Thèse de docteur de l'université Joseph Fourier – Grenoble 1", Grenoble (2005).

24. A. Titov, X. Biquard, D. Halley, S. Kuroda, E. Bellet-Amalric, H. Mariette, J. Cibert, A. E. Merad, G. Merad, M. B. Kanoun, E. Kulatov, and Yu. A. Uspenskii "X-ray Absorption Near-Edge Structure and Valence state of Mn in (Ga,Mn)N" Physical Review B **72**, 115209 (2005).

25. A. Wolos, M. Palczewska, M. Zajac, J. Gosk, M. Kaminska, A. Twardowski, M. Bockowski, I. Grzegory, and S. Porowski, "Optical and magnetic properties of Mn in bulk GaN", Physical Review B **69**, 115210 (2004).

26. C. Zener, "Interaction Between the d Shells in the Transition Metals. II. Ferromagnetic Compounds of Manganese with Perovskite Structure", Physical Review **82**, 403 (1951).

27. P. M. Krstajic, F. M. Peeters, V. A. Ivanov, V. Fleurov, K. Kikoin, "Double-exchange mechanisms for Mn-doped III-V ferromagnetic semiconductors", Physical Review B **70**, 195215 (2004).

28. K. M. Yu, W. Walukiewicz, T. Wojtowicz, I. Kuryliszyn, X. Liu, Y. Sasaki, and J. K. Furdina, "Effect of the location of Mn sites in ferromagnetic $Ga_{1-x}Mn_xAs$ on its Curie temperature", Physical Review B **65**, 201303(R) (2002).

29. J. Masek and F. Maca, "Interstitial Mn in (Ga,Mn)As: Binding energy and exchange coupling", Physical Review B **69**, 165212 (2004).

REFERENCES

30. L. Bergqvist, O. Eriksson, J. Kudrnovsky, V. Drchal, P. Korzhavyi, and I. Turek, "Magnetic Percolation in Diluted Magnetic Semiconductors", Physical Review Letters **93**, 137202 (2004).

31. J. L. Xu, M. van Schilfgaarde, G. D. Samolyuk, "Role of Disorder in Mn:GaAs, Cr:GaAs, and Cr:GaN", Physical Review Letters **94**, 097201 (2005).

32. Y. D. Park, A. T. Hanbicki, S. C. Erwin, C. S. Hellberg, J. M. Sullivan, J. E. Mattson, T. F. Ambrose, A. Wilson, G. Spanos, B. T. Jonker, "A Group-IV Ferromagnetic Semiconductor: Mn_xGe_{1-x}", Science **295**, 651 (2002).

33. S. Cho, S. Choi, S. Ch. Hong, Y. Kim, J. B. Ketterson, B.-J. Kim, Y. C. Kim, J.-H. Jung, "Ferromagnetism in Mn-doped Ge", Physical Review B **66**, 033303 (2002).

34. C. Jaeger, C. Bihler, T. Vallaitis, S. T. B. Goennenwein, M. Opel, R. Gross, M. S. Brandt, "Spin-glass-like behavior of Ge:Mn", Physical Review B **74**, 045330 (2006).

35. A. P. Li, J. F. Wendelken, J. Shen, L. C. Feldman, J. R. Thompson and H. H. Weitering, "Magnetism in Mn_xGe_{1-x} semiconductors mediated by impurity band carriers", Physical Review B **72**, 195205 (2005).

36. M. Jamet, A. Barski, T. Devillers, V. Poydenot, R. Dujardin, P. Bayle-Guillemaud, J. Rothman, E. Bellet-Amalric, A. Marty, J. Cibert, R. Mattana and S. Tatarenko, "High-Curie-Temperature ferromagnetism in self-organized $Ge_{1-x}Mn_x$ nanocolumns", Nature **5**, 653 (2006).

37. T. Dietl, H. Ohno and F. Matsukura, "Hole-mediated ferromagnetism in tetrahedrally coordinated semiconductors", Physical Review B **63**, 195205 (2001).

38. V. K. Dugaev, V. I. Litvinov, J. Barnas, and M. Vieira, "Exchange interaction and ferromagnetism in III-V semiconductors", Physical Review B **67**, 033201 (2003).

Conclusion

1.   T. Graf, M. Gjukic, M. S. Brandt, M. Stutzmann, and O. Ambacher, "The $Mn^{3+/2+}$ acceptor level in group III nitrides", Applied Physics Letters **81**, 5159 (2002).

2.   A. Wolos, A. Wysmolek, M. Kaminska, A. Twardowski, M. Bockowski, I. Grzegory, S. Porowski, and M. Potemski, "Neutral Mn acceptor in bulk GaN in high magnetic fields", Physical Review B **70**, 245202 (2004).

3.   S. Marcet, D. Ferrand, D. Halley, S. Kuroda, H. Mariette, E. Gheeraert, F. J. Teran, M. L. Sadowski, R. M. Galera, and J. Cibert, "Magneto-optical spectroscopy of (Ga,Mn)N epilayers", Physical Review **74**, 125201 (2006).

4.   E. Kulatov, H. Nakayama, H. Mariette, H. Ohta, and Yu. A. Uspenskii, "Electronic structure, magnetic ordering, and optical properties of GaN and GaAs doped with Mn", Physical Review B **66**, 045203 (2002).

5.   E. Kulatov, H. Mariette, J. Cibert, A. Titov, H. Nakayama, Yu. Uspenskii, "Electronic, optical spectra andthe distribution of Mn impurities in GaN and group-IV semiconductors", Journal of Crystal Growth **275**, e2239 (2005).

6.   S. Marcet, "Thèse de docteur de l'université Joseph Fourier – Grenoble 1", Grenoble (2005).

7.   R. Giraud, S. Kuroda, S. Marcet, E. Bellet-Amalric, X. Biquard, B. Barbara, D. Fruchart, D. Ferrand, J. Cibert, and H. Mariette, "Structural and magnetic properties of a $Ga_{0,985}Mn_{0,015}N$", Journal of Magnetism and Magnetic Materials, **272-276**, e1557 (2004).

8.   E. Sarigiannidou, F. Wilhelm, E. Monroy, R. M. Galera, E. Bellet-Amalric, A. Rogalev, J. Goulon, J. Cibert, and H. Mariette, "Intrinsic ferromagnetism in wurtzite (Ga,Mn)N semiconductor", Physical Review B **74**, 041306R (2006).

9.   T. Dietl, H. Ohno, F. Matsukura, J. Cibert, D. Ferrand, "Zener Model Description of Ferromagnetism in Zinc-Blende Magnetic Semiconductors", Science **287**, 1019 (2000).

10. P. M. Krstajic, F. M. Peeters, V. A. Ivanov, V. Fleurov, K. Kikoin, "Double-exchange mechanisms for Mn-doped III-V ferromagnetic semiconductors", Physical Review B **70**, 195215 (2004).

Université Joseph Fourier – Grenoble 1

A. M. Prokhorov Institut de Physique Générale de l'Académie des Sciences de Russie

THESE

pour obtenir le grade de

Docteur de l'Université Joseph Fourier – Grenoble 1

Spécialité: physique

présentée et soutenue publiquement par

TITOV Andrey

le 7 décembre 2006

Propriétés électroniques des semiconducteurs magnétiques dilués:

$Ga_{1-x}Mn_xN$, $Ga_{1-x}Mn_xAs$, $Ge_{1-x}Mn_x$

Résumé

Composition du jury:

Président:	Michel ZIGONE
Rapporteur:	Patrick BRUNO
Rapporteur:	Frédéric PETROFF
Codirecteur de thèse:	Henri MARIETTE
Directeur de thèse:	Erkin KULATOV
Directeur de thèse:	Joël CIBERT

Grenoble – 2006

Brève description de la thèse en français

Les semiconducteurs magnétiques dilués sont considérés aujourd'hui comme une base potentielle de composants pour l'électronique de spin, qui permettraient d'utiliser dans le traitement de l'information non seulement la charge des porteurs, mais aussi leur spin. L'extrapolation aux semiconducteurs à grande bande interdite du modèle du champ moyen [1,2] utilisé pour décrire les semiconducteurs dopés par le manganèse prédit pour ces matériaux un comportement ferromagnétique à température élevée [2]. Ainsi, le semiconducteur $Ga_{1-x}Mn_xN$ (x=0,053) serait ferromagnétique à température ambiante, à condition que le Mn substitue le Ga dans GaN sous la forme d'un ion Mn^{2+}. Dans ce cas, le Mn porte un spin 5/2 et joue le rôle d'un accepteur, assurant un dopage de type p, et des interactions d'échange entre les atomes de Mn sont induites par des trous libres. Une autre hypothèse raisonnable est que le Mn adopte la configuration Mn^{3+}, isoélectronique du gallium. Il est donc très important de déterminer le mode d'incorporation et l'état électronique du Mn dans (Ga,Mn)N. En outre, les propriétés électroniques de (Ga,Mn)As et (Ge,Mn) ont été étudiées. En effet, les propriétés de (Ga,Mn)As sont déjà bien connues et de nombreux résultats expérimentaux et théoriques sont disponibles. Dans ce travail nous utilisons (Ga,Mn)As comme une référence pour profiter de ces nombreux résultats. Le semiconducteur (Ge,Mn) est un autre matériau qui peut trouver de nombreux applications en électronique de spin: d'une part, la technologie de croissance du germanium est bien développée et d'autre part, des propriétés ferromagnétiques de (Ge,Mn) à température élevée (T_C~285K) ont été observées [3]. Dans ce travail la structure de bande de (Ge,Mn) a été calculée pour déterminer l'état électronique du Mn dans (Ge,Mn).

Les propriétés électroniques de (Ga,Mn)N ont été étudiées par spectroscopie d'absorption des rayons X au seuil K du Mn. Cette méthode a plusieurs avantages. Premièrement, elle permet d'étudier séparément les différents éléments chimiques dans un alliage complexe. Deuxièmement, l'intensité de ces spectres peut souvent être directement associée à la densité d'états p au dessus du niveau de Fermi. En outre, les spectres d'absorption au seuil K sont moins influencés par la surface des échantillons que les spectres au seuil L. Les spectres au seuil K permettent donc d'étudier les propriétés intrinsèques du cristal. Enfin, cette méthode est couramment utilisée à Grenoble et des résultats préliminaires étaient disponibles dans notre équipe.

Les couches de $Ga_{1-x}Mn_xN$ (x=0,003-0,057) ont été préparées par épitaxie par jets moléculaires [4]. La structure wurtzite de ces échantillons a été confirmée par des mesures de diffraction des rayons X. La forte dynamique de ces mesures a montré également que les couches de (Ga,Mn)N ne contiennent pas de phases secondaires, comme $GaMn_3N$ [4]. Les spectres d'absorption des rayons X au seuil K du Mn ont été enregistrés par X. Biquard et al. au Synchrotron Européen (ESRF, ligne BM30B) à Grenoble [5]. Une simulation de la partie EXAFS des spectres d'absorption au seuil K du Mn a confirmé que les atomes de Mn substituent les atomes de Ga dans GaN [5].
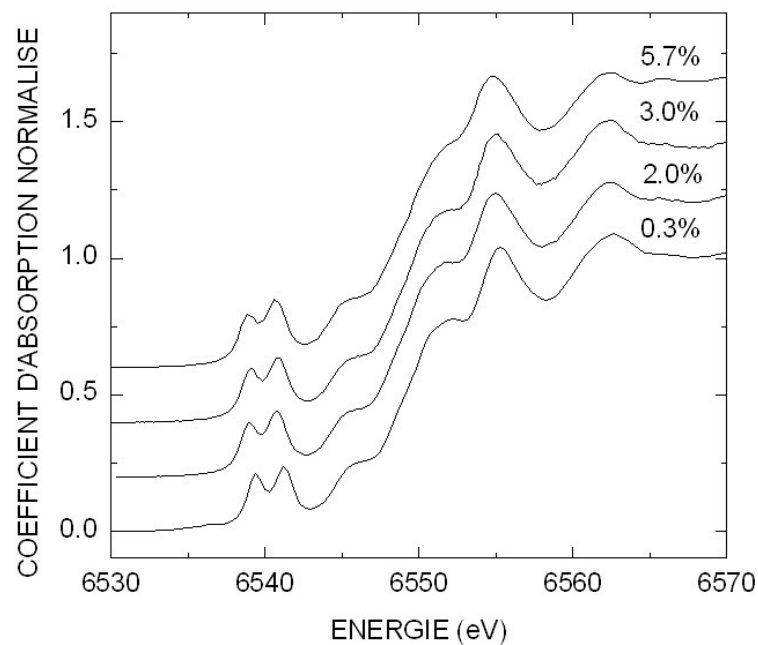

Fig. 1. La partie XANES des spectres d'absorption des rayons X au seuil du Mn dans $Ga_{1-x}Mn_xN$ (la concentration x du Mn est montrée sur la figure). Mesures: X. Biquard et al. [5].

Une information sur l'état électronique du Mn peut être obtenue à partir de la partie XANES des spectres d'absorption des rayons X (fig. 1). La forme du XANES ne dépend pas de la concentration de Mn dans $Ga_{1-x}Mn_xN$. L'état électronique du Mn et la structure cristalline locale autour du Mn sont donc les mêmes dans tous nos échantillons. Cependant, il est assez compliqué de trouver un lien entre le XANES et la structure électronique du cristal. Nous utilisons des calculs *ab-initio* pour obtenir une information quantitative à partir de ces spectres.
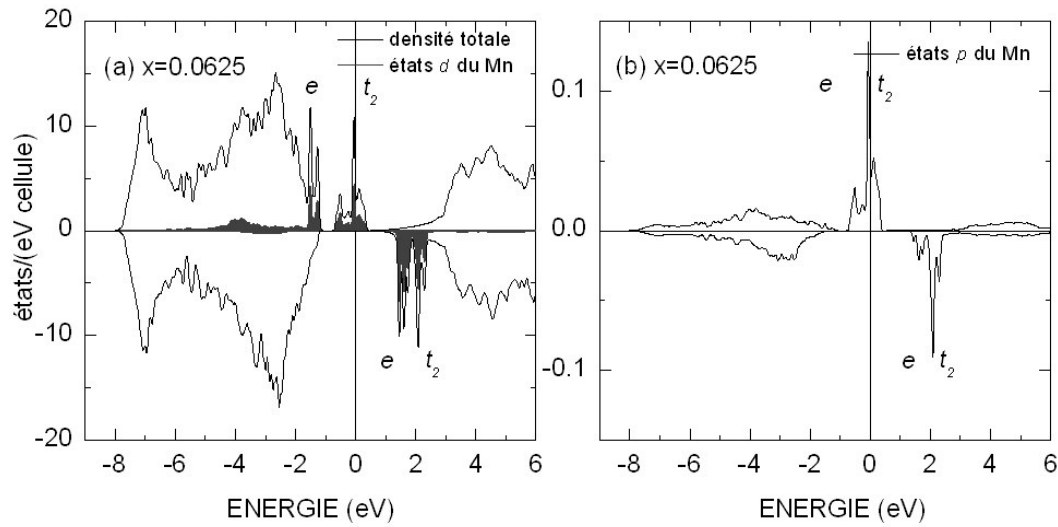
Fig. 2. (a) Densité d'états totale (ligne noire) et densité d'états 3*d* du Mn (ligne grise); (b) densité d'états *p* du Mn. Le niveau de Fermi est indiqué par une ligne verticale à 0 eV.

La structure de bandes de $Ga_{1-x}Mn_xN$ (*x*=0,0625) a été calculée par la méthode LAPW [6]. Les densités d'états de spin up (spin d'électron a la même direction que l'aimantation du cristal) et de spin down sont présentés sur la fig. 2a. Le haut de la bande de valence est constitué essentiellement par des états 2*p* des atomes d'azote, ces états se trouvent au-dessous de -1eV. Les états de la bande de conduction sont situés au-dessus de +2eV. Des états 3*d* du Mn sont localisés dans la bande interdite. L'interaction d'échange entre les électrons 3*d* d'un atome de Mn décale les états 3*d* de spin up vers les basses énergies par rapport aux états 3*d* de spin down et ce décalage est environ 2 eV (fig. 2a). Chaque atome de Mn dans (Ga,Mn)N a comme proches voisins quatre atomes d'azote. Ces quatre atomes forment un tétraèdre régulier autour du Mn. Le champ cristallin induit par ces quatre atomes d'azote lève la dégénérescence des états 3*d* du Mn et il divise ces états en deux bandes: *e* (deux états) et t_2 (trois états). Les orbitales 2*p* de l'azote agissent plus fortement sur les orbitales de la bande t_2 et cette interaction pousse la bande t_2 au-dessus de la bande *e* [7]. Le niveau de Fermi se trouve dans la bande t_2 de spin up et il devise cette bande en deux parties (remplie et vide) avec un rapport 2:1. Ainsi, la bande *e* de spin up est complètement remplie par 2 électrons, tandis que la bande t_2 est partiellement vide.

Les orbitales $4p$ du Mn acquièrent la symétrie t_2 dans le champ cristallin tétraédrique des quatre atomes d'azote. Une hybridation de ces orbitales aux états $3d$ du Mn dans les bandes t_2 est donc possible et une forte densité d'états p du Mn est présente dans les bandes t_2 de spin up et down (fig. 2b). Ainsi, il y a deux bandes avec une forte densité d'états p du Mn dans le gap: la bande t_2 de spin up et la bande t_2 de spin down. Les spectres d'absorption des rayons X au seuil K du Mn correspondent à transitions des électrons $1s$ du Mn vers des états vides. Selon la règle de sélection dipolaire l'intensité de ces transitions est très forte si les états finaux ont la symétrie p. Les deux bandes (t_2 de spin up et down) doivent donc apparaître dans les spectres. Une estimation montre que les transitions quadrupolaires sont dix fois plus faibles que les transitions dipolaires.
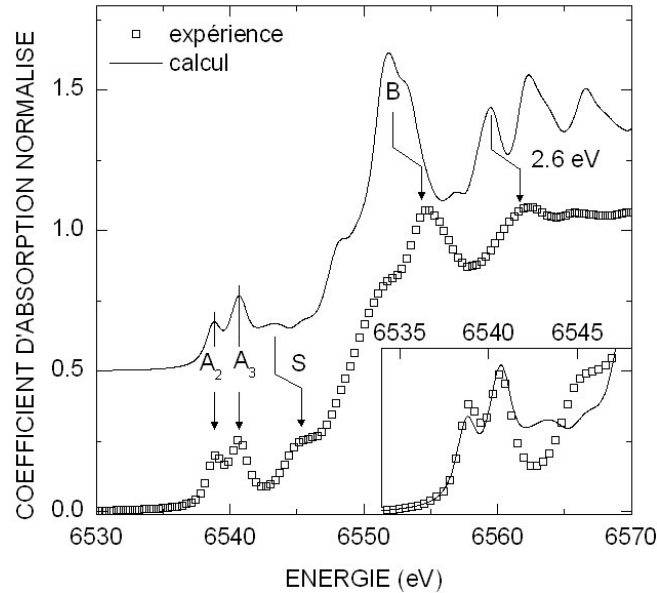

Fig. 3. Le spectre d'absorption des rayons X au seuil K du Mn: spectre expérimental de $Ga_{1-x}Mn_xN$ (x=0,057, carrés), spectre calculé de $Ga_{1-x}Mn_xN$ (x=0,0625, ligne).

Le spectre d'absorption des rayons X au seuil K du Mn dans $Ga_{1-x}Mn_xN$ (x=0,0625) a été calculé par la méthode LAPW [6], uniquement les transitions dipolaires ont été prises en compte. Puis, pour comparer ce calcul à nos résultats expérimentaux le spectre calculé a été élargi avec la fonction de Voigt $V(\Gamma_L, \Gamma_G)$, où le paramètre Γ_L est la largeur du niveau $1s$ (cette largeur est inversement proportionnelle au temps de vie du trou $1s$), Γ_G est la résolution du monochromateur. Le paramètre Γ_L vaut 1.16 eV [8] pour le niveau $1s$ du Mn, le paramètre Γ_G=0.5 eV a été ajusté pour obtenir un bon fit des raies d'absorption qui se trouvent devant le

seuil d'absorption (fig. 3). Deux raies d'absorption séparées par un intervalle de 2 eV sont présentes dans le spectre calculé: une raie (A_2) correspond à transitions vers la bande t_2 de spin up et une autre raie (A_3) correspond à transitions vers la bande t_2 de spin down. Deux pré-pics sont présents également dans nos spectres expérimentaux. Nous attribuons ces deux pré-pics aux transitions vers les bandes t_2 de spin up et down.
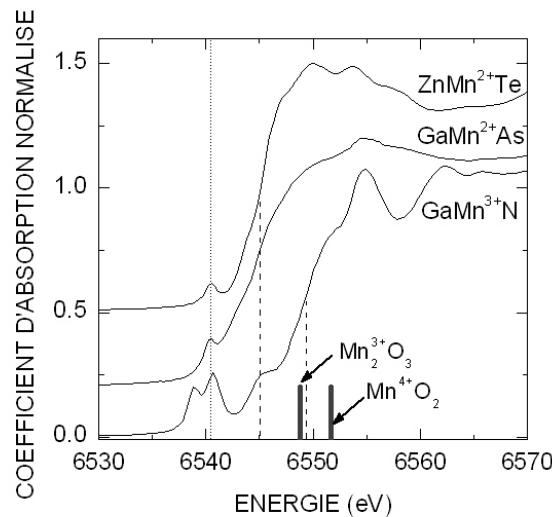

Fig. 4. Spectres d'absorption des rayons X au seuil du Mn (d'en haut): Mn^{2+} dans $Zn_{1-x}Mn_xTe:N$ (x=0,038), Mn^{2+} dans $Ga_{1-x}Mn_xAs$ (x=0,038) et Mn^{3+} dans $Ga_{1-x}Mn_xN$ (x=0,057). Les positions de seuil du Mn dans Mn_2O_3 et MnO_2 [5] sont également montrées. Mesures: X. Biquard et al. [5].

Cette attribution nous permet de déterminer l'état électronique du Mn dans (Ga,Mn)N. Si l'état électronique du Mn est $3d^5$ (Mn^{2+}), alors il y a cinq électrons d qui remplissent les bandes e et t_2 de spin up. Dans ce cas les transitions des électrons $1s$ vers la bande t_2 de spin up ne sont pas possibles et la raie A_2 ne doit pas apparaître dans le XANES du Mn. Effectivement, l'état électronique du Mn dans (Zn,Mn)Te et (Ga,Mn)As est Mn^{2+} et un seul pré-pic (A_3) est présent dans les spectres d'absorption des rayons X au seuil du Mn (fig. 4). Pourtant deux pré-pics sont présents dans les spectres du Mn dans (Ga,Mn)N. Cela signifie que la bande t_2 de spin up est partiellement vide et l'état électronique du Mn dans (Ga,Mn)N est Mn^{3+}.

La position du seuil d'absorption dépend de l'état électronique du Mn: lorsque la valence du Mn diminue, la position du seuil décale vers les basses énergies. Le seuil du Mn dans (Ga,Mn)N se trouve au-dessus de celui du Mn^{2+} dans (Zn,Mn)Te et dans (Ga,Mn)As

(fig. 4). Cette différence de position du seuil confirme donc que l'état électronique du Mn dans (Ga,Mn)N est 3+.

Cette conclusion est confirmée également par d'autres résultats expérimentaux:

- nos échantillons $Ga_{1-x}Mn_xN$ ont une conductivité de type *n* malgré la large gamme de concentration de Mn: *x*=0,003-0,057. De plus, nous n'observons pas de corrélation entre la concentration d'électrons et la concentration de Mn. Cela suggère que le Mn n'est pas accepteur dans (Ga,Mn)N, ce qu'il serait si son état électronique était Mn^{2+};
- une raie d'absorption à 1.4 eV est présente dans les spectres optiques d'absorption de (Ga,Mn)N [9]. Cette raie a été attribuée à une transition électronique interne du Mn: des électrons de la bande *e* de spin up passent vers la bande t_2 de spin up [10,11,12]. Cette transition est possible si la bande t_2 de spin up est partiellement vide (Mn^{3+}), cette raie n'est pas observée dans les spectres optiques d'absorption des semiconducteurs où le Mn a l'état électronique Mn^{2+}.
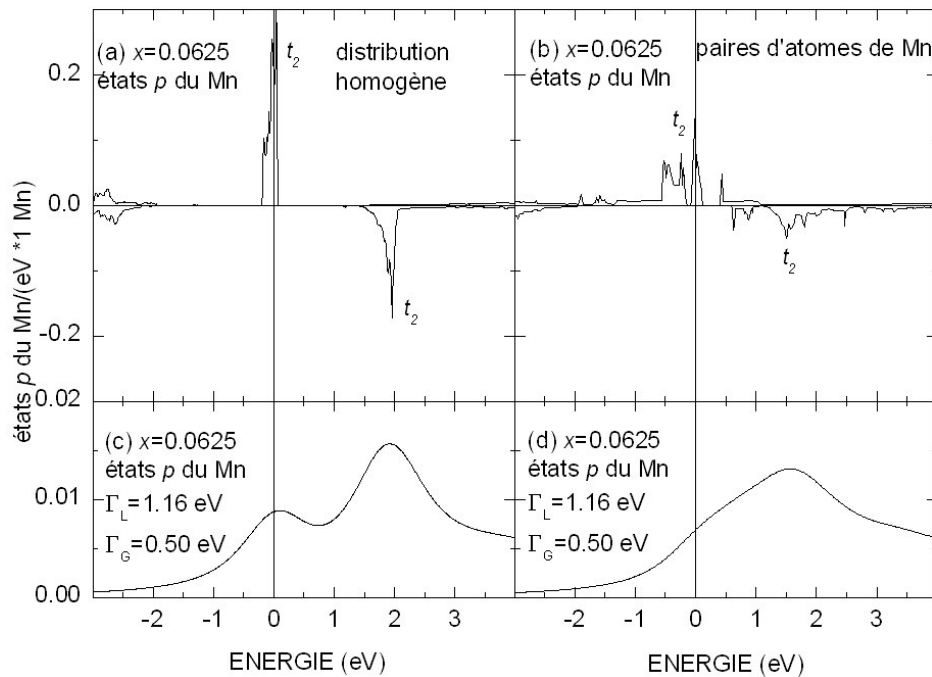

Fig. 5. La densité d'états *4p* du Mn dans $Ga_{1-x}Mn_xN$ (*x*=0,0625) de structure zinc-blende: (a) avec une distribution des atomes de Mn homogène; (b) avec formation de paires d'atomes de Mn en proches voisins. En (c) et (d) les densités d'états ont été élargies: (c) distribution des atomes de Mn homogène; (d) formation de paires d'atomes de Mn en proches voisins.

L'interprétation du XANES nous permet également d'étudier la distribution de Mn dans (Ga,Mn)N. Une simulation de la partie EXAFS permet de déterminer les distances entre le Mn et ses proches voisins, et le nombre de ces voisins. Par contre, il est très compliqué de dire à partir de cette simulation s'il y a un atome du Mn parmi d'autres seconds voisins – onze atomes de Ga. Cette information peut être obtenue à partir de la partie XANES et cela nous permet de tester l'hypothèse d'une formation privilégiée de paires d'atomes proches voisin. La largeur des bandes d dans le gap dépend des distances entre les atomes de Mn: si la distribution de Mn est homogène dans $Ga_{1-x}Mn_xN$ ($x=0,057$) (les distances entre les atomes de Mn sont grandes), alors les bandes t_2 dans le gap sont étroites (fig. 5a) et deux pré-pics bien résolus sont présents dans le XANES du Mn (fig. 5c); si au contraire, il y a une formation de paires d'atomes de Mn en proches voisins, alors les bandes t_2 s'élargissent de façon significative (fig. 5b) et nous ne sommes plus capable de résoudre les deux pré-pics dans les spectres d'absorption des rayons X (fig. 5d). La présence des deux pré-pics bien résolus dans tous nos spectres expérimentaux suggère donc que la distribution du Mn est homogène dans tous les échantillons étudiés (fig. 1).

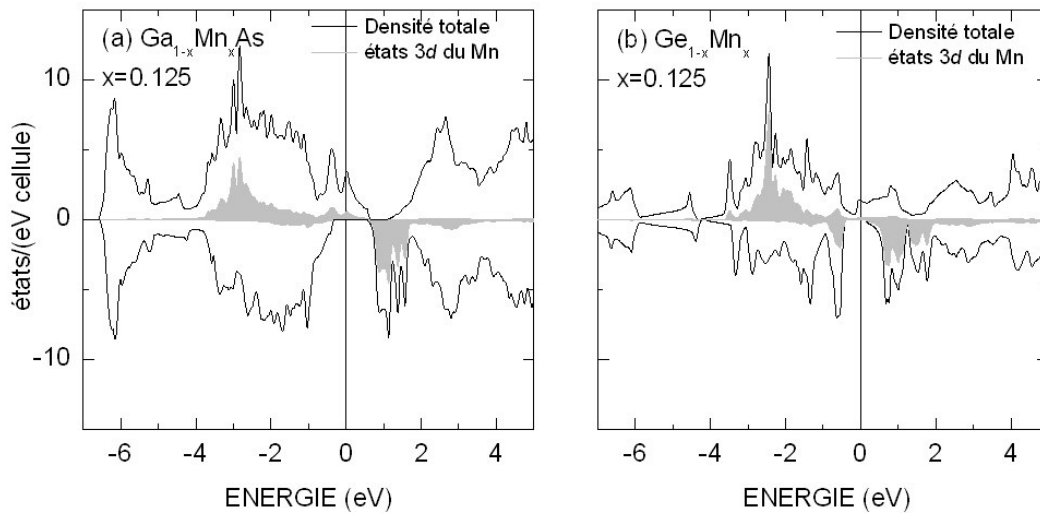Fig. 6. Calcul: densité d'états totale (ligne noire) et densité d'états $3d$ du Mn (ligne grise) dans (a) $Ga_{1-x}Mn_xAs$ ($x=0,125$) et (b) $Ge_{1-x}Mn_x$ ($x=0,125$).

La structure de bandes de $Ga_{1-x}Mn_xAs$ ($x=0,125$) et de $Ge_{1-x}Mn_x$ ($x=0,125$) a été calculée par la méthode LAPW [6]. Dans ces deux cas les états $3d$ du Mn de spin up se trouvent dans la

bande de valence: il sont totalement remplis par cinq électrons et fortement hybridés à la bande de valence (fig. 6). Le nombre calculé d'électrons $3d$ près de l'atome de Mn est 4.90 dans (Ga,Mn)As et 5.01 dans (Ge,Mn). Ainsi selon ce calcul la configuration électronique du Mn est $3d^5$ (Mn^{2+}) dans ces deux semiconducteurs. Selon l'interprétation de la structure du XANES, qui a été proposée ci-dessus, un seul pré-pic (A_3) doit être présent dans le XANES du Mn dans (Ge,Mn). Cependant cette conclusion doit être confirmée par l'expérience.

Des études expérimentales montrent que le ferromagnétisme à haute température que nous observons dans (Ga,Mn)As est induit par les trous libres: des échantillons de (Ga,Mn)As de type p avec une haute concentration des trous sont ferromagnétiques, en même temps des échantillons de (Ga,Mn)As électriquement compensés sont antiferromagnétiques [13]. L'état électronique du Mn dans (Ga,Mn)N est Mn^{3+}: le Mn n'est pas accepteur dans (Ga,Mn)N et ces échantillons ont une conductivité de type n. Le mécanisme d'échange induit par les trous libres entre les atomes de Mn n'est pas présent dans (Ga,Mn)N. Cela explique une faible valeur de la température de Curie ($T_C{\sim}8K$) que nous observons dans $Ga_{1-x}Mn_xN$ (x=0.063) [14]. Cependant un co-dopage par un accepteur [2] ou par un donneur [15] peut renforcer l'interaction d'échange entre les atomes de Mn dans (Ga,Mn)N. Dans le dernier cas un co-dopage par un donneur change l'état électronique d'une partie des atomes de Mn. Si la concentration de donneurs est plus basse que celle du Mn, alors une partie des atomes de Mn acquiert l'état Mn^{2+}, tandis qu'une autre partie reste dans l'état Mn^{3+}. Dans ce cas le mécanisme de double échange de Zener [16] apparaît, et il peut significativement renforcer interaction entre les atomes de Mn dans (Ga,Mn)N [15].

Conclusion

Dans ce travail nous avons essayé de combiner les recherches expérimentales et théoriques pour obtenir d'une part une information directe sur les propriétés des semiconducteurs et d'autre part pour optimiser notre recherche. Les objectifs principaux de ce travail sont:

- l'estimation des possibilités prédictives des calculs *ab-initio* en comparant les spectres expérimentaux d'absorption des rayons X à ceux calculés par des méthodes *ab-initio*;
- l'interprétation des spectres d'absorption des rayons X au seuil K du Mn;
- l'étude des propriétés électroniques des DMS.

Les résultats principaux:

- l'état électronique du Mn dans (Ga,Mn)N est Mn^{3+} (configuration électronique $3d^4$): une raie dans le spectre d'absorption des rayons X au seuil K du Mn est attendue dans le cas du Mn^{2+} ($3d^5$) parce que la bande t_2 de spin up est remplie et une seule transition vers la bande t_2 de spin down est possible, mais deux raies d'absorption sont présentes dans les spectres de (Ga,Mn)N et cela signifie que la bande t_2 de spin up est partiellement vide dans (Ga,Mn)N;

- Mn n'est pas accepteur dans (Ga,Mn)N; cette conclusion est confirmée par nos mesures de transport électrique: nos échantillons ont une conductivité de type *n*; nous n'observons pas de corrélation entre la concentration d'électrons et la concentration du Mn;

- les bandes $3d$ du Mn sont étroites dans (Ga,Mn)N et cela signifie que la distribution du Mn est homogène dans nos échantillons;

- l'interaction d'échange induite par les trous libres n'est pas présente dans (Ga,Mn)N et cela explique la basse valeur de la température de Curie de nos échantillons de (Ga,Mn)N;

- selon notre calcul *ab-initio*, l'état électronique du Mn dans (Ge,Mn) est Mn^{2+} et donc une seule raie d'absorption doit être présente dans le XANES du Mn, mais cette conclusion doit être confirmée expérimentalement.

Bibliographie

1. A. A. Abrikosov and L. P. Gor'kov, "On the nature of impurity ferromagnetism", Soviet Physics JETP **16**, number 6, 1575 (1963).

2. T. Dietl, H. Ohno, F. Matsukura, J. Cibert, D. Ferrand, "Zener Model Description of Ferromagnetism in Zinc-Blende Magnetic Semiconductors", Science **287**, 1019 (2000).

3. S. Cho, S. Choi, S. Ch. Hong, Y. Kim, J. B. Ketterson, B.-J. Kim, Y. C. Kim, J.-H. Jung, "Ferromagnetism in Mn-doped Ge", Physical Review B **66**, 033303 (2002).

4. S. Kuroda, E. Bellet-Amalric, R. Giraud, S. Marcet, J. Cibert, and H. Mariette, "Strong influence of Ga/N flux ratio on Mn incorporation into $Ga_{1-x}Mn_xN$ epilayers grown by plasma-assisted molecular beam epitaxy", Applied Physics Letters **83**, 4580 (2003).

5. X. Biquard, O. Proux, J. Cibert, D. Ferrand, H. Mariette, R. Giraud, and B. Barbara, "Local Structure and Valence State of Mn in $Ga_{1-x}Mn_xN$ Epilayers", Journal of Superconductivity **16**, 127 (2003).

6. P. Blaha, K. Schwarz, G. K. H. Madsen, D. Kvasnicka, and J. Luitz, WIEN2k, "An Augmented Plane Wave_Local Orbitals Program for Calculating Crystal Properties", Karlheinz Schwarz, Techn. Universität Wien, Austria, 2001, ISBN 3-9501031-1-2.

7. Z. S. Popovic, S. Satpathy, and W. C. Mitchel, "Electronic structure of substitutional versus interstitial manganese in GaN", Physical Review B **70**, 161308 (2004).

8. Web-site: http://www.esrf.fr/exp_facilities/BM30B/BM30Bb-en.html

9. S. Marcet, D. Ferrand, D. Halley, S. Kuroda, H. Mariette, E. Gheeraert, F. J. Teran, M. L. Sadowski, R. M. Galera, and J. Cibert, "Magneto-optical spectroscopy of (Ga,Mn)N epilayers", Physical Review **74**, 125201 (2006).

10. T. Graf, M. Gjukic, M. S. Brandt, M. Stutzmann, and O. Ambacher, "The $Mn^{3+/2+}$ acceptor level in group III nitrides", Applied Physics Letters **81**, 5159 (2002).

11. A. Wolos, M. Palczewska, M. Zajac, J. Gosk, M. Kaminska, A. Twardowski, M. Bockowski, I. Grzegory, and S. Porowski, "Optical and magnetic properties of Mn in bulk GaN", Physical Review B **69**, 115210 (2004).

12. E. Kulatov, H. Nakayama, H. Mariette, H. Ohta, and Yu. A. Uspenskii, "Electronic structure, magnetic ordering, and optical properties of GaN and GaAs doped with Mn", Physical Review B **66**, 045203 (2002).

13.   H. Ohno, "Making Nonmagnetic Semiconductors Ferromagnetic", Science **281** (1998).

14.   E. Sarigiannidou, F. Wilhelm, E. Monroy, R. M. Galera, E. Bellet-Amalric, A. Rogalev, J. Goulon, J. Cibert, and H. Mariette, "Intrinsic ferromagnetism in wurtzite (Ga,Mn)N semiconductor", Physical Review B **74**, 041306R (2006).

15.   P. M. Krstajic, F. M. Peeters, V. A. Ivanov, V. Fleurov, K. Kikoin, "Double-exchange mechanisms for Mn-doped III-V ferromagnetic semiconductors", Physical Review B **70**, 195215 (2004).

16.   C. Zener, "Interaction Between the d Shells in the Transition Metals. II. Ferromagnetic Compounds of Manganese with Perovskite Structure", Physical Review **82**, 403 (1951).

Appendix I: list of samples

Label	Mn content (x)	Layer thickness	Substrate	Laboratory
$Ga_{1-x}Mn_xN$ E166	0.3%	-	Lumilog (Al_2O_3/GaN)	CEA-CNRS-UJF (Grenoble)
$Ga_{1-x}Mn_xN$ E363b	2.0%	240 nm	Lumilog (Al_2O_3/GaN)	CEA-CNRS-UJF (Grenoble)
$Ga_{1-x}Mn_xN$ E414	3.0%	170 nm	Lumilog (Al_2O_3/GaN)	CEA-CNRS-UJF (Grenoble)
$Ga_{1-x}Mn_xN$ E476	5.7%	210 nm	Lumilog (Al_2O_3/GaN)	CEA-CNRS-UJF (Grenoble)
$Ga_{1-x}Mn_xAs$	8%	-	-	University of Nottingham
$Zn_{1-x}Mn_xTe:N$	3.8%	-	-	CEA-CNRS-UJF (Grenoble)

Appendix II: list of publications

1. A. Titov, D. Ferrand, J. Cibert, "Epitaxial film thickness measurement using reflectivity" (in Russian) // Scientific transactions of the MEPHI-2003 **1**, p. 97-98 (2003).

2. E. Kulatov, H. Mariette, J. Cibert, A. Titov, H. Nakayama, Yu. Uspenskii, "Electronic, optical spectra and the distribution of Mn impurities in GaN and group-IV semiconductors" // Proceedings of International Conference on Crystal Growth ICCG14, p. 12 (2004).

3. S. Marcet, E. Bellet, X. Biquard, C. Bougerol, J. Cibert, D. Ferrand, R. Giraud, D. Halley, E. Kulatov, S. Kuroda, H. Mariette, A. Titov, "Properties of $Ga_{1-x}Mn_xN$ epilayers grown by molecular beam epitaxy" // Proceedings of International Conference on the Physics of Semiconductors, American Institute of Physics, p. 365-366 (2004).

4. Yu. Uspenskii, E. Kulatov, A. Titov, H. Mariette, J. Cibert, K. Motizuki, H. Nakayama, H. Ohta, "Effect of $3d$-transition metal atoms distribution on exchange couplings and optical spectra in the dilute magnetic semiconductors of II-VI, III-V and IV groups" // Moscow International Symposium on Magnetism, Book of Abstracts, p. 303 (2005).

5. A. Titov, X. Biquard, D. Halley, S. Kuroda, E. Bellet-Amalric, H. Mariette, J. Cibert, E. Kulatov, and Yu. A. Uspenskii, "X-ray Absorption Near-Edge Structure of Mn in GaMnN" // Moscow International Symposium on Magnetism, Book of Abstracts, p. 305 (2005).

6.   E. Kulatov, H. Mariette, J. Cibert, A. Titov, H. Nakayama, Yu. Uspenskii, "Electronic, optical spectra and the distribution of Mn impurities in GaN and group-IV semiconductors" // Journal of Crystal Growth **275**, e2239-e2243 (2005).

7.   A. Titov, X. Biquard, D. Halley, S. Kuroda, E. Bellet-Amalric, H. Mariette, J. Cibert, A. E. Merad, G. Merad, M. B. Kanoun, E. Kulatov, and Yu. A. Uspenskii, "X-ray absorption near-edge structure and valence state of Mn in (Ga,Mn)N" // Physical Review B **72**, 115209 (2005).

8.   Yu. Uspenskii, E. Kulatov, A. Titov, H. Mariette, J. Cibert, K. Motizuki, H. Nakayama, H. Ohta, "Effect of 3*d*-transition metal atoms distribution on exchange couplings and optical spectra in the dilute magnetic semiconductors of II-VI, III-V and IV groups" // Journal of Magnetism and Magnetic Materials **300**, issue 1, p. 140-143 (2006).

9.   A. Titov, E. Kulatov, Yu. A. Uspenskii, X. Biquard, D. Halley, S. Kuroda, E. Bellet-Amalric, H. Mariette, and J. Cibert, "Pre-Edge Features in x-ray Absorption Structure of Mn in GaMnN, GaMnAs and GeMn" // Journal of Magnetism and Magnetic Materials **300**, issue 1, p. 144-147 (2006).

10.   A. Titov, E. Kulatov, Yu. A. Uspenskii, X. Biquard, D. Halley, S. Kuroda, E. Bellet-Amalric, H. Mariette, and J. Cibert, "Modeling of x-ray absorption spectra of diluted magnetic semiconductors GaN:Mn, GaAs:Mn, Ge:Mn" // Bulletin of the Lebedev Physics Institute (in English), Kratkie soobshchenia po fizike №4, p. 10-18 (in Russian) (2006).

11.   A. Titov, X. Biquard, D. Halley, S. Kuroda, E. Bellet-Amalric, H. Mariette, J. Cibert, E. Kulatov, and Yu. A. Uspenskii, "X-ray absorption near-edge structure and valence state of Mn in (Ga,Mn)N" // Abstracts of the French-US workshop on Spintronics, p. 57 (2006).

12. A. Titov, X. Biquard, D. Halley, S. Kuroda, E. Bellet-Amalric, E. Kulatov, Yu. A. Uspenskii, H. Mariette, J. Cibert, "Etude des propriétés électroniques de (Ga,Mn)N par spectroscopie d'absorption des rayons X" // Abstracts of the conference «10es Journées de la Matière Condensée», p. 382-383 (2006).

13. Yu. A. Uspenskii, J. F. Seely, B. Kjornrattanawanich, D. L. Windt, Ye. A. Bugayev, V. V. Kondratenko, I. A. Artyukov, A. A. Titov, E. T. Kulatov, A. V. Vinogradov, "Determination of the optical constants of amorphous carbon in the EUV spectral region 18-450 eV" // Proceedings of the SPIE **6317**, p. 631713-631717 (2006).

14. A. Titov, X. Biquard, D. Halley, S. Kuroda, E. Bellet-Amalric, E. Kulatov, Yu. A. Uspenskii, H. Mariette, and J. Cibert, "X-ray absorption near-edge structure and valence state of Mn in (Ga,Mn)N", Réunion finale du GdR SESAME, Palaiseau (2006).

Résumé

Les propriétés électroniques de (Ga,Mn)N ont été étudiées par spectroscopie d'absorption des rayons X au seuil K du Mn. Des calculs *ab-initio* ont été utilisés pour interpréter les spectres d'absorption de (Ga,Mn)N. Deux pré-pics sont présents dans le seuil du Mn: le premier pré-pic est attribué aux transitions électronique vers les états $3d$ du Mn de spin up, tandis que le second pré-pic correspond aux transitions vers les états $3d$ du Mn de spin down. Cette interprétation nous permet de déterminer que l'état électronique du Mn dans (Ga,Mn)N est Mn^{3+}: deux pré-pics sont présents dans les spectres d'absorption du Mn^{3+} et un seul pré-pic reste dans les spectres du Mn^{2+}. Ce changement des spectres a été vérifié expérimentalement sur des échantillons de $(Zn,Mn^{2+})Te$ et $(Ga,Mn^{2+})As$. De plus, cette interprétation permet d'étudier la distribution du Mn dans (Ga,Mn)N: la forme des spectres d'absorption suggère que la distribution du Mn est homogène dans nos échantillons de (Ga,Mn)N.

Mots-clés: semiconducteurs magnétiques dilués, GaN:Mn, GaAs:Mn, Ge:Mn, XANES, spectroscopie d'absorption des rayons X, *ab-initio*, valence

Abstract

Electronic properties of the diluted magnetic semiconductor (Ga,Mn)N were studied by x-ray absorption spectroscopy at the K-edge of Mn. The measured x-ray absorption spectra were further interpreted using the *ab-initio* calculations. Two pre-edge absorption lines are observed in the x-ray absorption spectra: the first line was attributed to electronic transitions into $3d$ states of Mn of spin up, while the second line corresponds to transitions into $3d$ states of Mn of spin down. This interpretation allows us to determine the valence state of Mn: two absorption lines are present in the pre-edge structure of Mn^{3+} and only one line remains in case of Mn^{2+}. Such a change of the pre-edge structure was checked experimentally on $(Zn,Mn^{2+})Te$ and on $(Ga,Mn^{2+})As$. In addition, the distribution of Mn in (Ga,Mn)N can be studied using the interpretation: the shape of the spectra points to a homogeneous distribution of Mn in our (Ga,Mn)N samples.

Keywords: diluted magnetic semiconductor, GaN:Mn, GaAs:Mn, Ge:Mn, XANES, x-ray absorption spectroscopy, *ab-initio*, valence